Cellular and Molecular Mechanisms of lean MAFLD

Mohammad Alarabi

The University of Sydney

A thesis submitted in fulfilment of the requirements for the degree of Doctor of Philosophy

Sydney Medical School

The Westmead Institute for Medical Research

The University of Sydney

NSW, Australia

2026

Statement of Originality

The work in this thesis was performed towards a degree under the supervision of Professor Mohammed Eslam and Dr. Ziyan Pan at the Storr Liver Centre, Westmead Institute for Medical Research, University of Sydney. I certify that to the best of my knowledge, the content of this thesis is my own work. This thesis has not been submitted towards any other degree or purpose. I certify that the intellectual content of this thesis is the product of my own work and that all the assistance received in preparing this thesis and sources have been acknowledged.

Mohammad Alarabi

15 Feb 2026

Acknowledgements

I begin by expressing gratitude to Almighty Allah because His divine mercy and wisdom and blessings have sustained me throughout this entire experience. Through His divine will all things begin and end, so I reached this milestone because He guided me. I express my most sincere gratitude to Him. Through my prayers I extend peace to the most excellent human being Prophet Muhammad (Peace be upon him) who guides people toward knowledge and integrity through service to others.

The work has evolved through many years of continuous work and many obstacles and received backing from faithful believers. Many people played a crucial role in this achievement because their guidance and contributions exceed any number of words can convey.

I want to express my sincere gratitude to Professor Mohammed Eslam for your exceptional guidance throughout this field and your enduring patience and motivational support. You provided me with freedom to develop but remained available whenever I needed guidance. Your feedback provided precise and helpful guidance which strengthened my understanding and your trust in my abilities proved more important than you understand. I feel honoured to have studied under your leadership.

Deep thanks to Dr. Ziyan Pan, for your time and the effort to teach me the experiments and huge thanks for other facilities in Westmead institute for medical research for providing instruments and knowledge that helped me in pursuing my studies.

Special thanks to my parents and my wife for their praying and support that helped me mentally to finish my studies. Extended gratitude to my brothers and sisters for their constant emotional support. Your support and understanding have been a great source of strength, and I am very thankful for your presence in my life.

Authorship Attribution Statement

Chapter 3 and 4 of this thesis has been published as [*Alarabi M, Pan Z, Romero-Gómez M, George J, Eslam M. Telomere length and mortality in lean MAFLD: the other face of metabolic adaptation. Hepatology International. 2024;18(5):1448-58.*]. I designed the study, analysed the data and wrote the drafts of the manuscript.

Chapter 5 and 6 of this thesis has been accepted to published as [*Differential DNAm-GDF15 and Mitochondrial profile in lean MAFLD. Clinical and Experimental Medicine]*. I designed the study, analysed the data and wrote the drafts of the manuscript.

In addition to the authorship attribution statements above, in cases where I am not the corresponding author of a published item, permission to include the published material has been granted by the corresponding author.

Student: Mohammed Alarabi

Signature:

As supervisor for the candidature upon which this thesis is based, I can confirm that the authorship attribution statements above are correct.

Lead Supervisor: Prof. Mohammed Eslam

Signature:

Artificial Intelligence Statement

Artificial intelligence tools (Microsoft Copilot) were used solely for language-related assistance, including paraphrasing, sentence structure, and spelling/grammar correction. No AI tools were used for data analysis, interpretation, or generation of original scientific content. The author retains full responsibility for the work

Table of Contents

List of Figure

List of tables

List of Abbreviations

Abbreviation	Full Form
MAFLD	Metabolic dysfunction-associated fatty liver disease
ALD	Alcohol-associated liver disease
NAFLD	Non-alcoholic fatty liver disease
HCC	Hepatocellular carcinoma
WHO	World Health Organization
DALYs	Disability-adjusted life years
T2DM	Type 2 diabetes mellitus
BMI	Body mass index
HSCs	Hepatic stellate cells
MASH	Metabolic dysfunction-associated steatohepatitis
GWAS	Genome-wide association studies
SNPs	Single-nucleotide polymorphisms
PNPLA3	Patatin-like phospholipase domain-containing protein 3
TM6SF2	Transmembrane 6 superfamily member 2
MBOAT7	Membrane-bound O-acyltransferase domain-containing 7
GCKR	Glucokinase regulatory protein
FGF21	Fibroblast growth factor 21
FNDC5	Fibronectin type III domain-containing protein 5
MERTK	MER proto-oncogene tyrosine kinase
TGF-β	Transforming growth factor beta
MRI-PDFF	Magnetic resonance imaging-proton density fat fraction
CAP	Controlled attenuation parameter
ALT	Alanine aminotransferase
AST	Aspartate aminotransferase
NFS	NAFLD fibrosis score
FIB-4	Fibrosis-4 index
APRI	AST-to-platelet ratio index
HOMA-IR	Homeostasis model assessment of insulin resistance
HDL	High-density lipoprotein
FFAs	Free fatty acids
TNF-α	Tumour necrosis factor alpha
IL-6	Interleukin-6
LPS	Lipopolysaccharides
TLRs	Toll-like receptors
CNV	Copy number variation
XPO4	Exportin-4

FXR	Farnesoid X receptor
GDF-15	Growth differentiation factor-15
DNAm-GDF15	DNA methylation-predicted GDF-15
CpG	Cytosine-phosphate-guanine
ISR	Integrated stress response
ER	Endoplasmic reticulum
UPR	Unfolded protein response
NF-κB	Nuclear factor-kappa B
ROS	Reactive oxygen species
mtDNA	Mitochondrial DNA
ETC	Electron transport chain
ATP	Adenosine triphosphate
NADH	Nicotinamide adenine dinucleotide
$FADH_2$	Flavin adenine dinucleotide
TCA	Tricarboxylic acid cycle
PCR	Polymerase chain reaction
RT-PCR	Reverse transcription polymerase chain reaction
ELISA	Enzyme-linked immunosorbent assay
RNA-seq	RNA sequencing
ATAC-seq	Assay for Transposase-Accessible Chromatin sequencing
CUT&Tag-seq	Cleavage Under Targets and Tagmentation sequencing
TEM	Transmission electron microscopy
SEM	Standard error of the mean
ANOVA	Analysis of variance
SPSS	Statistical Package for the Social Sciences
NHANES	National Health and Nutrition Examination Survey
NDI	National Death Index

Chapter 1: Literature Review

1. Burden of liver disease

1.1 Global mortality and morbidity

Liver diseases are major causes of morbidity and mortality in the world as they cause almost 2 million deaths per year (1, 2). Cirrhosis is the 11th major cause of death and liver cancer is the 16th major cause of death. Collectively, the two conditions cause 3.5% of all deaths globally (3). According to the Global Burden of Disease 2019 study, cirrhosis and chronic liver diseases accounted for approximately 46.2 million disabilities adjusted life years (DALYs) globally, representing 1.6–1.8% of total DALYs (4).

1.2 Etiological contributors

Among the major causes of cirrhosis is metabolic dysfunction-associated fatty liver disease (MAFLD), a rapidly growing public health concern affecting nearly 25% of the global population (5). Alcohol-associated liver disease (ALD) is another cause of chronic liver injury resulting from excessive alcohol consumption and can progress to steatosis, steatohepatitis, fibrosis, and cirrhosis. Harmful alcohol use is responsible for approximately three million deaths globally each year across all causes, while ALD specifically accounts for a substantial proportion of cirrhosis-related mortality worldwide, contributing to approximately one quarter to one third of global cirrhosis deaths (6).

Another major cause behind the liver disease is viral hepatitis, caused by numerous viruses including “hepatitis A to G”, which is a leading contributor to cirrhosis, liver failure, and hepatocellular carcinoma (HCC) (7). The world health organisation (WHO) has documented an estimated 325 million people across the globe who have been suffering from hepatitis B or C, with annual deaths amounting to 1 million caused by viral hepatitis (8).

With effective drugs available to treat viral hepatitis as well as the wide implementation of

screening and vaccination programs for hepatitis B, the trend of liver diseases associated with viral hepatitis is decreasing worldwide. On the contrary, with lifestyle changes, including an increase in obesity and other manifestations of metabolic dysfunction and unsafe alcohol consumption, the trend of ALD and MAFLD has been increasing (5, 9).

2 Metabolic dysfunction associated fatty liver disease (MAFLD)

2.1 Definition and nomenclature shift

Over the past few years, fatty liver disease attributed to metabolic dysfunction has been subject of redefinition process that include an update in nomenclature from non-alcoholic fatty liver disease (NAFLD) to more apt one, MAFLD (10, 11), and change of the accompanied diagnostic criteria of exclusion of NAFLD to a positive diagnostic criteria for MAFLD that require evidence of hepatic steatosis together with metabolic risk factors to establish diagnosis (12).

This redefinition of the disease aims to recognise the role of metabolic dysfunction, including insulin resistance, obesity, type 2 diabetes mellitus (T2DM), and dyslipidaemia as the principal driver of disease pathogenesis, even in individuals without obesity (13). The utility of the new definition has been validated in numerous studies, which have shown that it has a higher ability to identify both hepatic and extra-hepatic outcomes, increase disease awareness and recognition of liver in the metabolic health spectrum, among many other positive attributes (14, 15).

2.2 Epidemiology and global burden

MAFLD is the most common chronic liver disease in the worldwide, affecting approximately 25-30% of the global population (Fig. 1.1). The prevalence is increasing in line with the rising trends of obesity, sedentary behaviour, and T2DM (5, 16), as consequences of the global changes in dietary habits and other lifestyle behaviours, such as the intake of

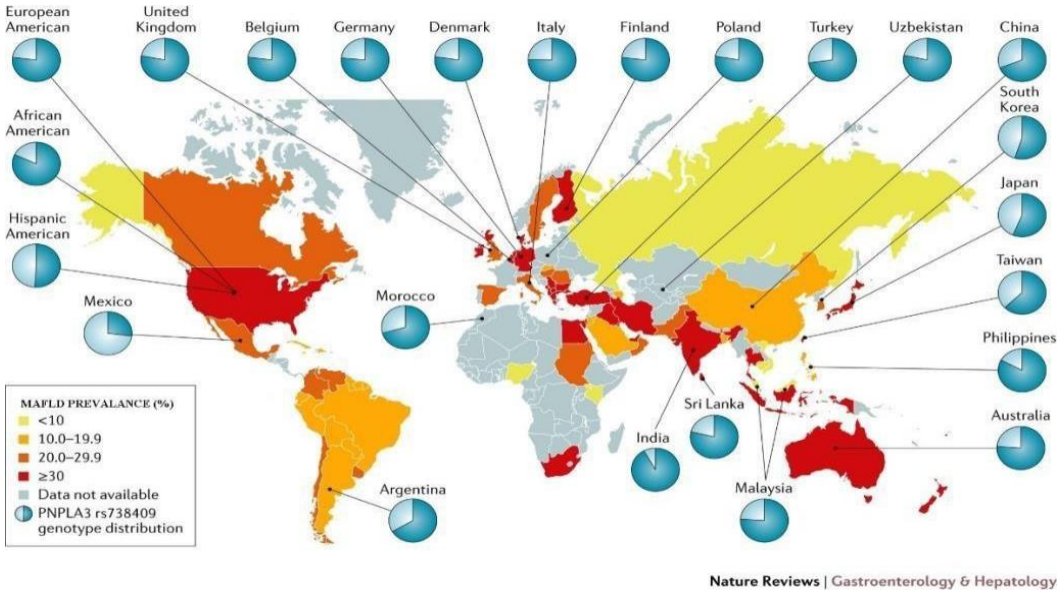

processed calorie-dense diet and a lack of physical activity.

Figure 1.1 Global distribution of MAFLD prevalence and patatin-like phospholipase domain-containing 3 (PNPLA3) genetic susceptibility (17).

The accelerating rate of urbanization has led to an increased prevalence of metabolic risk factors in places formerly classified as low risk. Consequently, the prevalence of MAFLD is also rising in many low- and middle-income countries (18). Alarmingly, this rise in MAFLD is also being observed among children, coinciding with the growing rates of childhood obesity. This surge in MAFLD across different populations and different age groups is a concerning trend (19).

In addition to hepatic sequelae, MAFLD is now considered a multisystem metabolic disease

linked with highly elevated risks of cardiovascular disease, chronic kidney disease, and a variety of cancers, which result in significant non-liver morbidity and mortality (20).

Despite its high prevalence and significant implications, MAFLD remains underdiagnosed and under-managed, which hinders proper intervention (21), indicating the need for more efficient policies, including enhancing disease awareness, appropriate active case findings protocols, and referral care pathways (22).

2.3 Spectrum and natural history of MAFLD

MAFLD spectrum spans from hepatic steatosis, metabolic dysfunction-associated steatohepatitis (MASH), fibrosis, cirrhosis, and HCC (23).

In the early stages, MAFLD is usually asymptomatic and is often discovered incidentally through elevated liver enzyme levels or imaging tests conducted for unrelated issues. As the disease advances, some patients may start to experience nonspecific symptoms such as fatigue or discomfort in the right upper quadrant of the abdomen, and hepatomegaly may be detected during a clinical examination (13, 24). Most patients remain asymptomatic until the disease has progressed significantly or complications arise, which can lead to delays in diagnosis and management (25).

In a small subset of patients, steatosis can progress to MASH, formerly known as NASH (26). This form of the disease is more aggressive, characterized by hepatocellular ballooning, lobular inflammation, and varying degrees of fibrosis (27). Identifying individuals at risk remains a significant clinical challenge (28).

Repeated cycles of hepatocellular injury and inflammation can activate hepatic stellate cells (HSCs), leading to deposition of extracellular matrix and the development of fibrosis (29), which subsequently increases the risk of HCC. Notably, HCC may also arise in non-cirrhotic

livers in MAFLD, particularly among patients with diabetes or metabolic comorbidities, highlighting the systemic nature of the disease (30).

Recognising MAFLD as a spectrum disorder is important in clinical practice and research. Disease progression is neither linear nor uniform, as some individuals may remain in a static and stable state for decades. In contrast, others may rapidly progress to develop advanced fibrosis over a short time span (31). Factors such as age, sex, ethnicity, comorbidities, and lifestyle behaviours influence this trajectory (32). For example, patients with T2DM and MAFLD are at particularly high risk for rapid progression and adverse outcomes, making them a priority population for screening and intervention (33).

2.4 Pathophysiology of MAFLD

The pathophysiology of MAFLD is complex and shaped by a myriad of factors, including genetic susceptibility, metabolic milieu, and lifestyle habits, as depicted in Fig. 1.2 (34).

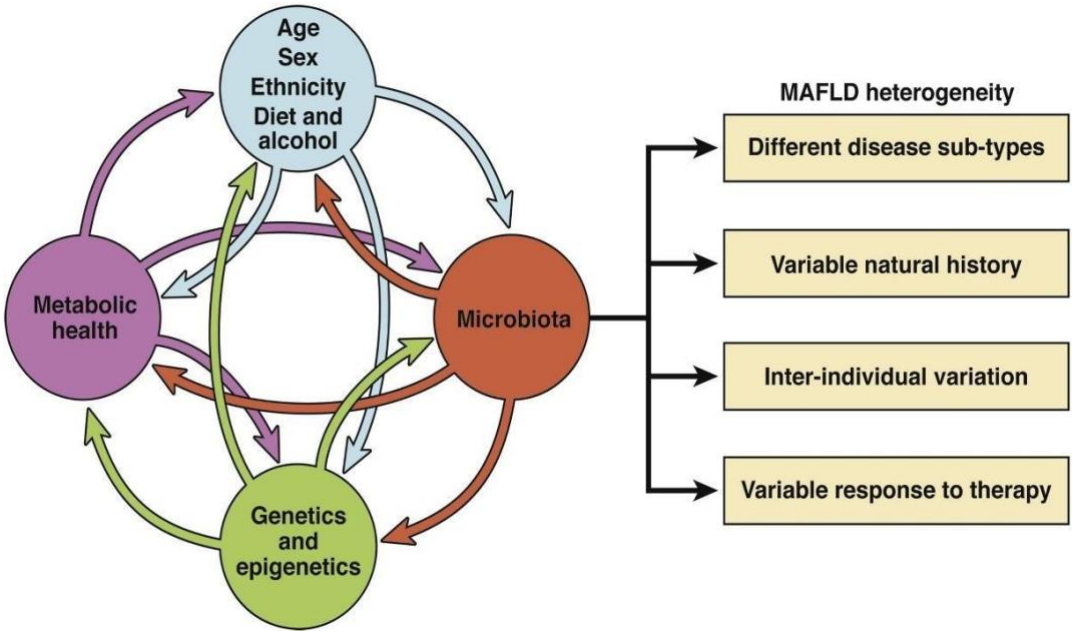

Figure 1.2 Multifactorial drivers of MAFLD heterogeneity and their impact on disease subtypes, progression, and treatment response (10).

A crucial factor in this process is insulin resistance, which leads to increased hepatic de novo lipogenesis, reduced fatty acid oxidation, and increased adipose tissue lipolysis (35). The outcome is an excess influx of free fatty acids (FFAs) into the liver that cannot be safely stored or metabolised by hepatocytes (36). This subsequent lipotoxic environment promotes oxidative stress, mitochondrial dysfunction and endoplasmic reticulum (ER) stress, ultimately leading to hepaocellular injury and inflammatory signaling (37).

Additionally, systemic inflammation and adipose tissue dysfunction play significant roles in disease progression (38). In insulin-resistant individuals, the adipocytes produce more pro-inflammatory cytokines, including tumour necrosis factor-alpha (TNF-α) and interleukin-6 (IL-6), while producing less adiponectin, an anti-inflammatory and insulin-sensitizing hormone (39). This imbalance exacerbates hepatic inflammation, facilitates fibrosis, and links MAFLD to broader cardiometabolic conditions.

Another layer of complexity arises from the close anatomical and functional relationship between the liver and the gut through the portal vein. When intestinal permeability increases—often referred to as "leaky gut" bacterial endotoxins and metabolites, including lipopolysaccharides (LPS), can translocate into the liver (40). This gut–liver axis triggers toll-like receptors (TLRs) activation and hepatic immune cells infiltration, further worsening hepatic inflammation and fibrosis (41). The pathogenesis of MAFLD is also associated with dysbiosis, involving alterations in bile acid metabolism, short-chain fatty acid production, and pro-inflammatory compounds (Fig. 1.3) (42).

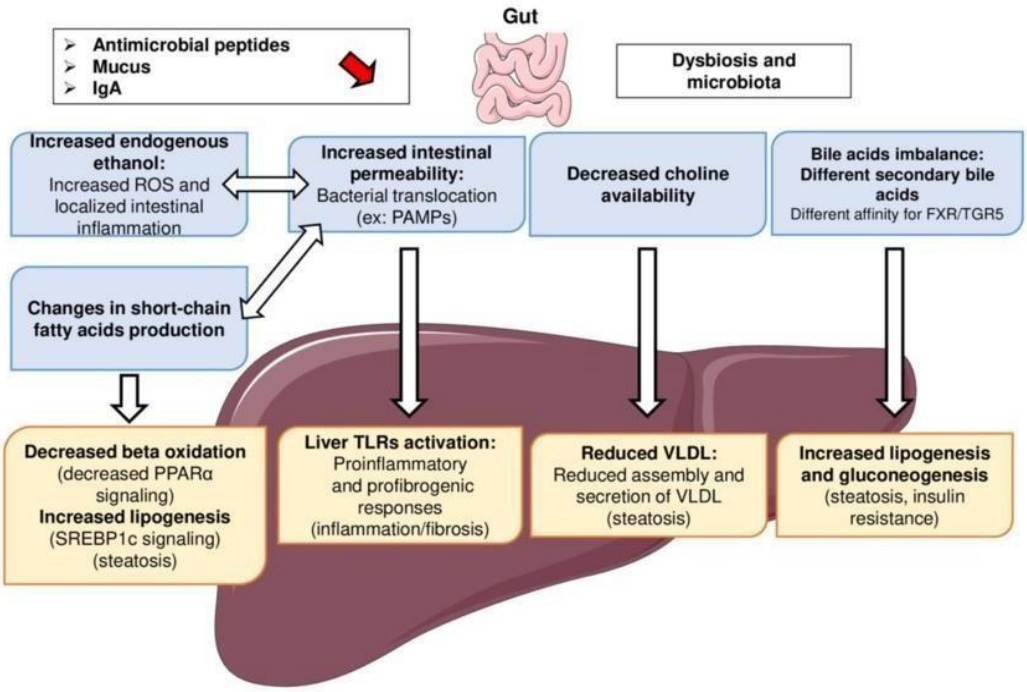

Figure 1.3 The crucial role of gut-liver axis in the pathophysiology of MAFLD (43).

Despite often being linked to unhealthy lifestyle choices, indeed, MAFLD has a significant genetic component, with heritability estimated at around 50% for both steatosis and fibrosis (44, 45). Multiple Genome-Wide Association Studies (GWAS) and large multiple candidate gene studies have identified several single-nucleotide polymorphisms (SNPs) that have been linked to increased susceptibility to the disease and its progression (46).

The most notable of these is the variant of the patatin-like phospholipase domain-containing 3 (PNPLA3) gene (rs738409), which is associated with the entire spectrum of the disease (47). In addition to PNPLA3, other variants such as those in transmembrane 6 superfamily member 2 (TM6SF2) (48), membrane-bound O-acyltransferase domain-containing 7 (MBOAT7) (49), and glucokinase regulatory protein (GCKR) have been identified (50).

Some other genetic variants regulating key processes involved in metabolic and immune signalling have also been implicated in MAFLD pathogenesis. Such as those in fibroblast growth factor 21 (FGF21) gene which plays a key role in hepatic metabolic regulation and mitochondrial stress responses through endocrine and transcriptional mechanisms that modulate lipid handling and energy homeostasis (49), fibronectin type III domain-containing protein 5 (FNDC5) that contributes to systemic energy balance and metabolic adaptation (51), and MER proto-oncogene tyrosine kinase (MERTK) influences MAFLD progression via macrophage-mediated efferocytosis and immune regulation, and transforming growth factor beta (TGF-β) signalling modulation, with dysregulated signalling promoting persistent inflammation and fibrogenesis (52).

In addition to SNPs, other types of variants were also identified, such as copy number variation (CNV) in the exportin-4 (XPO4), which has been associated with MAFLD severity, with reduced hepatic XPO4 expression linked to hepatic stellate cell activation and fibrosis through dysregulation of SMAD3/4 signalling (49)

Advancing our understanding of the genetic basis of MAFLD may help in future risk stratification and the development of personalized management plans (49).

2.5 Diagnosis and risk stratification

Ultrasound is the first-line imaging modality for steatosis evaluation due to its accessibility and low cost. However, its sensitivity can be limited, particularly in cases of mild steatosis or among individuals with a high BMI (53). Advanced imaging modalities, such as magnetic resonance imaging-proton density fat fraction (MRI-PDFF) and the controlled attenuation parameter (CAP) via transient elastography, provide more accurate quantification of hepatic fat, although their availability may be restricted in some healthcare settings (54).

Detecting liver injury through routine liver enzyme tests can be challenging, as alanine aminotransferase (ALT) and aspartate aminotransferase (AST) levels often remain normal in the early stages of MAFLD (55).

Risk stratification for fibrosis can be performed through multiple non-invasive scoring systems which could also predict liver-related outcomes (56). Some commonly employed scoring systems include the NAFLD Fibrosis Score (NFS), the Fibrosis-4 (FIB-4) index, and the AST to platelet ratio index (APRI) (57). The scores evaluate the likelihood of advanced fibrosis through a combination of age, BMI, AST, ALT, platelet count and albumin levels. The FIB-4 is often preferred in both primary and specialty care because of its simplicity and reliable performance. Patients with indeterminate or elevated scores may require further evaluation with elastography or liver biopsy to determine fibrosis severity (58, 59). Despite several limitations, these tools remain valuable (60). For instance, age can significantly influence the interpretation of FIB-4 scores, with older adults more likely to have scores that overestimate fibrosis risk (61). Conversely, the accuracy of fibrosis scores may be lower in younger individuals or those with fewer comorbidities (62).

Transient elastography (FibroScan) is widely used as a second-step test to quantify liver stiffness, providing a non-invasive assessment of fibrosis severity and helping refine risk stratification after FIB-4 (63).

Liver biopsy remains the gold standard for confirming steatohepatitis and assessing the stage of fibrosis (64). Histological evaluation enables the direct identification of key features such as hepatocyte ballooning, lobular inflammation, and fibrosis, which collectively indicate the severity of disease progression (65). However, the biopsy is invasive procedure that is costly and carries risks, including bleeding and sampling variability (66). For these reasons, it is typically reserved for patients with inconclusive or conflicting non-invasive test results, or

when histological confirmation is necessary before initiating therapies that involve significant risks (67).

3 Lean MAFLD

Increasing evidence indicates substantial heterogeneity in MAFLD presentation. Although MAFLD is commonly associated with overweight and obesity, a proportion of individuals with normal BMI develops MAFLD, a subset commonly referred to as lean MAFLD. This subgroup represents a distinct clinical entity with important diagnostic, metabolic, and prognostic considerations.

3.1 Definition and diagnostic criteria of lean MAFLD

Lean MAFLD refers to the presence of hepatic steatosis accompanied by metabolic dysfunction in individuals with a normal BMI (68). According to the international consensus criteria (69) and the Asian pacific association for the study of the liver (APASL) guidelines (70), diagnosis of lean MAFLD requires evidence of hepatic steatosis along with the presence of metabolic dysfunction defined by at least two metabolic risk abnormalities out of seven predefined criteria (increased waist circumference based on ethnicity-specific cut-offs, blood pressure ≥130/85 mmHg or use of antihypertensive medication, plasma triglycerides ≥1.70 mmol/L or use of lipid-lowering therapy, plasma high-density lipoprotein (HDL) cholesterol <1.0 mmol/L in men or <1.3 mmol/L in women, prediabetes, defined as fasting plasma glucose 5.6–6.9 mmol/L, 2-h post-load glucose 7.8–11.0 mmol/L, or HbA1c 5.7–6.4%, insulin resistance, defined by a homeostasis model assessment of insulin resistance (HOMA-IR) score ≥2.5, and plasma high-sensitivity C-reactive protein >2 mg/L). A healthy weight is determined based on ethnicity-specific BMI thresholds, which are defined as a BMI of less than 25 kg/m² for

Western/Caucasian populations and less than 23 kg/m² for Asian populations (Fig 1 .4) (71). Lean patients with MAFLD are often under-recognised in routine clinical practice, which might be partly due to the common practice of using BMI as an initial indicator of metabolic risk. When BMI falls within the normal range, clinical suspicion for fatty liver disease decreases, even if metabolic dysfunction is present. Consequently, hepatic steatosis in lean individuals is frequently identified incidentally rather than through targeted evaluation, leading to delays or a lack of further metabolic or hepatic investigations (24, 72, 73).

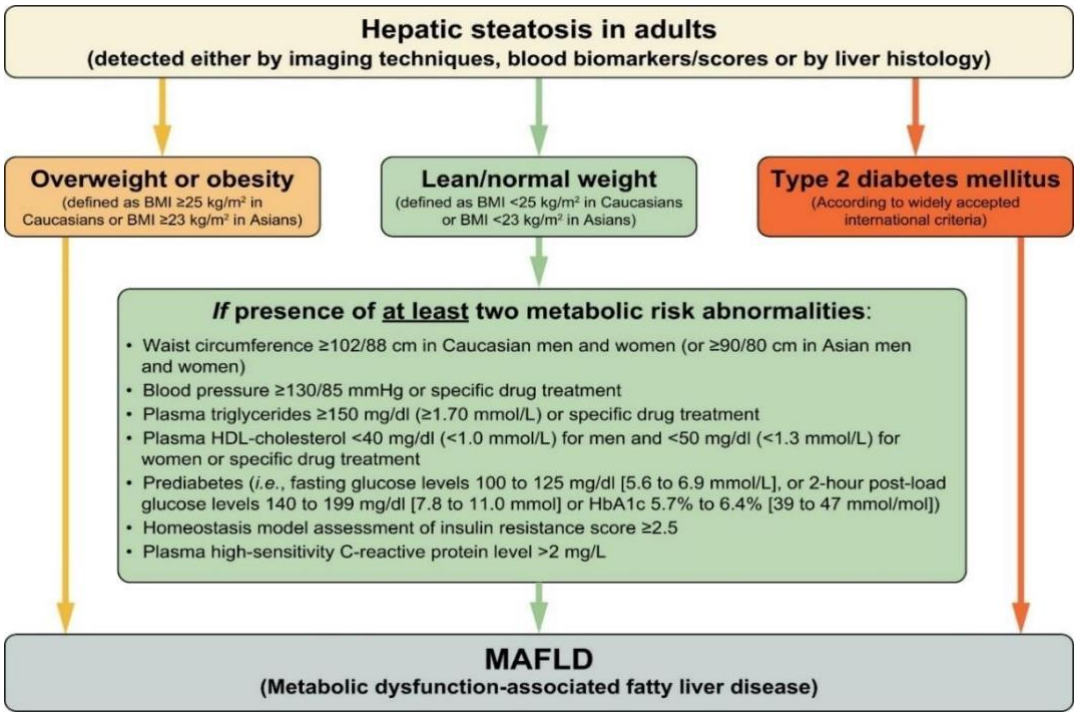

Figure 1.4 Flowchart for the diagnostic criteria for MAFLD (13).

3.2 Epidemiology and risk factors of lean MAFLD

Lean MAFLD accounts for approximately 10–20% of MAFLD cases globally, with even higher rates observed in East and South Asian populations, where it can reach up to 40% (74-78). This variability persists after adjustment for lifestyle factors, and this could be at least partly attributed to differences in body composition specific to these populations, as well as the

fact that metabolic dysfunction and visceral fat accumulation can occur at lower BMI levels in South Asian individuals, along with underlying genetic susceptibility (Fig. 1.5).

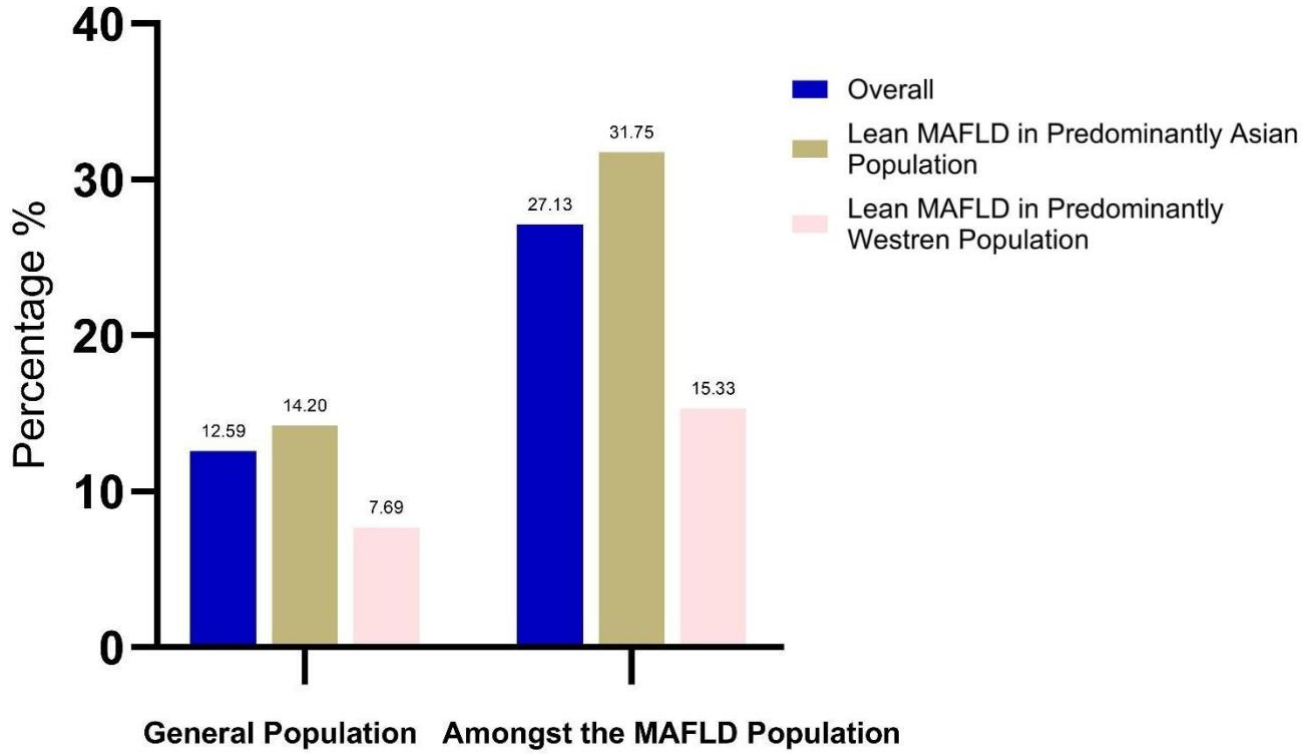

Figure 1.5 Prevalence of lean MAFLD among general population and MAFLD (79).

3.3 Clinical outcomes of lean MAFLD

Lean MAFLD patients present with a relatively favourable metabolic and histological profile, including hepatic inflammation and fibrosis at baseline compared to their obese counterparts. However, longitudinal cohort studies demonstrate that lean MAFLD is not a benign phenotype and is associated with clinically significant long-term hepatic and extrahepatic outcomes despite a normal BMI (80).

With respect to liver-related outcomes, observational studies and meta-analyses indicate that rates of cirrhosis and HCC in lean MAFLD are comparable to those observed in obesity-

associated MAFLD. Several cohorts report increased liver-related and all-cause mortality in lean MAFLD after adjustment for metabolic and fibrosis-related confounders, despite a favourable baseline metabolic and histological profile (81, 82).

Cardiovascular disease represents the leading cause of death across MAFLD phenotypes, including lean individuals (83). Compared with metabolically healthy lean populations, lean MAFLD is associated with increased risks of cardiovascular disease, T2DM, and all-cause mortality (81, 82).

Collectively, these observations highlight a clinical paradox in lean MAFLD, whereby individuals with a relatively favourable metabolic and histological profile at baseline experience adverse long-term outcomes that are comparable to or exceed those observed in obesity-associated MAFLD. The biological mechanisms underlying this discordance remain incompletely understood and form the basis for the mechanistic investigations undertaken in this thesis.

3.4 Pathophysiology of lean MAFLD

While the key biological pathways underpinning the disease development and progression, including those mediating hepatic lipid accumulation, insulin resistance, oxidative stress, inflammation, and fibrogenesis, seem to be shared between MAFLD among lean and non-lean individuals, a fundamental difference lies in the fact that these pathways are activated at lower total adiposity among lean subjects.

One explanation for this observation is that the body’s peripheral buffering capacity is limited. When the expandability of subcutaneous adipose tissue is restricted, the body's ability to store excess energy safely in peripheral depots is compromised. Additionally, low muscle mass and visceral adiposity can contribute to a high-risk lean phenotype characterized by metabolic

inflexibility and increased hepatic stress (Fig. 1.6) (84, 85).

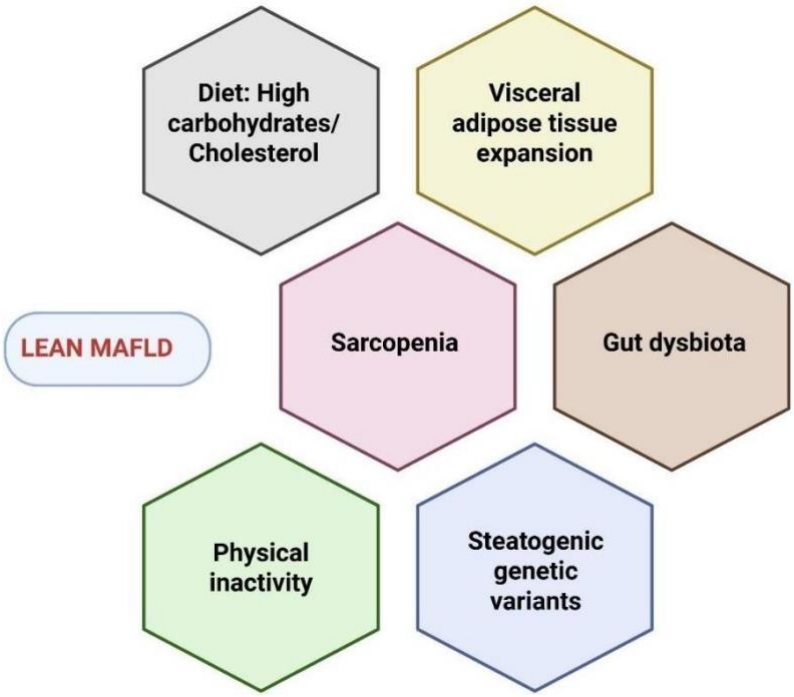

Figure 1.6 Lean MAFLD pathogenesis (86).

Even though individuals with lean MAFLD may have a body weight within the normal range according to BMI, they often experience higher levels of visceral adiposity. This increased amount of visceral fat, along with a higher ratio of visceral to subcutaneous fat, is considered a key risk factor for the disease. Visceral adipose tissue is more lipolytically active and contributes to the production of inflammatory cytokines such as tumor necrosis factor-alpha (TNF-α) and interleukin-6 (IL-6). These cytokines play a propagating role in inflammatory and fibrogenic signaling in the liver (87, 88). Additionally, visceral fat facilitates the delivery of FFAs via the portal vein to liver cells, increasing the liver's lipid load, even in individuals with relatively low overall body fat (89).

Insulin resistance in lean MAFLD results in impaired suppression of adipose lipolysis mediated by insulin, leading to inappropriate hepatic glucose production and an increased hepatic

substrate delivery, upregulating transcriptional regulators such as sterol regulatory element-binding protein-1c (SREBP-1c) and carbohydrate-responsive element-binding protein (ChREBP), augmenting lipogenesis and ultimately, enhancing the synthesis of intrahepatic triglycerides, even if elevated BMI is absent (85).

Moreover, high-energy diets rich in refined carbohydrates, sugar-sweetened soft drinks, and saturated fats can stimulate hepatic de novo lipogenesis and oxidative stress without leading to apparent obesity. Physical inactivity further exacerbates insulin sensitivity and mitochondrial oxidative capacity (90, 91).

At elevated lipid loads, more toxic lipid species accumulate in hepatocytes, triggering inflammatory responses and cell death pathways, which can progress to steatohepatitis, and fibrosis (37, 92, 93). Whether individuals with lean MAFLD may be particularly vulnerable when mitochondrial reserve capacity is compromised or when the degree of anti-oxidant capacity does not adequately match the level of oxidative stress is yet to be clarified.

Another pathway that activates the hepatic immune system involves disruptions in the gut-liver axis. Increased intestinal permeability and dysbiosis can enhance the portal translocation of bacterial products, such as LPS, which activates Kupffer cells via TLRs signalling, leading to chronic inflammation and fibrogenesis (94, 95). Additionally, studies have shown that the microbiome profiles in individuals with lean MAFLD are distinct from those in individuals with obese MAFLD (95).

Sarcopenia, defined as reduced skeletal muscle mass and/or low muscle quality, is more prevalent in lean MAFLD compared to metabolically healthy lean counterparts and is linked to impaired glucose metabolism and poor metabolic health phenotypes (96, 97). As muscle is a primary site for glucose uptake during insulin action, having low muscle mass or strength can increase the availability of substrates in the circulation, which in turn, may contribute to

heightened hepatic lipogenesis and insulin resistance in the liver (97).

Genetic factors are also implicated in the pathogenesis of lean MAFLD, with the identified genetic variants that impact hepatic lipid metabolism and response to liver injury, such as PNPLA3, TM6SF2, and MBOAT7 variants, have also been demonstrated to be linked with greater hepatic fat levels and the risk of more severe fibrosis among subjects with lean MAFLD (77, 98).

Collectively, existing data suggest considering lean MAFLD as a phenotype shaped by the outcome of dynamic interaction of genetic susceptibility and various environmental factors, including adverse body composition, metabolic dysregulation, inherited vulnerability, and lifestyle exposures- and not by BMI alone (68, 71).

3.5 Metabolic adaptation in lean MAFLD

Metabolic adaptation refers to the coordinated capacity of metabolically active tissues, particularly the liver, adipose tissue, and skeletal muscle, to adjust substrate utilisation, energy storage, and fuel selection in response to changes in nutrient availability and physiological demand (99, 100). In metabolically healthy states, this adaptive flexibility limits ectopic lipid deposition, preserves mitochondrial function, and maintains metabolic homeostasis during periods of nutrient excess (101).

Clinical and mechanistic studies from our team indicate that lean MAFLD represents a distinct entity characterized by a dynamic and transient metabolic adaptation. This adaptation is mediated by bile acid and Farnesoid X Receptor (FXR) activation, which aims to maintain metabolic homeostasis. Bile acids and FXR are critical regulators of hepatic metabolic adaptation and metabolic homeostasis. The intricate interplay between bile acids, FXR, and gut microbiota forms a key axis in suppressing hepatic lipogenesis, promoting β-oxidation,

enhancing insulin sensitivity, and limiting inflammatory signalling (102).

Early in the disease course, these compensatory hepatic mechanisms can partially offset limited peripheral lipid buffering capacity, allowing for near-normal metabolic function and contributing to an obesity-resistant phenotype. This occurs before the adaptive reserves are exhausted (80, 86, 103, 104). As repeated exposure to increased lipid and glucose flux in the context of constrained adipose storage progressively challenges these adaptive responses, which tend to weaken as the disease advances.

Endotoxemia results in widespread epigenetic reprogramming that blocks bile acid signaling, identified as a key mechanism mediating the loss of metabolic adaptation (104). Over time, this may lead to metabolic inflexibility, characterized by an impaired ability to switch between lipid and glucose oxidation, increased mitochondrial stress, and a heightened susceptibility to lipotoxic injury (80, 86). These features suggest that the outcomes of lean MAFLD are influenced by variations in the integrity of metabolic adaptation, which determines vulnerability as metabolic stress persists.

In the following sections, I will turn the focus to discuss some of the key pathways in MAFLD pathogenesis that are relevant to my thesis.

4 Telomere

Chronic liver diseases, including MAFLD, are characterised by sustained cellular stress, repeated cycles of hepatocellular injury and repair, and progressive limitations in regenerative capacity (105). At the cellular level, these processes place cumulative demands on mechanisms that preserve genomic stability during cell division (106). Telomeres play a central role in this context by maintaining chromosomal integrity and determining the replicative capacity (107). An understanding of telomere structure and biological function is therefore essential for

interpreting how chronic metabolic stress may influence cellular resilience, tissue repair, and long-term disease progression.

4.1 Structure and biological function of telomeres

Telomeres are specialised nucleoprotein structures located at the termini of linear chromosomes and are composed of tandem TTAGGG DNA repeat sequences (Fig. 1.7) (108). In humans, telomeres span several kilobases and serve a fundamental protective function by preventing chromosome ends from being recognised as DNA double-strand breaks, thereby preserving chromosomal stability during cell division (109).

This protective function is mediated by the shelterin complex, which consists of six core proteins: telomeric repeat-binding factor 1 (TRF1), telomeric repeat-binding factor 2 (TRF2), protection of telomeres 1 (POT1), TRF1-interacting nuclear protein 2 (TIN2), TIN2-interacting protein 1 (TPP1), and repressor/activator protein 1 (RAP1). Together, these proteins stabilise telomeric DNA and regulate the interaction between chromosome ends and DNA damage response pathways (110, 111).

Telomere length decreases progressively with successive cell divisions as a consequence of the end-replication problem, whereby conventional DNA polymerases are unable to fully replicate the 3′ termini of linear DNA molecules (112). In most somatic tissues, telomerase activity is either low or absent, which limits telomere maintenance and leads to gradual telomere attrition over time (113, 114).

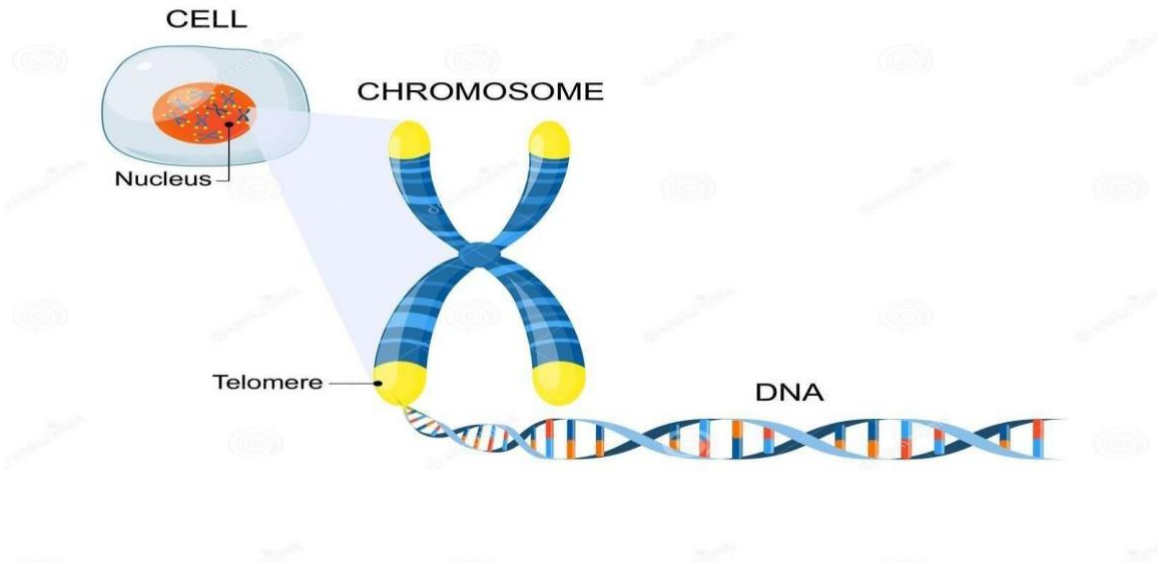

Figure 1.7 Schematic representation of telomeres at the ends of linear chromosomes (115).

4.2 Telomere attrition in lean MAFLD

Telomere integrity is crucial for sustaining hepatocyte proliferative capacity and supporting tissue regeneration following injury (116). While hepatic tissue exhibits substantial regenerative potential, this capacity is finite and depends on the replicative reserve of hepatocytes and hepatic progenitor cells (117).

Experimental models and clinical studies consistently demonstrate that reduced telomere length is associated with more advanced stages of liver fibrosis, cirrhosis, and HCC (118-120). Thus, telomere length has emerged as a biomarker of cumulative cellular stress burden and mortality risk, with particular relevance to chronic metabolic liver diseases such as MAFLD (121).

Telomere attrition has emerged as an important biological process linking sustained metabolic stress to progressive liver injury in MAFLD (122, 123). Persistent exposure to lipotoxicity, inflammatory signalling, and oxidative stress increases hepatocyte turnover and places sustained demand on regenerative pathways, thereby accelerating telomere shortening via stress-dependent, cell division–independent mechanisms (124, 125). Telomere shortening

constrains hepatocyte replicative reserve, limiting effective tissue repair and increasing vulnerability to chronic injury, fibrosis, and functional decline (117). Oxidative stress can induce telomere shortening independently of cell division, indicating that telomere erosion in MAFLD reflects cumulative cellular stress exposure rather than replicative processes (126). In advanced MAFLD and MASH, telomere damage is particularly pronounced (122). However, if there is a differential telomere attrition rate between lean and obese MAFLD, and if it represents a plausible biological contributor linking metabolic stress to disease progression, explaining the paradoxical adverse long-term outcomes of lean MAFLD is unknown.

Critically shortened telomeres in HSCs induce a senescent but metabolically active phenotype characterised by a senescence-associated secretory profile enriched in pro-inflammatory cytokines, growth factors, and extracellular matrix components (122, 127). This senescence-associated secretory activity sustains inflammatory signalling and extracellular matrix deposition, thereby actively promoting fibrotic remodelling rather than representing a passive consequence of cellular senescence (128-130).

Telomere instability has been associated with chromosomal abnormalities and increased susceptibility to HCC (131). Telomere dysfunction also contributes to genomic instability and malignant transformation. Critically shortened telomeres promote chromosomal rearrangements, impair cell-cycle regulation, and increase susceptibility to oncogenic transformation (132, 133). In chronically inflamed and fibrotic livers, where hepatocyte turnover is increased and DNA repair capacity is compromised, telomere dysfunction may contribute to telomere crisis and promote the development of HCC (134, 135).

5. GDF-15 and DNAm-GDF15 in lean MAFLD

Given the central role of chronic oxidative and mitochondrial stress in MAFLD and their contribution to telomere attrition, signalling pathways that integrate cellular stress responses

are highly relevant to disease pathophysiology. Growth differentiation factor-15 (GDF-15) represents one such pathway, functioning as a systemic indicator of cellular and mitochondrial stress in lean MAFLD.

5.1 Biological roles of GDF-15

Growth differentiation factor-15 (GDF-15) is a stress-responsive cytokine belonging to the transforming growth factor-β (TGF-β) superfamily and is increasingly recognised as an integrative marker of cellular stress and tissue injury (136). GDF-15 is expressed at low levels in most tissues but is robustly induced in response to various forms of stress, including inflammatory, metabolic, oxidative, and mitochondrial stress. The stress-inducible expression profile positions GDF-15 as a downstream readout of integrated stress signalling rather than a constitutively active signalling molecule (137).

Circulating GDF-15 concentrations are consistently elevated in individuals with insulin resistance, T2DM, dyslipidaemia, and visceral adiposity, and correlate with markers of oxidative stress and low-grade inflammation (138). GDF-15 levels rise in proportion to disease severity across multiple cardiometabolic conditions, including atherosclerosis, chronic kidney disease, and heart failure, supporting its role as a biomarker of cumulative metabolic burden (138, 139).

Similarly, in MAFLD, numerous population-based studies demonstrated that circulating GDF-15 levels are significantly elevated and correlate with indices of hepatic steatosis and fibrosis independent of adiposity measures (140). These associations indicate that GDF-15 reflects metabolic and hepatic stress rather than excess body weight alone.

In hepatocytes, GDF-15 expression is strongly upregulated in response to metabolic overload. Experimental models demonstrate that early steatosis, lipotoxicity, and exposure to saturated

FFA stimulate GDF-15 transcription, establishing a direct link between its induction and hepatic metabolic stress.(141, 142). Multiple stress-response pathways converge on the GDF-15 promoter, including oxidative and ER stress signalling through transcription factors such as tumour protein p53 (p53), activating transcription factor-4 (ATF4), and C/EBP homologous protein (CHOP), which identifies GDF-15 as an essential component of the integrated stress response (ISR) (143).

Furthermore, mitochondrial dysfunction is a major driver of GDF-15 induction. Factors such as impaired oxidative phosphorylation, activation of the mitochondrial unfolded protein response (UPR), defective β-oxidation, and electron transport chain dysfunction have all been shown to stimulate GDF-15 expression in both hepatic and extrahepatic tissues (144). Collectively, these mitochondrial stress-induced changes position GDF-15 at the critical interface between mitochondrial stress sensing and systemic stress signalling, enabling it to indicate metabolic imbalance before overt tissue injury becomes clinically apparent (142).

GDF-15 plays a significant role in the inflammatory pathways of the liver. It modulates nuclear factor-κB (NF-κB) signalling and influences the production of cytokines by hepatic macrophages and Kupffer cells. Proinflammatory mediators such as tumour necrosis factor-α (TNF-α), interleukin-1, and interferon-related pathways further enhance GDF-15 expression. This creates a feedback loop between inflammatory activation and cellular stress signaling. (141). During fibrogenesis, activated macrophages and HSCs contribute to increased hepatic GDF-15 expression, which complements signals derived from hepatocytes and strengthens its association with chronic liver injury and tissue remodeling (142, 145).

5.2 Epigenetic control and DNAm-GDF15

Epigenetic mechanisms play a central role in regulating hepatocellular responses to metabolic

stress, and DNA methylation has emerged as a key regulator of GDF15 transcription (146). DNA methylation at cytosine–phosphate–guanine (CpG) dinucleotides modulates gene expression by altering chromatin accessibility and transcription factor binding, thereby shaping stress-responsive signalling pathways relevant to metabolic liver disease (147). The GDF15 locus contains multiple regulatory CpG sites within promoter and enhancer regions that are sensitive to inflammatory, oxidative, and mitochondrial stress signals (148, 149).

Variation in DNA methylation at these CpG sites, commonly referred to as DNA methylation–derived GDF-15 (DNAm-GDF15), shows a strong correlation with circulating GDF-15 concentrations and reflects long-term regulation of GDF15 expression (150, 151). The transcriptional control of GDF15 is closely linked to CpG methylation at regulatory regions located near binding motifs for stress-activated transcription factors such as, p53, ATF4, and CHOP, which are central components of the integrated stress response and UPR pathways (152).

Hypomethylation at these regulatory CpG sites increases chromatin accessibility and facilitates transcription factor binding, thereby enhancing GDF15 transcription during metabolic and oxidative stress. In contrast, hypermethylation suppresses promoter activity and reduces transcriptional inducibility. Epigenome-wide association studies consistently demonstrate that systemic oxidative stress, mitochondrial dysfunction, and chronic low-grade inflammation are associated with differential methylation at the GDF15 locus (150, 153, 154).

DNAm-GDF15 has emerged as a widely validated epigenetic marker of long-term metabolic and inflammatory stress exposure. Cohort studies demonstrate strong associations between DNAm-GDF15 and major cardiometabolic outcomes, including T2DM, cardiovascular disease, MAFLD, and other chronic inflammatory conditions (51, 150). DNAm-GDF15 predicts long-term cardiometabolic disease risk and mortality independently of adiposity, BMI,

and conventional metabolic risk factors (150). These associations mirror those observed for circulating GDF-15 across cardiometabolic outcomes, and DNAm-GDF15 exhibits low short-term variability, supporting the notion that DNAm-GDF15 reflects long-term biological stress exposure rather than transient physiological fluctuations or acute stress responses (150). Recent multi-omic integration studies demonstrate that DNAm-GDF15 correlates with systemic markers of lipid peroxidation, cumulative inflammatory load, and impaired metabolic flexibility across diverse demographic groups (151, 155).

6 Mitochondria

Mitochondrial function represents a central determinant of hepatic metabolic health and a convergent pathway through which many of the stressors described in earlier sections exert their effects.

6.1 Mitochondrial physiology and morphology

Mitochondria are double-membraned organelles that function as highly dynamic structures responsible for essential metabolic and signalling processes in eukaryotic cells (156). Structurally, mitochondria consist of an outer membrane, an intermembrane space, an inner membrane folded into cristae, and the matrix compartment (157). The outer membrane contains porins that permit diffusion of small molecules, whereas the inner membrane houses the electron transport chain (ETC) and ATP synthase, enabling oxidative phosphorylation (158). The matrix contains enzymes of the tricarboxylic acid (TCA) cycle, mitochondrial DNA (mtDNA), and the molecular machinery required for mtDNA transcription and replication (159). This compartmentalised architecture enables tight coordination between structure and function, allowing mitochondria to efficiently meet hepatocellular metabolic demands (Fig.

1.8) (160).

Maintenance of a healthy mitochondrial population depends on coordinated regulation of mitochondrial fusion, fission, and mitophagy (161). Fusion facilitates the exchange of mitochondrial contents and supports metabolic adaptability, whereas fission segregates damaged mitochondrial components for removal (161, 162). Mitophagy selectively eliminates dysfunctional mitochondria, thereby limiting ROS accumulation and preserving cellular homeostasis (163). Dysregulation of these quality-control mechanisms results in mitochondrial dysfunction and has been increasingly implicated in the pathogenesis of various metabolic diseases, including MAFLD (37).

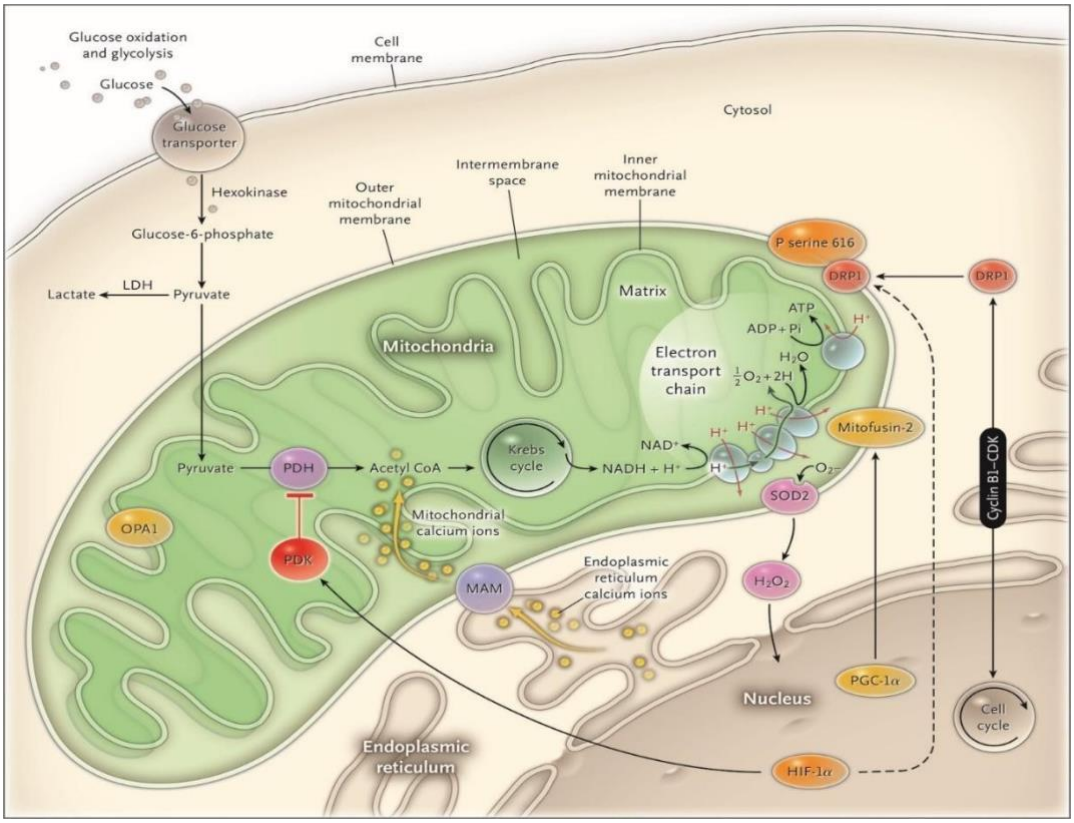

Figure 1.8 Metabolism and dynamics in mitochondria (164).

Maintenance of both mitochondrial structural integrity and functional competence is therefore essential for maintaining hepatic metabolic homeostasis, and mitochondrial dysfunction is increasingly recognised as a key driver of metabolic liver diseases, including MAFLD (37, 92). Hepatic energy metabolism relies heavily on mitochondrial ATP production through oxidative phosphorylation (165). Substrates derived from carbohydrates, lipids, and amino acids are oxidised via the TCA cycle to generate the electron carriers nicotinamide adenine dinucleotide (NADH) and flavin adenine dinucleotide ($FADH_2$) (166). These reducing equivalents donate electrons to the ETC, generating a proton gradient across the inner mitochondrial membrane that drives ATP synthesis via ATP synthase (167, 168). Because the liver must continuously adapt to fed and fasted states, sustained mitochondrial ATP production is essential for maintaining metabolic homeostasis (169).

Mitochondria also play a central role in hepatic lipid metabolism through β-oxidation of long-chain fatty acids (170). FFAs are transported into the mitochondrial matrix via the carnitine shuttle system, where they are converted to acyl-CoA and sequentially oxidised to generate acetyl-CoA (171-173). This process supplies substrates for the TCA cycle and ATP generation while preventing lipid accumulation. Tight regulation of β-oxidation is therefore critical, as impairment of this pathway promotes hepatic steatosis and represents a key pathogenic mechanism in MAFLD development (37, 174).

In addition to energy and lipid metabolism, mitochondria are major regulators of cellular redox balance. During normal ETC activity, small amounts of electrons leak from complexes I and III, generating ROS as by-products (175, 176). Under physiological conditions, antioxidant systems including superoxide dismutase, glutathione peroxidase, and catalase neutralise ROS and preserve redox homeostasis (177). However, impaired mitochondrial respiration and substrate overload increase ROS production, leading to oxidative damage to proteins, lipids,

and DNA (178). In hepatocytes, excessive ROS accumulation contributes to inflammation, activation of fibrogenic pathways, and progressive liver injury (179).

Mitochondria further contribute to hepatic detoxification through participation in the urea cycle, which occurs partially within the mitochondrial matrix. This pathway converts toxic ammonia into urea for renal excretion, and disruption of mitochondrial urea cycle function can result in hyperammonaemia and hepatic encephalopathy in advanced liver disease (180, 181). Mitochondria also regulate programmed cell death through release of cytochrome c and other pro-apoptotic factors during mitochondrial outer membrane permeabilisation, initiating caspase-dependent apoptosis (182, 183). Dysregulated mitochondrial apoptosis contributes to hepatocyte loss and disease progression from steatosis to steatohepatitis and fibrosis (184, 185). Finally, mtDNA integrity is increasingly recognised as critical for hepatic mitochondrial function. The proximity of mtDNA to the ETC and the absence of protective histones render it particularly susceptible to oxidative damage (186). Impaired mtDNA transcription and replication reduce ETC component availability, further diminishing respiratory efficiency and amplifying ROS production in a self-perpetuating cycle (187). Studies in MAFLD demonstrate reduced mtDNA copy number, increased mtDNA mutations, and impaired respiratory chain function, particularly with advancing disease severity (188).

6.2 Mitochondrial implications in the hepatic metabolism

Hepatocytes have particularly high metabolic demands, requiring substantial mitochondrial capacity to support energy production, redox balance, lipid metabolism, and detoxification pathways (189). Accordingly, the liver contains a dense mitochondrial population, reflecting its central role in nutrient processing, intermediary metabolism, and xenobiotic detoxification (169, 190). Maintaining both the structural integrity and functional competence of mitochondria is essential for preserving hepatic metabolic homeostasis. Mitochondrial

dysfunction is increasingly recognised as a key driver of metabolic liver diseases, including MAFLD (37, 92).

Hepatic energy metabolism heavily relies on mitochondrial ATP production through oxidative phosphorylation (165). Substrates derived from carbohydrates, lipids, and amino acids are oxidised via the TCA cycle to generate the electron carriers nicotinamide adenine dinucleotide (NADH) and flavin adenine dinucleotide ($FADH_2$) (166). These reducing equivalents donate electrons to the ETC, generating a proton gradient across the inner mitochondrial membrane that drives ATP synthesis via ATP synthase (167, 168). Because the liver must continuously adapt to fed and fasted states, sustained mitochondrial ATP production is essential for maintaining metabolic homeostasis (169).

Mitochondria also play a central role in hepatic lipid metabolism through β-oxidation of long-chain fatty acids (170). FFAs are transported into the mitochondrial matrix via the carnitine shuttle system, where they are converted to acyl-CoA and sequentially oxidised to generate acetyl-CoA (171-173). This process not only supplies substrates for the TCA cycle and ATP generation but also prevents lipid accumulation. Therefore, tight regulation of β-oxidation is critical, as impairment of this pathway can lead to hepatic steatosis and is a key pathogenic mechanism in the development of MAFLD (37, 174).

In addition to energy and lipid metabolism, mitochondria are major regulators of cellular redox balance. During normal ETC activity, small amounts of electrons leak from complexes I and III, generating ROS as by-products (175, 176). Under physiological conditions, antioxidant systems, including superoxide dismutase, glutathione peroxidase, and catalase, neutralise ROS and preserve redox homeostasis (177). However, impaired mitochondrial respiration and substrate overload increase ROS production, leading to oxidative damage to proteins, lipids, and DNA (178). In hepatocytes, excessive ROS accumulation contributes to inflammation,

activation of fibrogenic pathways, and progressive liver injury (179).

Mitochondria also regulate programmed cell death by releasing cytochrome c and other pro-apoptotic factors during mitochondrial outer membrane permeabilisation, thereby initiating caspase-dependent apoptosis (182, 183). Dysregulated mitochondrial apoptosis contributes to hepatocyte loss and disease progression from steatosis to steatohepatitis and fibrosis (184, 185). mtDNA integrity is increasingly recognised as critical for hepatic mitochondrial function. The proximity of mtDNA to the ETC and the absence of protective histones render it particularly susceptible to oxidative damage (186). Impaired mtDNA transcription and replication reduce ETC component availability, further diminishing respiratory efficiency and amplifying ROS production in a self-perpetuating cycle (187). Studies in MAFLD demonstrate reduced mtDNA copy number, increased mtDNA mutations, and impaired respiratory chain function, particularly with advancing disease severity (188).

Finally, mitochondria contribute to hepatic detoxification through their involvement in the urea cycle, which partially occurs within the mitochondrial matrix. This pathway converts toxic ammonia into urea for renal excretion. Disruption of mitochondrial urea cycle function can result in hyperammonaemia and hepatic encephalopathy, particularly in advanced liver disease (180, 181).

6.3 Core mitochondrial abnormalities in MAFLD

Mitochondrial dysfunction represents a cardinal feature underlying MAFLD progression across the disease spectrum and is observed irrespective of overall adiposity (103). Histological, biochemical, and molecular analyses of liver tissue from patients with MAFLD consistently demonstrate structural and functional mitochondrial alterations (191). While mitochondrial dysfunction is detectable at early stages of steatosis, its severity increases in

parallel with hepatic inflammation and fibrosis, indicating progressive deterioration of mitochondrial homeostasis with advancing disease (191).

In healthy hepatocytes, mitochondria maintain energy homeostasis, coordinate lipid metabolism, and regulate cellular stress responses. Disruption of these functions destabilises hepatic metabolic balance and contributes to disease progression (192, 193). These include impaired oxidative phosphorylation, excessive generation of ROS, disruption of mitochondrial quality-control pathways, and abnormalities affecting mtDNA integrity (Fig. 1.9) (194).

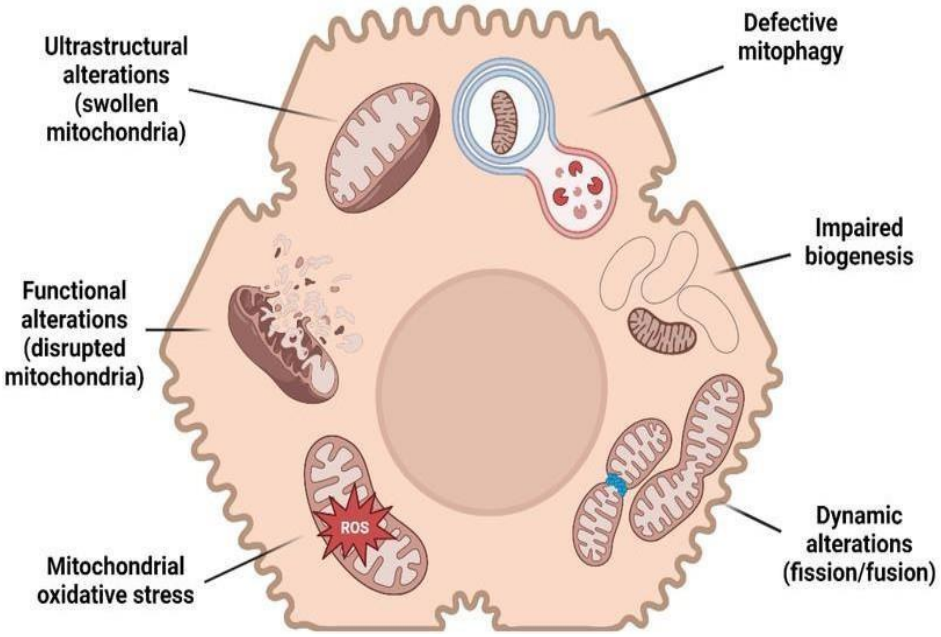

Figure 1.9 Changes in mitochondria and MAFLD. A schematic representation of the key mitochondrial alterations in hepatocytes that contribute to MAFLD (42).

Defects within the ETC are a prominent feature of mitochondrial dysfunction in MAFLD. Studies of liver biopsy specimens demonstrate reduced enzymatic activity of respiratory chain complexes, particularly complexes I and IV, resulting in diminished ATP synthesis and increased electron leakage (191, 195). Experimental models of MAFLD, including high-fat

diet and methionine–choline-deficient feeding paradigms, recapitulate these mitochondrial abnormalities, demonstrating mitochondrial swelling, reduced ETC activity, increased ROS generation, and enhanced hepatocyte apoptosis (196).

At the cellular level, mitochondrial dysfunction promotes hepatocyte death through activation of intrinsic apoptotic and necroptotic pathways. Liver tissue from patients with steatohepatitis shows increased expression of pro-apoptotic proteins, including Bax, enhanced cytochrome c release, and activation of downstream effector caspases such as cleaved caspase-3 (197). Escaping electrons react with molecular oxygen to generate superoxide and other ROS, overwhelming endogenous antioxidant defences and promoting oxidative damage to lipids, proteins, and nucleic acids (198-200). This oxidative stress directly contributes to hepatocellular injury and amplifies inflammatory and fibrogenic signalling pathways (201).

Metabolomic and lipidomic profiling further reveal accumulation of incomplete β-oxidation products, including acylcarnitines and ceramides, within MAFLD livers (202). These lipotoxic intermediates impair mitochondrial membrane integrity, disrupt enzymatic activity, and exacerbate oxidative stress (203). Their accumulation correlates with histological features of hepatocyte ballooning, inflammation, and disease severity, supporting a direct link between mitochondrial lipid overload and liver injury (204, 205).

Mitochondrial quality-control mechanisms are also consistently impaired in MAFLD, with defective mitophagy resulting in the accumulation of damaged mitochondria within hepatocytes. Reduced expression of key mitophagy regulators, including PTEN-induced kinase 1 (PINK1) and Parkin, has been observed in human steatohepatitis and experimental models, leading to inefficient clearance of dysfunctional organelles (206). Ultrastructural analyses using electron microscopy demonstrate swollen mitochondria with disrupted cristae architecture, consistent with impaired mitochondrial turnover (207).

In parallel, mitochondrial dynamics are altered, with an imbalance favouring excessive fission over fusion. Dysregulated expression of dynamin-related protein 1 (DRP1), mitofusin 2 (MFN2), and optic atrophy 1 (OPA1) has been documented in MAFLD, resulting in mitochondrial fragmentation and loss of structural integrity (196). Fragmented mitochondria exhibit reduced respiratory efficiency and increased susceptibility to oxidative damage, further aggravating hepatocellular stress (201).

Genetic disruption of key mitochondrial maintenance genes, such as mitochondrial transcription factor A (TFAM) or DNA polymerase gamma (POLG), accelerates hepatic steatosis and fibrosis under metabolic stress, underscoring the causal role of mitochondrial dysfunction in disease progression (208).

Together, these findings identify mitochondria as central executioners linking metabolic stress to hepatocellular injury, inflammation, fibrosis, and disease progression in MAFLD.

7 Summary of the literature review

There is growing evidence that lean MAFLD is a clinically significant condition, although its underlying mechanisms are not as well understood. Individuals with lean MAFLD often exhibit a more favorable metabolic and histological profile. However, paradoxically, they are associated with worse liver-related outcomes and higher mortality rates compared to their obese counterparts.

Despite the absence of overt obesity, lean individuals with MAFLD frequently exhibit visceral adiposity, limited adipose tissue expandability, impaired metabolic flexibility, and heightened susceptibility to oxidative stress and inflammation. Recent evidence indicates that differential metabolic adaptation mediated by bile acid–FXR signalling and alterations in gut–liver axis function play a crucial role in defining the lean MAFLD phenotype and determining outcomes.

While considerable progress has been made in characterizing the epidemiology and clinical

profile of lean MAFLD, the biological basis for the disproportionately adverse outcomes observed in these patients remains incompletely defined. Factors such as mitochondrial dysfunction, telomere biology, and stress-response pathways have emerged as potential contributors. However, their roles in lean MAFLD and their interactions have not yet been integrated into a comprehensive pathogenic framework.

7.1 Open questions and knowledge gaps

Despite growing recognition of lean MAFLD as a clinically important phenotype, several critical knowledge gaps persist. A major unresolved question is why lean individuals may display relatively modest metabolic or histological abnormalities at presentation yet experience disproportionately poor long-term outcomes. Accelerated telomere attrition driven by heightened oxidative stress has been proposed as a contributing mechanism; however, the extent to which oxidative stress specifically accelerates telomere shortening in lean MAFLD, and how this relates to fibrosis progression and mortality risk, remains poorly understood.

Another important gap concerns epigenetic regulation of stress-response pathways. Lean MAFLD has been reported to exhibit lower circulating GDF-15 despite evidence of increased metabolic stress and markedly elevated DNAm-GDF15. This discordant pattern may impair mitochondrial stress adaptation and has been linked to telomere attrition and mortality risk, yet its mechanistic significance has not been fully elucidated.

In addition, it remains unclear whether lean MAFLD is characterised by a distinct mitochondrial phenotype. Available evidence suggests the presence of enlarged but dysfunctional mitochondria, reduced respiratory efficiency, and lower mtDNA content, consistent with heightened mitochondrial vulnerability. The contribution of impaired mitochondrial biogenesis altered fusion–fission dynamics, defective mitophagy, and increased

ER stress to disease progression in lean MAFLD also remains insufficiently defined. Collectively, these gaps highlight the need for an integrated mechanistic framework capable of explaining the distinct pathogenesis and adverse clinical outcomes characteristic of lean MAFLD.

7.2 Central hypotheses

This thesis addresses the central hypothesis that the paradox of higher mortality in lean MAFLD, despite a favourable histological and metabolic profile, is driven by biological stress pathways linking telomere attrition with impaired mitochondrial stress adaptation. I hypothesize that lean MAFLD is characterized by increased oxidative stress and accelerated telomere shortening, alongside epigenetic dysregulation of GDF-15 that limits appropriate mitochondrial stress responses, which is associated with a distinct mitochondrial profile in lean MAFLD, thereby promoting disease progression and adverse clinical outcomes.

7.4 Aims of the thesis

The aims of this thesis are:

- To determine whether lean MAFLD is associated with accelerated telomere attrition and to clarify the contribution of oxidative stress to this process.
- To determine the relationship between circulating GDF-15, DNAm-GDF15, telomere biology, and oxidative injury, and to assess their relevance to clinical outcomes.
- To determine the mitochondrial structural and functional features of lean MAFLD, including mitochondrial morphology, respiratory efficiency, and mtDNA content.

- To determine mitochondrial quality-control pathways, including biogenesis, fusion and fission dynamics, mitophagy, and ER oxidative stress responses, to identify mechanisms contributing to mitochondrial dysfunction.

Chapter 2: Materials and Methods

2. Materials

The materials used in this study were obtained from the sources listed in Table 2.1.

Table 2.1 Commercial Kits

Name	Company
Human GDF-15 ELISA kit	Thermo scientific (EHGDF15)
Malondialdehyde ELISA kit	Abcam (ab287797)
Absolute Human Telomere Length and Mitochondrial DNA Copy Number Dual Quantification qPCR Assay Kit	Sciencell (8958)
TRAPeze® Telomerase Detection Kit	Merck-Sigma-Aldrich (S7700)
Tissue Total RNA Purification Mini Kit	Favorgen Biotech Corp.
Random Hexamer and dNTP Mix	Meridian Bioscience
Total DNA DNeasy Blood & Tissue Kit (250)	Qiagen, Germany
Absolute Mouse Mitochondrial DNA Copy Number Quantification qPCR Assay Kit	ScinceCell (M8948)

Table 2.2 Reagents

Name	Company
Human GDF-15/MIC-1 Recombinant Protein, PeproTech	Thermo scientific (120-28C-20UG)
SYBR Green PCR Master Mix	Invitrogen
Bovine serum albumin (BSA),	Sigma Aldrich
RIPA buffer	Sigma Aldrich

Trypsin	Sigma Aldrich
Protease inhibitors	Sigma Aldrich
Dimethyl sulfoxide (DMSO),	Sigma Aldrich
β-mercaptoethanol,	Sigma Aldrich
EDTA (Ethylenediaminetetraacetic acid)	Sigma Aldrich
Penicillin	Gibco BRL through Life Technologies
Streptomycin	Gibco BRL through Life Technologies
Dulbecco's Modified Eagle Medium (DMEM)	Lonza
BEBM Bronchial Epithelial Cell Basal Medium	Lonza
Phosphate buffered saline (PBS)	Lonza
Glutamine solution	In Vitro Technologies
Ethanol, absolute	POCD Healthcare
D-Mannitol	Merck-Sigma-Aldrich (M4125)
Sucrose	Merck-Sigma-Aldrich (S0389)
HEPES, free acid	Astral scientific (BIOHB0264)
Magnesium chloride hexahydrate ($MgCl_2 \cdot 6H_2O$)	Avantor (25108.260)
Potassium dihydrogen phosphate (KH2PO4)	Avantor (0781)
(EGTA) Ethylene glycol-bis(2-aminoethylether)-N, N,	Merck-Sigma-Aldrich (E3889)

N′, N′-tetraacetic acid	
Ficoll-Paque PLUS GE Healthcare	GE Healthcare
Mito-TEMPO	Sigma-Aldrich (SML0737)
2,7-Dichlorodihydrofluorescein diacetate	Merck (D6883-50mg)

Table 2.3 Antibodies

Name	Company
GAPDH	Abcam (ab181602)
Vinculin	Abcam(ab129002)
Anti-human 8-Hydroxy-2'-deoxyguanosin (8-OHdG)	NOVUS (NB600-1508)
Mouse monoclonal anti-4 Hydroxynonenal (4-HNE)	Abcam (AB48506)
Total OXPHOS Rodent WB Antibody Cocktail	Abcam (ab110413)
Anti-IRE1 antibody	Abcam (ab37073)
Anti-beta Actin antibody	Abcam (ab8226)

Table 2.4: siRNAs

Name	Company
DHA-L-HUMAN-XX-0005 ON TARGETplus SMARTpool - 5 nmol ON-TARGETplus Human GDF15 (9518) siRNA- SMARTpool	Millennium Science (horizon, L01987500-00055 nmol)

Table 2.5: Software and Algorithms

Name	Company
ImageJ	BD https://imagej.nih.gov/ij/
GraphPad Prism 10	http://www.graphpad.com/scientificsoftware/prism/
StepOne Software v2.3	Applied Biosystems
IBM SPSS statistics	https://www.ibm.com/products/spss-statistics/features
R Studio	Version 4.5.1 (2025-06-13)

Table 2.6: qPCR primer sequences

Name		Sequences
M36b4	For	AAGCGCGTCCTGGCATTGTCT
	Rev	CCGCAGGGGCAGCAGTGGT
Chop	For	CCACCACACCTGAAAGCAGAA
	Rev	AGGTGAAAGGCAGGGACTCA
Xbp1s	For	TTACGGGAGAAAACTCACGGC
	Rev	GGGTCCAACTTGTCCAGAATGC
Ire1 (Ern1)	For	GACCGGCAGTTCCAGTACAT
	Rev	TGGTCTGATGAAGCAAGGTG
Perk	For	ACTCCTGTCTTGGTTGGGTCTGAT

	Rev	CGTGCTCCGCTTATTCCTTTCT
Atf-6	For	TCGCCTTTTAGTCCGGTTCTT
	Rev	GGCTCCATAGGTCTGACTCC
Ndufv1	For	CCAGTTCCTCAGCCTCAGTG
	Rev	ATGGATAGACGCAGGACAGC
Opa1	For	TGGAAAATGGTTCGAGAGTCAG
	Rev	CATTCCGTCTCTAGGTTAAAGCG
Bnip3	For	TCCTGGGTAGAACTGCACTTC
	Rev	CTGTTGGTATCTTGTGGTGTCTG
Optn	For	GGACAGCCCTTGTGAGACCC
	Rev	TCAAATCGCCCTTTCATAGC
Fundc1	For	TGTAATGGGTGGCGTGACTG
	Rev	CCACGAAGCCGCTGGATATC
Pink1	For	TTCTTCCGCCAGTCGGTAG
	Rev	CTGCTTCTCCTCGATCAGCC
Mt-co1	For	TCAACATGAAACCCCCAGCCA
	Rev	GCGGCTAGCACTGGTAGTGA
Tfam	For	GCCCGGCAGAGACGGTTAAA
	Rev	GCCGAATCATCCTTTGCCTCC
Drp1	For	CCTCAGATCGTCGTAGTGGGAAC
	Rev	GAAACGTGGACTAGCTGCAGAA
Mfn2	For	AGCTGCCCGGGTTAGTACAGAA

	Rev	GCTTGTAGCAAGGCAGGGATG
Mfn1	For	AGCGGGATTGGTCACACAAC
	Rev	CCTTCGGTCATAAGGTAGGCTT
Stat2	For	GCATTTGGCTACCTGGATTGA
	Rev	GGCCTTGGCGTCATCACT
Atp5a1	For	AATGTTCAAGCAGAGGAGATGGT
	Rev	TCCATCAATAGCATTACCGAGGG
Uqcrc2	For	TCCCTCAAAGTTGCCCC
	Rev	GCAAGACGTAGTAAATGTGAG
Sdhb	For	CGAAAGCGACATGGCGGTTC
	Rev	GGTCCTGGAGAAATGCTGACAC
Fam73b	For	GGAGGACTGAGGGTATGTCCA
	Rev	CAAGGGCTGTGGCAAAAAGA
Mief1	For	GCTTCGCTACACTGATCGAGACT
	Rev	CTCAAGCTTCTGATTTTTCCTGAAT
Sirt1	For	ACTGCAGAAAC TTTTAGCCTTTCAA
	Rev	GGCAATGTTCC AAAGAAGTCTGT
Nrf1	For	GCACCTTTGGAGAATGTGGT
	Rev	CTGAGCCTGGGTCATTTTGT
GAPDH	For	AAGGTGAAGGTCGGAGTCAAG
	Rev	GGGGTCATTGATGGCAACAATA
TERT	For	CAAGTTCCTGCACTGGCTGATG

	Rev	CAAGTGCTGTCTGATTCCAATGC
TERC	For	TCTAACCCTAACTGAGAAGGGCGTAG
	Rev	GTTTGCTCTAGAATGAACGGTGGAAG
TRF1	For	CGAGTGCCAGGTGCAGGTGG
	Rev	ATAATAGCCTCTGCGCTGTTGCGG
TRF2	For	GGGTAGCCGGTACGGGGACT
	Rev	GGATTCCGTAGCTGCCTTGCG
POT1	For	TTGTTCGCTTTCACAGGCTGAAGA
	Rev	TGTCCTGGTGCCATCCCATACCTTT

3. Ethics

The human studies were approved by the Human Research Ethics Committee of the Sydney West Area Health Service and the University of Sydney (HREC/17/WMEAD/433) and the University of Sydney and the Ethics Committee of Valme University Hospital, Seville, Spain. All participants provided written informed consent prior to their involvement.

Animal experimental protocols received approval from the Western Sydney Local Health District animal ethics committee (Ethics protocol: 4249, 4302) and adhered to the guidelines set by the Australian Council on Animal Care.

4. In-house human cohorts

4.1 Telomere length patient cohort

The study comprised 303 patients with biopsy-proven MAFLD (152 patients in the initial cohort from Westmead hospital, Australia and 151 in the validation cohort from Valme University Hospital, Spain).

MAFLD was diagnosed according to the international consensus criteria (209). Individuals with concomitant diagnoses were excluded, including excess alcohol intake ((> 20 g per day for female and (> 30 g per day for male)), chronic viral hepatitis (hepatitis B and hepatitis C), and drug-induced liver injury.

Weight (in kilograms) and height (in centimeters) were measured by staff at the time of biopsy and used to calculate BMI, expressed as kg/m2. Following WHO criteria for Western populations, patients with BMI of < 25 kg/m2 were defined as lean and ≥ 25 kg/m2 as non-lean (68). Hypertension was defined as a registered diagnosis in patient medical records, a resting blood pressure of ≥ 140/90 mm Hg, or having any antihypertensive medication prescribed. Type 2 diabetes mellitus (T2DM) was defined as a registered diagnosis in patient medical records, a fasting plasma glucose value ≥ 7 mmol/L (or 126 mg/dL) or having any antidiabetic medication prescribed.

4.2 Human liver biopsy for TEM study

Liver sections from four patients with biopsy-proven lean and non-lean MAFLD were assessed by electron microscopy. The diagnosis of MAFLD was made according to international consensus criteria (209). Patients were excluded from the study if they had dual etiology conditions, such as excessive alcohol consumption (more than 20 grams per day for females or more than 30 grams per day for males), chronic viral hepatitis (hepatitis C or hepatitis B), or drug-induced liver injury.

5. National Health and Nutrition Examination Survey (NHANES)

The study of the association of telomere length and DNAm-GDF15 with morality was undertaken on the National Health and Nutrition Examination Survey (Continuous NHANES) database 1999 to 2002 (210).

For telomere length analysis, DNA samples were collected from participants (≥ 20 years age). 7,827 out of the 21,004 participants provided DNA specimens and consented for future research.

Of the 7,827 participants with available leucocyte telomere length, participants who were 85 years of age and older were eliminated from the study (n = 226) to mitigate survivor bias. Pregnant individuals (n = 445), participants who did not have the essential laboratory tests for defining liver disease (n = 13) such as platelet count, ALT, and AST levels, as well as subjects with viral hepatitis (HBV or HCV) (n = 176), were excluded from the analysis. Thus, the study cohort comprised 6,967 individuals.

Liver fibrosis was assessed based on the AST-to-platelet ratio index (APRI; 100 X [AST/AST upper limit of normal]/ [platelet count]) or the FIB-4 index calculated as follows: age (years) × AST (IU/L)/ (platelets (109/L) × (ALT(IU/L))1/2. A threshold of APRI greater than or equal to 1.5 or FIB-4 greater than or equal to 2.7 was used to define advanced fibrosis.

Suspected MAFLD was defined as serum ALT > 30 U/L for male and > 19 for female in the absence of other causes of chronic liver disease. The iteration of The National Death Index (NDI) (a database of all deaths in the United States) used in these analyses had follow-up data for the NHANES 1999–2002 participants.

Mortality outcome was not available for only three participants from the telomere analysis cohort allowing analysis of the relationship between telomere length and all-cause mortality among the 6,964 participants.

For DNAm-GDF15 analysis, the database collected blood samples from adults aged 50 years and above for DNA purification purposes (210).

Among the 21,004 participants in the NHANES dataset, 2,532 had DNAm-GDF15 measured. After excluding 189 participants due to incomplete mortality data, the final analysis cohort

consisted of 2,343 individuals. In this cohort, DNA was extracted, bisulfite-converted using the Zymo EZ kit, and analyzed with the Illumina Infinium EPIC BeadChip. Methylation data were processed with the iScan system, and cell type proportions were estimated using the IDOL probe set and the FlowSorted.Blood. EPIC_ref dataset. DNAm-predicted GDF15 levels were derived through regression modeling incorporating age, sex, and relevant CpGs.

5.1 All-cause, cardiovascular, cancer, and other cause mortality

Mortality data were obtained by linking participant information from NHANES to the NDI. Follow-up time was calculated from the date of the initial survey to the earlier of either the most recent mortality update or the NDI database cut-off date (December 31, 2019). The main outcomes assessed were deaths from all-cause mortality, cardiovascular, cancer, and other-cause mortality.

6. Animal models

Several dietary models for MAFLD have been developed such as the Methionine-Choline-Deficient (MCD) diet and the High Cholesterol (ChR) diet model, which represent lean MAFLD, as well as the High-Fat Diet (HFD) model for non-lean disease.

6.1 Methionine-Choline-Deficient (MCD) diet model & Methionine Choline Sufficient (MCS)

The study was carried out using eight-week-old male mice on a C57Bl/6 background. Mice in the experiment were fed a Methionine-Choline-Deficient (MCD) diet for six weeks. this dietary model is used to replicate features of lean MAFLD (Specialty Feeds, Glen Forrest, Western Australia, Cat.No. SF13-136). Methionine choline sufficient (MCS) diet as control (Specialty Feeds, Glen Forrest, Western Australia, Cat. No. SF13-137). The mice were maintained in a

temperature-controlled facility under a 12-hour light–dark cycle and had free access to standard chow and water.

6.2 High Cholesterol (ChR) diet model & Normal chow (NC)

The study was carried out using eight-week-old male mice on a C57Bl/6 background. The animals used in the experiment were given a high-cholesterol meal for 8 weeks, this dietary model is used to replicate features of lean MAFLD (Specialty Feeds in Glen Forrest, Western Australia, with the Cat.No SF09-080). Normal chow as control (NC) (Specialty Feeds, Glen Forrest, Western Australia, Cat.No. SF09-079). The mice were maintained in a temperature-controlled facility under a 12-hour light–dark cycle and had free access to standard chow and water.

6.3 High-Fat Diet (HFD) model

The study was carried out using eight-week-old male mice on a C57Bl/6 background. Male mice, aged 6 to 8 weeks, were administered a high-fat diet, this dietary model is used to replicate features of non-lean MAFLD (Specialty Feeds, Glen Forrest, Western Australia, Cat.No. SF04–001) for a duration of 24 weeks. Normal chow as control (Specialty Feeds in Glen Forrest, Western Australia, with the Cat.No SF00-100). The mice were maintained in a temperature-controlled facility under a 12-hour light–dark cycle and had free access to standard chow and water.

7. Tissue culture

Immortalized Human Hepatocytes (IHH) (Kind gift from Prof. Stephan Urban, Heidelberg University) were cultured in Williams' medium E (ThermoFisher Scientific, catalog 12,551,032) containing 10% fetal bovine serum and 1% penicillin/streptomycin solution. Mycoplasma testing and simple sequences or short tandem repeats (STR) profiling of cell lines

are done routinely. Cells were treated with H2O2 (300 nM) with or without Mito-TEMPO (10 μM), a ROS inhibitor for the indicated times and cells were harvested for further analysis.

8. Gene expression mRNA

8.1 RNA Extraction

The protocol was adapted from previously published methods (211, 212) . Total RNA was isolated from cultured cells immortalized human hepatocyte cell line (IHH) or frozen mouse tissues using the FavorPrep Tissue Total RNA Extraction Mini Kit (Favorgen Biotech), following the manufacturer's instructions. Frozen tissue approximately 25 mg was homogenized in 350 μL of FARB buffer supplemented with 1% β-mercaptoethanol and then incubated at room temperature for 5 minutes.

The lysate was then transferred to a filter column placed in a collection tube and centrifuged at 16000×g for 2 minutes. The resulting flow-through was moved to a new microcentrifuge tube, mixed with 350 μL of 70% ethanol, and loaded onto a fresh FARB mini-column.

After centrifugation at 14,000 rpm for 1 minute, the flow-through was discarded. The column was subsequently washed with Wash Buffer one of 500 μL and centrifuged again for 1 minute at 14000 rpm. A second wash was performed using Wash Buffer two of 750 μL, followed by centrifugation at the same speed for 1 minute; this step was repeated two times.

An additional 3 minute centrifugation was performed to ensure complete drying of the membrane. The mini-column was then placed into a 1.5-mL RNase-free tube, and RNA was eluted with 50 μL of RNase-free water, incubated for 1 minute, and centrifuged at 14000 rpm for 1 minute. For purity and RNA concentration were measured using a NanoDrop spectrophotometer at 260 and 280 nm.

8.2 cDNA Synthesis

The protocol was adapted from previously published methods (211). Complementary DNA (cDNA) was generated from 100 ng of total RNA using the qScript® cDNA SuperMix (Quanta Biosciences, Gaithersburg, MD). For each reaction, 10 µL of RNA (containing 100 ng) was mixed with 2.5 µL of qScript Reaction Mix in a 500-µL Eppendorf tube. The tubes were placed in a thermal cycler and processed according to the following program: 25°C for 5 minutes, 42°C for 30 minutes, and 85°C for 5 minutes, after which the reactions were held at 4°C. The resulting cDNA was subsequently used for quantitative real-time PCR analysis.

8.3 Real-time Quantitative PCR

Real-time polymerase chain reaction (PCR) was conducted using Applied Biosystems equipment (Foster City, CA, USA). SYBR and forward and reverse primers were used for each gene of interest, along with SYBR Select Master Mix. The results were normalized to the expression of glyceraldehyde 3-phosphate dehydrogenase (GAPDH) for human hepatocyte cell line (IHH) and M36b4 for mouse frozen tissue. Quantification was achieved by calculating the ΔCT value (ΔCT = CT [GAPDH or M36b4] – CT [target]), with results expressed as 2^−ΔCT.

9. DNA extraction

Genomic DNA was extracted using the DNeasy Blood & Tissue Kit according to the manufacturer's instructions for tissue and cultured cell samples (Qiagen, 69506, Germany). All centrifugation steps were performed at room temperature (15–25°C), and frozen tissues or cell pellets were equilibrated to room temperature prior to processing. An incubator was preheated to 56°C before starting the procedure.

Tissue pieces (≤10 mg spleen or ≤25 mg of other soft tissues) were excised and transferred into 1.5-mL microcentrifuge tubes. Samples were immersed in 180 µL of Buffer ATL, followed by

the addition of 20 µL proteinase K. Tubes were vortexed thoroughly to ensure complete mixing and then incubated at 56°C until the tissue was fully lysed.

During incubation, samples were vortexed intermittently to facilitate enzymatic digestion. Immediately before proceeding to the binding step, lysates were vortexed again for approximately 15 seconds to ensure homogeneity.

For cultured cell pellets, up to 5×10^6 cells were collected by centrifugation at 300 × g for 5 minutes. The supernatant was discarded, and the pellet was gently resuspended in 200 µL PBS. Proteinase K (20 µL) was added directly to the resuspended cells, and the mixture was briefly vortexed to ensure uniform distribution of the enzyme.

Following pretreatment, 200 µL of Buffer AL was added to each sample (tissue lysate or cell suspension). Samples were mixed thoroughly by vortexing and incubated at 56°C for 10 minutes to ensure complete lysis. After incubation, 200 µL of 96–100% ethanol was added to each tube, followed by vigorous vortexing to promote nucleic acid binding efficiency.

The entire lysate–ethanol mixture was then transferred to a DNeasy Mini spin column placed in a 2-mL collection tube. Columns were centrifuged at ≥6000 × g (approximately 8000 rpm) for 1 minute. Flow-through was discarded, and the spin column was transferred to a new collection tube.

A first wash was performed by adding 500 µL of Buffer AW1 to the column, followed by centrifugation for 1 minute at ≥6000 × g. The flow-through was discarded, and the column was placed into a fresh 2-mL collection tube.

A second wash was performed by adding 500 µL of Buffer AW2, followed by centrifugation at 20,000 × g (14,000 rpm) for 3 minutes to remove residual contaminants. After centrifugation, the flow-through and collection tube were discarded.

The spin column was transferred to a clean 1.5- or 2-mL microcentrifuge tube. DNA was eluted

by adding 200 µL of Buffer AE directly onto the center of the membrane. After incubation for 1 minute at room temperature, the column was centrifuged at ≥6000 × g for 1 minute to recover the purified DNA. A second elution step using an additional 200 µL Buffer AE was optional to increase total DNA yield.

10. Absolute mtDNA quantification

Mitochondrial DNA (mtDNA) copy number was quantified using the Absolute Mouse Mitochondrial DNA Copy Number Quantification qPCR Assay Kit (ScienCell, Cat. M8948), following the manufacturer's protocol.

The lyophilized mouse mtDNA and single-copy reference (SCR) primers were reconstituted with nuclease-free water and stored at −20°C before use. For each DNA sample, two qPCR reactions were prepared: one amplifying a conserved region of the mouse mitochondrial genome and one amplifying the nuclear single-copy reference gene on chromosome 10 to enable normalization. Each 20 µL reaction contained the 2X GoldNStart TaqGreen master mix, the corresponding primer set, genomic DNA (0.5–5 ng), and nuclease-free water.

Reactions were run on a real-time PCR instrument using the recommended cycling conditions (95°C for 10 min followed by 32 cycles of 95°C for 20 s, 52°C for 20 s, and 72°C for 45 s), with melting-curve analysis performed to confirm specificity of amplification. A reference mouse genomic DNA sample with a known mtDNA copy number (537 ± 20 copies per diploid cell) was included in each run for calibration.

Relative mtDNA content was calculated using the ΔΔCq method, in which mtDNA Cq values were normalized to the SCR gene and then compared with the reference DNA to determine fold change (2^−ΔΔCq). Absolute mtDNA copy number per diploid cell was derived by multiplying the fold change value by the known mtDNA content of the reference genomic DNA.

11. Absolute telomere length

Genomic DNA was extracted from all samples using a standard DNA isolation method (Qiagen, Germany). Telomere length was quantified using the Absolute Human Telomere Length and Mitochondrial DNA Copy Number Dual Quantification qPCR Assay Kit (ScienCell, Cat. 8958), following the manufacturer's instructions.

The lyophilized telomere and single-copy reference (SCR) primers supplied in the kit were reconstituted with nuclease-free water and stored at −20°C until use. For each sample, two parallel qPCR reactions were prepared, one amplifying the telomeric repeats and the other amplifying the SCR locus for normalization. Each 20 µL reaction contained the 2X GoldNStart TaqGreen master mix, the corresponding primer set, genomic DNA (0.5–5 ng), and nuclease-free water.

Reactions were run on a real-time PCR platform using the recommended cycling conditions (95°C for 10 min, followed by 40 cycles of 95°C for 20 s, 52°C for 20 s, and 72°C for 45 s), with melt-curve analysis confirming amplification specificity. A reference genomic DNA sample with a known telomere length (1.23 Mb per diploid cell) provided with the kit was included in each run. Telomere length was calculated using the ΔΔCq method, where telomere and SCR Cq values of each sample were normalized to the reference DNA to derive relative telomere content (2^−ΔΔCq), which was subsequently converted to absolute telomere length per diploid cell. Average telomere length per chromosome end was obtained by dividing the total telomere length by 92 chromosomal termini.

12. Telomerase activity (TRAP) assay

The telomerase repeat amplification procedure test was used to measure telomerase activity. This assay was conducted using the TRAPeze telomerase detection kit (S7700, Sigma-Aldrich) in accordance with the instructions provided by the manufacturer.

Cells were cultured until they reached a confluence of 70‑80% when they were lysed using CHAPS buffer. Each process used a lysate volume equivalent to 5000 cells. Negative controls were prepared by subjecting samples to a temperature of 85 ℃ for 10 min. A positive control provided in the kit was included for comparison. The PCR reaction mixture consisted of 25 μL, comprising 16 μL of PCR water, 2.5 μL of 10 × TRAP reaction buffer, 0.5 μL of 50 × dNTP mix, 3 μL of AuNP − TS primer (TS-modified AuNPs were incorporated into the PCR reaction system at a suitable concentration), 0.5 μL of TRAP primer mix, 0.5 μL of Taq polymerase (5 units/μL), and 2 μL of cell extract. Subsequently, the tubes were subject to incubation in a thermocycler set at 30 °C for 30 min, facilitating the process of telomerase elongation.

Subsequently, a three-step polymerase chain reaction (PCR) protocol consisting of denaturation at 94 °C for 30 s, annealing at 62.9 °C for 30 s, and extension at 72 °C for 1 min was executed for 33 cycles. Electrophoresis was conducted on a 2% agarose gel to facilitate the creation of polymerase chain reaction (PCR) products. The gel was stained with ethidium bromide at a concentration of 1 μg/ml, and the resulting bands were analysed using the ChemiDoc Touch Imaging system manufactured by Bio-Rad.

13. Enzyme-linked immunosorbent assay (ELISA)

13.1 Growth differentiation factor-15 (GDF-15)

GDF-15 concentrations were measured using a commercially available Human GDF-15 ELISA kit (ThermoFisher Scientific, EHGDF15), following the manufacturer's instructions. Serum samples were collected, centrifuged to remove debris, and stored at −80 °C until analysis. Prior to the assay, samples were thawed on ice and diluted in the supplied Assay Diluent (1×) according to recommended ranges.

Standards were prepared to generate a calibration curve (range: 1.1–800 pg/mL). Aliquots of 100 µL of standards and diluted samples were added to pre-coated wells and incubated at room temperature. After washing, wells were incubated sequentially with biotin- conjugated anti-GDF-15 antibody and HRP-streptavidin. Colour development was achieved using TMB substrate and stopped with the provided stop solution. Absorbance was measured at 450 nm using a microplate reader.

Sample concentrations were calculated by interpolation from a four-parameter logistic (4-PL) standard curve and corrected for the dilution factor. According to the manufacturer, the assay sensitivity is 2 pg/mL, with intra- and inter-assay coefficients of variation <10% and <12%, respectively.

13.2 Malondialdehyde (MDA)

Malondialdehyde concentrations were measured using a quantitative competitive ELISA kit (Abcam, ab287797) following the manufacturer's instructions. This assay is based on the binding of MDA present in samples to an MDA-BSA conjugate immobilized on the microplate. Serum samples were clarified by centrifugation and diluted in the sample diluent supplied with the kit to fall within the assay's dynamic range (0.156–10 µM).

Standards were prepared by serial dilution of the provided MDA standard solution to generate a calibration curve for quantification. Samples and standards were incubated with the MDA-specific primary antibody and then added to the pre-coated wells, allowing competitive binding between plate-bound antigen and free MDA in the sample.

After washing to remove unbound components, an HRP-conjugated secondary antibody was added, followed by TMB substrate for color development. The reaction was terminated with acidic stop solution, and absorbance was recorded at 450 nm using a microplate reader. Lower

optical density corresponds to higher MDA concentrations due to the competitive nature of the assay.

MDA levels in each sample were calculated by fitting absorbance values to the standard curve using a four-parameter logistic (4-PL) regression model. All samples were analyzed in duplicate, and values outside the linear portion of the curve were excluded from downstream analysis.

14. Immunohistochemistry (IHC)

4-μm sections were mounted onto saline-coated glass slides to ensure section adhesion through subsequent staining procedures. Slides were stained using the BOND RX Fully Automated Research Stainer (Leica Biosystems) using the Bond Polymer Refine Detection Method Algorithm as per manufacturer instructions (DS9800 Leica). The slides were incubated with a dilution of 1:500 goat polyclonal anti-human 8-hydroxy-2′ - deoxyguanosine (8- OHdG) (NOVUS, NB600-1508) and a dilution of 1:5000 mouse monoclonal anti-4- hydroxynonenal (4-HNE) (Abcam, AB48506). Negative controls were carried out using rabbit serum diluted to the same concentration as the primary antibody. The extent of 8-OHdG and 4-HNE immunostaining was assessed using ImageJ.

15. Immunofluorescence (IF)

Frozen mouse sections underwent two rinses with PBS and were permeabilized in 0.3% Triton X-100 for 10 minutes. They received an overnight incubation at 4°C with Anti-IRE1 antibody with a dilution of 1:500 as primary antibody (Abcam, ab37073), followed by a one-hour incubation at room temperature with a FITC-conjugated anti Rabbit with a dilution of 1:500 as secondary antibody (Abcam, ab6717). Ultimately, the sections were visualised using a confocal microscope (Leica).

16. Western blot analysis (WB)

We utilised SDS-PAGE to fractionate the tissue contents and subsequently transferred these fractions onto a polyvinylidene difluoride (PVDF) membrane in accordance with the manufacturer's instructions (Bio-Rad, Hercules, CA).

To prevent any non-specific binding, the membranes were treated with a solution containing 5% non-fat milk in TBST (50 mM Tris, pH 7.4, 150 mM NaCl, 0.05% Tween −20) for 1 hour at room temperature following the transfer.

The membranes were rinsed twice with TBST and then exposed to primary antibodies (Total OXPHOS Rodent WB Antibody Cocktail, Abcam ab110413) which were diluted in a solution of 5% skim milk and TBST. This incubation process took place overnight at a temperature of 4 °C. After the incubation period, the membranes were rinsed three times for 10 minutes with TBST solution. Then, they were exposed to secondary antibodies, which were diluted in a solution of 5% skim milk and TBST. This exposure lasted for 1 hour in a dark environment at room temperature.

The blots underwent three washes with TBST and were then subjected to development using Super Signal West Pico PLUS Chemiluminescent and Super Signal West Femto Maximum Sensitivity Substrates (Life Technologies, Australia), following the instructions provided by the manufacturer. The membranes were analysed using the ChemiDoc Touch Imaging system (Bio-Rad, Hercules, CA).

17. Cellular reactive oxygen species (ROS) assay

The procedure commenced by homogenizing frozen liver tissue in 2 mL of PBS, followed by centrifugation at 10,000 × g for 5 minutes at 4°C. The supernatant was collected, and the pellet was discarded for immediate use. Next, 50 µL of PBS was pipetted into a black 96-well plate with a clear bottom (Corning) and 50 µL of the prepared sample was added.

To this, 100 µL of 2′,7′-Dichlorodihydrofluorescein diacetate (final concentration 10 µM,

dissolved in DMSO; D6883-50mg, Merck) was added. The mixture was incubated in the dark at 37°C for 30 minutes.

Fluorescence readings were taken using a plate reader set to an excitation wavelength of 482 nm and an emission wavelength of 528 nm. A blank sample was used to measure background fluorescence which was subtracted from the sample readings. For normalization, the protein concentration of each sample was determined using the BCA protein assay.

18. Transmission electron microscope (TEM)

Human liver biopsies and mouse frozen liver samples were collected, cut into ~ 1 mm^3 pieces, and fixed in 2.5% glutaraldehyde. The samples were embedded following the protocol outlined in Table 17.1 and sectioned into ultrathin slices of 70 nm thickness. The prepared tissue sections were examined using transmission electron microscopy (TEM) (Jeol 1400 Flash, 120 kV).

Table 17.1 TEM protocol

VIAL	SOLUTION	TIME	TEMP
1	NaCac buffer	5min	20°C
2	NaCac buffer	5min	20°C
3	OsO4	60 mins	20°C
4	Distilled water	3min	20°C
5	Distilled water	3min	20°C
6	Uranyl acetate	60 mins	20°C
7	50 % Ethanol	10 mins	20°C
8	70 % Ethanol	10 mins	20°C

9	95 % Ethanol	10 mins	20°C
10	100 % Ethanol	10 mins	20°C
11	100 % Ethanol	10 mins	20°C
12	Acetone	10mins	20°C
13	1:1 Acetone/ resin	30mins	20°C
14	100% Resin	30mins	60°C
15	100% Resin	30mins	60°C
16	100% Resin	30mins	60°C

19. Statistical analysis

Multiple logistic regression models were used to assess factors independently associated with lean MAFLD and fibrosis. A set of Cox regression models was used to estimate the effect of telomere length on the risk of mortality in the full analysis cohort and in subjects with suspected MAFLD, stratified by obesity status. Models were adjusted for age, sex, fibrosis, and race. Telomere length was as continuous and categorical variable (quartiles of telomere lengths).

To assess the impact of DNAm-GDF15 on mortality risk, Cox regression models were employed on the full analysis cohort and in subjects with suspected MAFLD, stratified by obesity status. Models were adjusted for age, sex, ethnicity, ALT and AST. DNAm-GDF15 was assessed both as a continuous variable and as a categorical variable (quartiles). The correlation between DNAm-GDF15 and telomere length was analyzed using the Wilcoxon rank-sum test. Mediation analysis was performed to determine the indirect effect of DNAm-GDF15 on the relationship between telomere length and mortality. This analysis was used to

quantify the proportion of the relationship between telomere length and mortality that is mediated by DNAm-GDF15.

Statistical analysis was performed using SPSS or GraphPad Prism. Data is represented as mean ± standard error of the mean (SEM). The Mann-Whitney test was used for comparisons between two groups. Statistical significance was defined as $p < 0.05$.

Chapter 3: Telomere length and mortality in lean MAFLD

3.1 Introduction

MAFLD affects up to a third of the global population and is a leading cause of end-stage liver disease, liver cancer, and liver transplantation. While typically linked to overweight or obesity, a considerable proportion of patients are normal weight and frequently called “lean-MAFLD” (68, 213).

The metabolic profile in lean MAFLD patients often presents with lower insulin resistance and more favorable lipid profiles compared to their non-lean counterparts (100, 214). Similarly, histologically, lean MAFLD patients show less severe steatosis, inflammation, fibrosis, and lower NAFLD activity score (NAS) compared to their non-lean counterparts (100, 214, 215). Despite these favourable metabolic and histologic characteristics of the lean MAFLD patients, multiple studies and meta-analyses demonstrate that lean MAFLD patients exhibit poorer long-term outcomes and an increased risk of mortality compared to their non-lean counterparts (216), highlighting the paradox between these features.

I reasoned that differential telomere length might be one possible explanation for this paradox. Telomeres are protective structures located at the ends of eukaryotic chromosomes, and their progressive shortening has been associated with chronic disease progression and increased mortality (217, 218). The maintenance of telomeres requires significant energy resources. In periods of sustained metabolic stress, cells may prioritize immediate survival needs over long-term genomic maintenance, resulting in accelerated telomere attrition (219). The combination of ongoing stress and telomere erosion leads to adverse health outcomes in lean MAFLD.

Telomeres also show high vulnerability to oxidative damage (220). Mitochondria produce reactive oxygen species (ROS) as part of normal ATP generation, and excessive ROS can accelerate telomere erosion (220). This process links oxidative stress to telomere attrition and may help explain long-term disease progression in lean MAFLD patients.

Based on this, I hypothesize that differential telomere length mediated by oxidative stress contributes to the adverse clinical outcomes observed in lean MAFLD. To test this hypothesis, the studies in this chapter aim to compare telomere length between lean and non-lean MAFLD patients, investigate the relationship between telomere length and key pathological features, including fibrosis, inflammation, and mortality, and experimentally explore if oxidative stress contributes to telomere shortening in lean MAFLD using both clinical samples and experimental models.

3.2 Method

3.2.1 Patient cohort

A total of 303 patients with biopsy-proven MAFLD were included across an initial and validation cohort from Westmead hospital, Australia and Valme University Hospital, Spain, respectively.

Lean MAFLD was defined according to consensus guidelines (209). Individuals with concomitant diagnoses were excluded, including excess alcohol intake (> 20 g per day for female and (> 30 g per day for male)), chronic viral hepatitis (hepatitis B and hepatitis C), and drug-induced liver injury.

Ethics approval was obtained from the Human Research Ethics Committees of the Western Sydney Local Health District and the University of Sydney and the Ethics Committee of Valme University Hospital, Seville, Spain.

3.2.2 Cell culture and molecular assays

IHH were cultured in Williams' E medium supplemented with 10% fetal bovine serum and 1% penicillin/streptomycin. To model oxidative stress, cells were treated with 300 nM hydrogen

peroxide (H_2O_2), with or without 10 μM Mito-TEMPO. Total RNA was extracted and converted to cDNA, and gene expression of shelterin complex components was assessed using RT-PCR (reverse transcription-polymerase chain reaction). Protein expression of TERT (Telomerase reverse transcriptase) was examined by Western blot analysis using liver tissue lysates.

For oxidative DNA damage assessment, IHC was performed on liver tissue sections using antibodies against 8-OHdG and 4-HNE. Oxidative stress levels were further evaluated using ELISA to measure serum MDA concentrations.

3.2.3 Telomere length and Telomerase activity assay

Telomere length was measured using a qPCR-based absolute quantification method on extracted genomic DNA.

Telomerase activity was measured using the TRAPeze telomerase detection kit. Cell lysates were processed with telomerase repeat amplification procedure (TRAP) PCR under standard cycling conditions. Products were separated by agarose gel electrophoresis and visualized with ethidium bromide using a ChemiDoc imaging system.

3.2.4 Statistical analysis

The data analysis was conducted with GraphPad Prism software version 10. The data were provided as the mean ± standard error of the mean (SEM). The one-way analysis of variance (ANOVA) was used for performing a multi-group research, whereas the student's t-test was applied for assessing two groups. IBM SPSS Statistics was used for the study of public datasets. P-value <0.05 denote the presence of a statistically significant difference.

3.3 Results

3.3.1 Clinical and histopathological characteristics of MAFLD patients in the initial cohort

The initial cohort comprised of 156 biopsy-proven patients from MAFLD, of them 26 were lean MAFLD, and 130 were non-lean MAFLD. The mean age was comparable between lean MAFLD (51±11.2 years) and non-lean MAFLD groups (49±13.1 years, P=0.6) and there were no significant differences between groups in gender distribution.

As expected, BMI was significantly lower in the lean MAFLD group (23.1±1.2 kg/m²) compared to the non-lean MAFLD group (32.6±6 kg/m²; P<0.001). Notably, Homeostatic Model Assessment for Insulin Resistance (HOMA-IR) in lean MAFLD (2.4±2.1) was lower than non-lean MAFLD (5.2±5.9; P=0.01). While gamma-glutamyl transferase (GGT) was higher in lean MAFLD (164.9±203.8 IU/L) than non-lean MAFLD (104.1±115.9 IU/L; P=0.03). While there were no significant differences between groups in hypertension, dyslipidaemia, ALT, AST, fasting blood sugar test (BSL), platelets count or histological features (**Table. 3.1**).

Table 3.1: Clinical and histological characteristics of lean and non-lean patients with MAFLD in the initial cohort.

	Lean MAFLD (n = 26)	Non-lean MAFLD (n = 130)	P Value
Age (years)	51 ± 11.2	49 ± 13.1	0.6
Male (%) **Female (%)**	13 (50) 13 (50)	72 (55.4) 58 (44.6)	0.6
BMI (kg/m2)	23.1 ± 1.2	32.6 ± 6	< 0.001
Hypertension (%)	9 (34.6)	47 (36.2)	1
Dyslipidaemia (%)	13 (52)	80 (61.5)	0.3
Homa-IR	2.4 ± 2.1	5.2 ± 5.9	0.01
ALT (IU/mL)	70.2 ± 43.9	71.5 ± 45.4	0.8
AST (IU/mL)	61.2 ± 51.7	49.1 ± 27.5	0.08
GGT (IU/L)	164.9 ± 203.8	104.1 ± 115.9	0.03
Fasting BSL (mmol/L)	6.4 ± 3.3	6.3 ± 2.3	0.8
Platelets (×109/L)	250.1 ± 81.5	250.8 ± 69.7	0.9
Total cholesterol (mmol/L)	5.2 ± 1.2	5.2 ± 1.2	0.8
HDL-C (mmol/L)	1.4 ± 0.6	1.2 ± 0.37	0.04
LDL-C (mmol/L)	3.1 ± 0.9	3 ± 1	0.7
Triglyceride (mmol/L)	2.4 ± 2.2	2.1 ± 1.3	0.2
Severe fibrosis (F3-F4) (%)	6 (23.1)	22 (17.1)	0.5
Moderate/severe steatosis (S≥2) (%)	7 (28)	50 (39.7)	0.3
Inflammation (≥A1) (%)	4 (15.8)	12 (9.4)	0.2

P value was calculated using independent t-test. Abbreviations: BMI: Body Mass Index; Homa-IR: Homeostatic Model Assessment for Insulin Resistance; ALT: Alanine Aminotransferase; AST: aspartate aminotransferase; GGT: gamma-glutamyl transferase; Fasting BSL: fasting blood sugar test; HDL-C: high-density lipoprotein cholesterol; LDL-C: low-density lipoprotein cholesterol.

3.3.2 Telomere length is associated with inflammation and fibrosis in MAFLD in the initial cohort

To explore the changes of telomere length among patients with MAFLD, I first examined the association between telomere length and liver histology in the initial cohort. No differences in telomere length were noted between patients with mild (S1–S2) compared with severe steatosis (S3) (**Fig. 3.1a**).

Higher grades of lobular inflammation were associated with shorter telomere length (P=0.01) (**Fig. 3.1b**). Similarly, patients with significant fibrosis (≥F3) had shorter telomere lengths compared with those with none/ mild fibrosis (F0–F2) (P=0.02) (**Fig. 3.1c**).

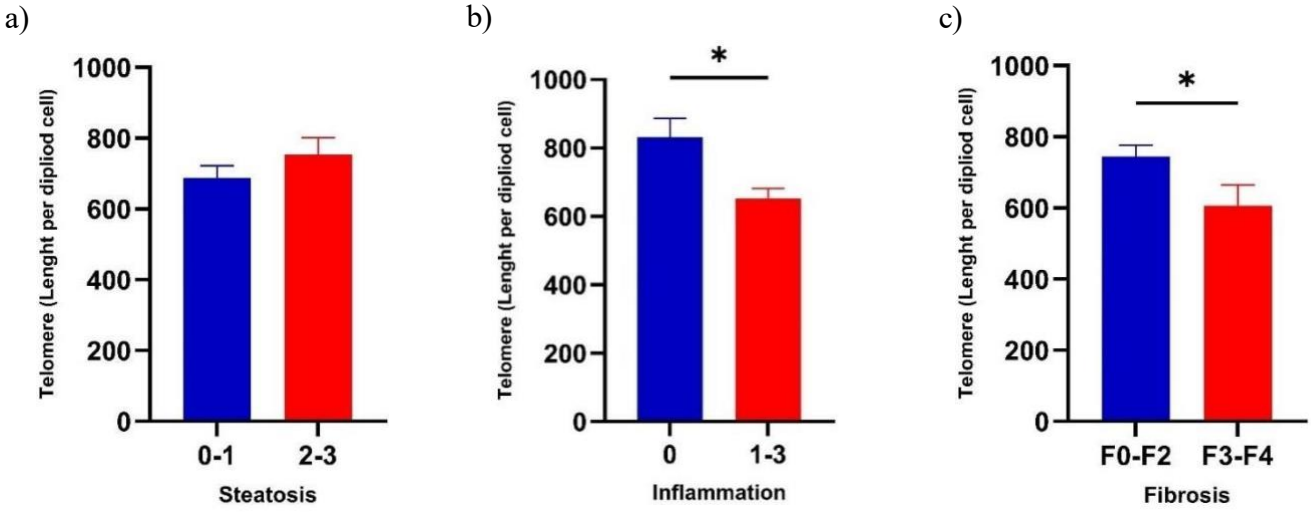

Figure 3.1 Telomere length and histological features in patients with MAFLD: a) steatosis, **b)** inflammation, **c)** fibrosis. Data are represented by vertical bars and are mean ± SEM. Statistical differences between groups are assessed by Mann–Whitney test. *P<0.05, **P<0.01, ***P<0.001, ****P<0.0001.

To determine whether telomere length is independently associated with fibrosis severity. I used multivariable logistic regression. The association between telomere length and fibrosis remained significant after adjusting for age, BMI, sex, ALT, and platelets in a multivariable logistic regression analysis (OR=0.998; 95% CI: 0.998–0.997; P=0.03) (**Table. 3.2**).

Table 3.2: Multivariate analysis of factors associated with fibrosis stage ≥3 in the initial cohort.

Variable	Odd Ratio	95% C.I	P value
Telomere (length per diploid cell)	0.998	0.998-0.997	0.03
Sex	1.919	0.693-5.315	0.2
Age (Years)	1.019	0.976-1.064	0.3
ALT (IU/mL)	1.008	0.998-1.018	0.1
Platelets (×109/L)	0.988	0.980-0.996	0.004

P value was calculated using univariable logistic regression analysis. Abbreviations: ALT: Alanine Aminotransferase.

3.3.3 Lean MAFLD patients have shorter telomere length in the initial cohort

I next explored the differential telomere lengths between patients with lean and non-lean MAFLD in initial cohort. Interestingly, patients with lean MAFLD had shorter telomere lengths compared with those with non-lean MAFLD (P=0.0003) (**Fig. 3.2**).

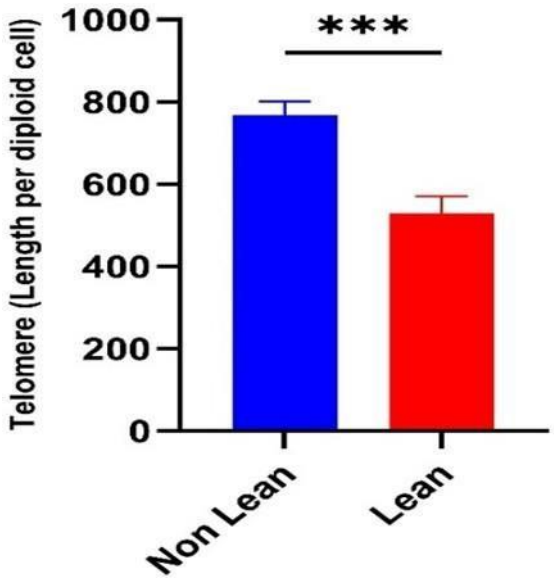

Figure 3.2: Telomere length in initial cohort. Data are represented by vertical bars and are mean ± SEM (n=156). Statistical differences between groups are assessed by Mann–Whitney test. *P<0.05, **P<0.01, ***P<0.001, ****P<0.0001.

Then I assessed whether lean MAFLD status was independently associated with shorter telomere length. A multivariable analysis was performed, adjusting for age, sex, ALT, fibrosis stage, diabetes, and the presence of risk variants in Patatin-like phospholipase domain-containing protein 3 (PNPLA3) and Transmembrane 6 superfamily member 2 (TM6SF2). Telomere length remained significantly associated with lean MAFLD (OR=1.003; 95% CI, 1.001–1.006; P=0.003) (**Table 3.3**).

Table 3.3: Multivariable logistic regression: telomere length and other predictors of lean MAFLD status in the initial cohort.

Variable	Odd Ratio	95% C.I (L-U)	P value
Telomere (length per diploid cell)	1.003	1.001-1.006	0.003
Male	0.749	0.266-2.11	0.5
Age (years)	1.001	0.957-1.047	0.9
Diabetes	2.522	0.678-9.378	0.1
ALT (IU/mL)	1.001	0.989-1.014	0.8
Significant fibrosis (≥ F2)	0.716	0.184-2.793	0.6
TM6SF2 rs58542926 (CT/TT)	2.452	0.735-8.181	0.1
PNPLA3 rs738409 (GG)	0.665	0.232-1.907	0.4

P value was calculated using univariable logistic regression analysis. Abbreviations: ALT: Alanine Aminotransferase; TM6SF2: Transmembrane 6 superfamily member 2; PNPLA3: Patatin-like phospholipase domain-containing protein 3.

3.3.4 Correlation between telomere length and clinical parameters in MAFLD patients

To further clarify the relationship between telomere length and continuous clinical and histological variables, I next undertook a correlation analysis to identify continuous predictors of telomere length across the full MAFLD cohort. BMI was positively significant (r2=0.289; P=<0.001) consistent with previous findings that lower BMI is associated with shorter telomeres, (**Table 3.4**) and depicted in (**Fig 3.3a**). Inflammation (r2=-0.178; P=0.02) and fibrosis (r2=-0.177; P=0.02) were negatively significant associated with telomere length (Table. 3.4). Notably, no correlation between telomere length and age was discerned (**Fig. 3.3b**).

Table 3.4: Correlation between telomere length and clinical variables in the initial cohort

Telomere	r2	P Value
BMI (kg/m2)	0.289**	<0.001
Age (years)	-0.012	0.8
Hypertension	-0.004	0.9
Diabetes	-0.048	0.5
Dyslipidemia	-0.078	0.3
HOMA-IR	0.089	0.2
ALT (IU/mL)	0.005	0.9
AST (IU/mL)	-0.056	0.4
GGT (IU/L)	0.009	0.9
Fasting BSL (mmol/L)	-0.087	0.2
Platelets (×109/L)	-0.007	0.9
Total cholesterol (mmol/L)	-0.109	0.1
HDL-C (mmol/L)	-0.073	0.3
LDL-C (mmol/L)	-0.090	0.2
Triglyceride (mmol/L)	0.018	0.8
Moderate or severe steatosis (S≥2)	0.082	0.3
Inflammation (≥A1)	-0.178*	0.02
Severe fibrosis (F3-F4)	-0.177*	0.02
NAS (≥5)	-0.055	0.4

P value was calculated using Pearson's correlation coefficient. Abbreviations: BMI: Body Mass Index; Homa-IR: Homeostatic Model Assessment for Insulin Resistance; ALT: Alanine Aminotransferase; AST: aspartate aminotransferase; GGT: Gamma-glutamyl transferase; Fasting BSL: fasting blood sugar test; HDL-C: high-density lipoprotein cholesterol; LDL-C: low-density lipoprotein cholesterol; NAS: NAFLD Activity Score.

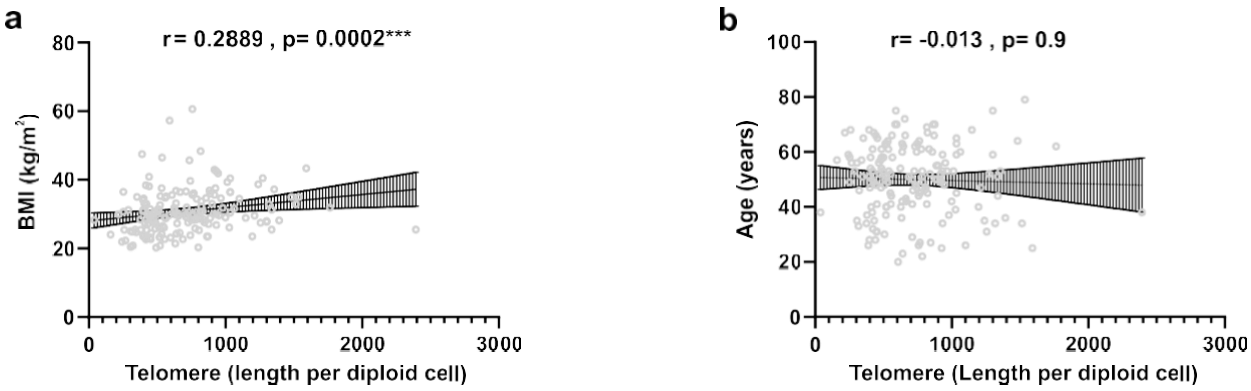

Figure 3.3: Correlation of telomeres length and a) BMI, and **b)** Age in patients with MAFLD. Data were analysed using Spearman's rank correlation. *P<0.05, **P<0.01, ***P<0.001, ****P<0.0001.

3.3.5 Characteristics of clinical and histopathological features between lean and non-lean MAFLD in validation cohort

To ascertain the validity of my findings discerned in the initial cohort, I apted to test it in an independent validation cohort of MAFLD patients recruited at Valme University Hospital, Spain.

This cohort comprised of 151 patients, including 25 with lean MAFLD, and 126 were non-lean MAFLD. The mean age was comparable between lean MAFLD (47.4±15.3 years) and non-lean MAFLD groups (46.5±11 years; P=0.7). As expected, BMI was significantly lower in the lean MAFLD group (22.5±1.9 kg/m²) compared to the non-lean MAFLD group (41.5±8.7 kg/m²; P<0.001).

Notably, lean MAFLD was lower in HOMA-IR (P=0.01), ALT (P=<0.001), AST (P=0.03), GGT (P=0.02), fasting blood glucose (P=0.02) and severe steatosis (P=0.005) than non-lean MAFLD. While HDL-C was higher in lean MAFLD (P=0.02) than non-lean MAFLD. While there were no significant differences between groups in gender distribution, dyslipidaemia, albumin, platelets count, total cholesterol, and triglyceride or histological features (**Table. 3.5**).

Table 3.5: Clinical and histological characteristics of patients with lean and non-lean MAFLD in the validation cohort

	Lean MAFLD (n = 25)	Non-lean MAFLD (n = 126)	P Value
Age (years)	47.4 ± 15.3	46.5 ± 11	0.7
Male (%) **Female (%)**	8 (32) 17 (68)	58 (46) 68 (54)	0.2
BMI (kg/m2)	22.5 ± 1.9	41.5 ± 8.7	< 0.001
Hypertension (%)	5 (20)	73 (58.9)	< 0.001
Dyslipidaemia (%)	1 (52)	40 (36.4)	1
Homa-IR	2.1 ± 2.3	5.4 ± 3.6	< 0.001
ALT (IU/mL)	29.7 ± 33.2	47.8 ± 38.7	< 0.001
AST (IU/mL)	26.2 ± 17.8	33.7 ± 26.7	0.03
GGT	43 ± 43.3	72.9 ± 111.7	0.01
Fasting BSL (mmol/L)	5.2 ± 0.6	6.2 ± 2.1	0.02
Albumin	43.1 ± 3.1	43 ± 3	0.8
Platelet (×109/L)	250.4 ± 75.3	237.5 ± 63	0.4
Total cholesterol (mmol/L)	5.2 ± 1.2	5 ± 0.9	0.5
HDL-C (mmol/L)	1.3 ± 0.3	1.1 ± 0.4	0.01
LDL-C (mmol/L)	3.4 ± 0.8	2.8 ± 1	0.2
Triglyceride (mmol/L)	1.4 ± 0.5	1.7 ± 1.1	0.1
Adverse Fibrosis (%)	2 (8)	29 (23)	0.1
Severe Steatosis (%)	4 (37.5)	85 (69.1)	0.005
Severe Inflammation (%)	0	15 (11.9)	0.1

P value was calculated using independent t-test. Abbreviations: BMI: Body Mass Index; Homa-IR: Homeostatic Model Assessment for Insulin Resistance; ALT: Alanine Aminotransferase; AST: aspartate aminotransferase; GGT: gamma-glutamyl transferase; Fasting BSL: fasting blood sugar test; HDL-C: high-density lipoprotein cholesterol; LDL-C: low-density lipoprotein cholesterol.

3.3.6 Lean MAFLD patients have shorter telomere length in validation cohort

Consistently, patients with lean MAFLD had shorter telomere lengths compared with those with non-lean MAFLD in validation cohort (P=0.07) (**Fig. 3.4a**) as well as in the pooled cohort (P=<0.001) (**Fig. 3.4b**).

a)

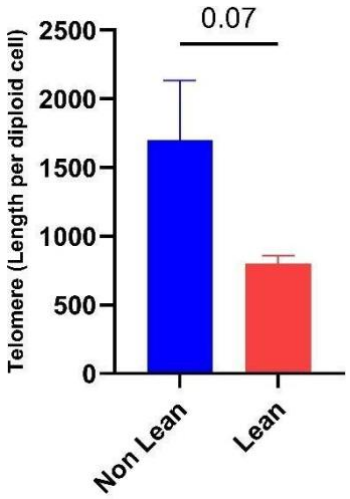

b)

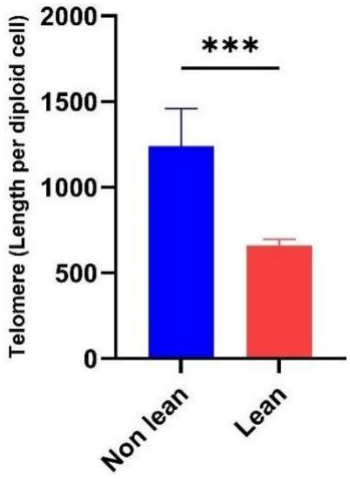

Figure 3.4: Telomere length is shorter in lean patients with MAFLD: a) validation cohort (n=151). **b)** Total cohort (n=303). Data are represented by vertical bars and are mean ± SEM. Statistical differences between groups are assessed by Mann‑Whitney test. *P<0.05, **P<0.01, ***P<0.001, ****P<0.0001.

3.3.7 Increased serum Malondialdehyde (MDA) in lean MAFLD

Having established robustly that lean MAFLD patients have shorter telomere length. I next explored potential mechanisms underlying this finding.

Oxidative stress is known to cause DNA damage and accelerate telomere shortening (220). I hypothesis that oxidative stress contributes to telomere attrition and poor outcomes in lean MAFLD.

To this end, serum levels of MDA, a marker of lipid peroxidation (221), were measured using ELISA, including 100 with lean MAFLD, and 100 were non-lean MAFLD. recruited at the Westmead hospital and with available serum samples. Consistently, compared to non-lean MAFLD, MDA levels were more frequently detected in serum from lean MAFLD patients (P=< 0.0001) (**Fig. 3.5**).

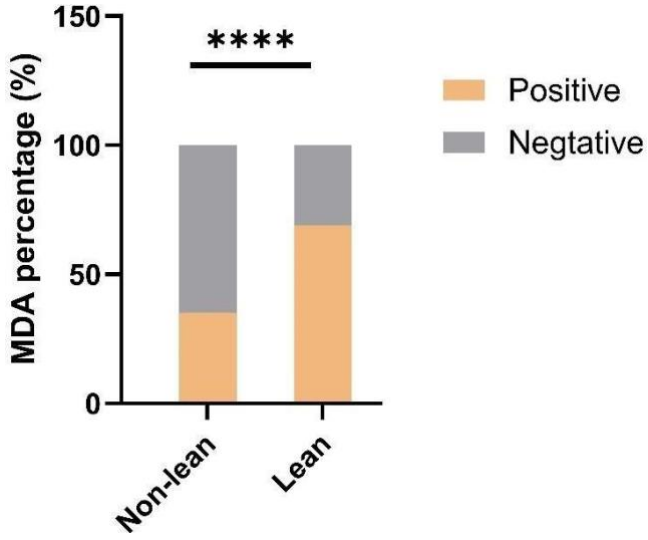

Figure 3.5: MDA positive percentage measured in the MAFLD cohort. Data are represented by vertical bars. Statistical differences between groups are assessed by Fisher's exact test (n=153). *P<0.05, **P<0.01, ***P<0.001, ****P<0.0001.

3.3.8 Patients with lean MAFLD have higher oxidative stress levels

To confirm this finding in liver, I examined 8-hydroxy- 2′-deoxyguanosine (8-OHdG), a marker of oxidative DNA damage, and 4-hydroxynonenal (4-HNE), a marker of lipid peroxidation and oxidative stress expression by immunohistochemistry (**Fig. 3.6a**) (222). This analysis showed that the expression of 8-OHdG and 4-HNE was increased in the liver of lean MAFLD patients compared to their non-lean counterparts (**Fig. 3.6b**).

a)

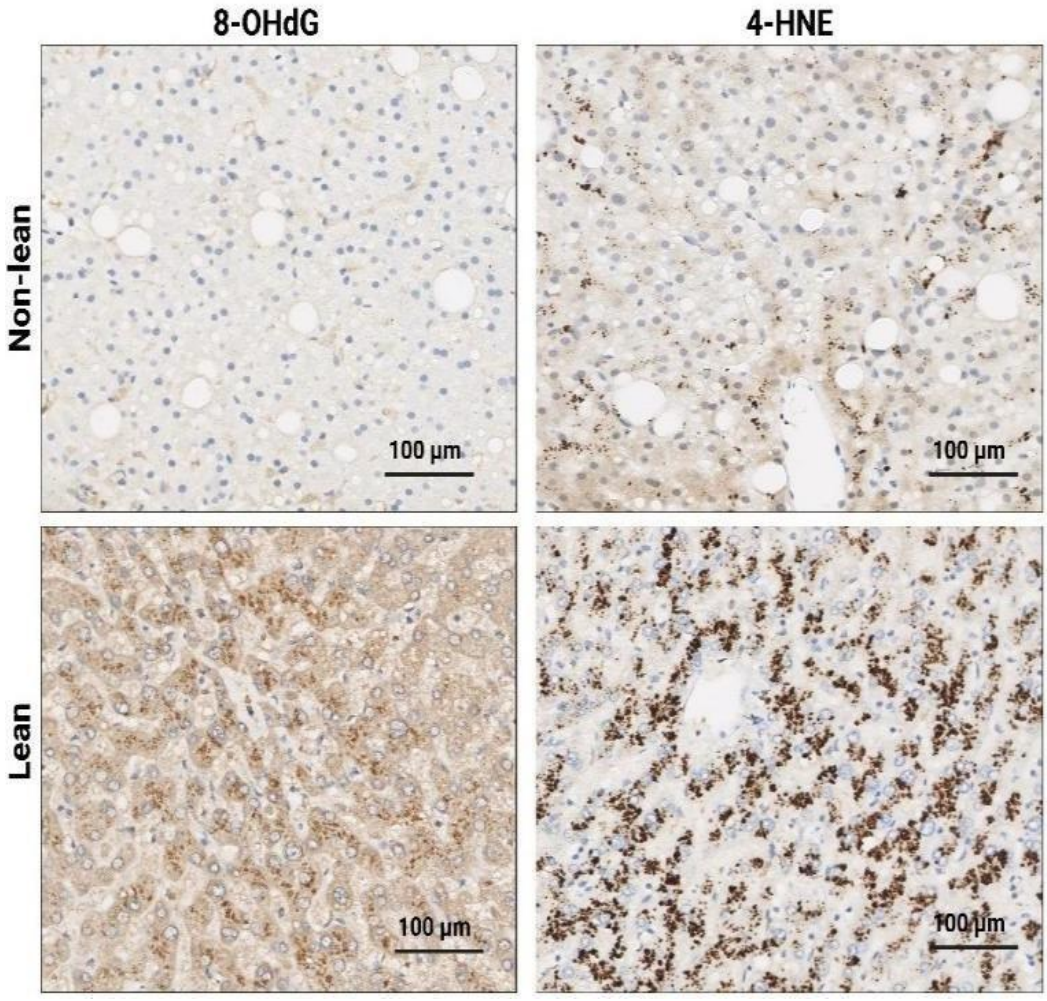

b)

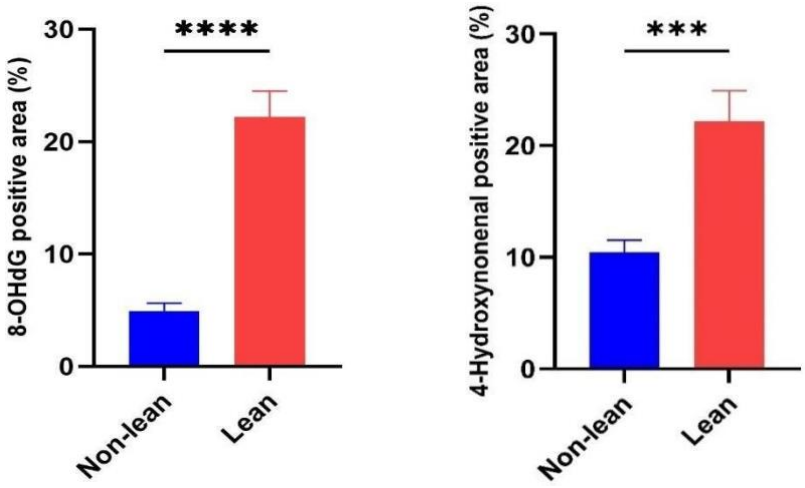

Figure 3.6: Oxidative stress measured in lean MAFLD. a) ROS signals including 8-OHdG and 4-HNE were measured by immunohistochemistry in lean and non-lean MAFLD patients (n=6). The scale bar in the images represents a length of 100 µm. **b)** quantification of 8-OHdG and 4-HNE by ImageJ. Data are represented by vertical bars and are mean ± SEM. Statistical differences between groups are assessed by Mann–Whitney test. *P<0.05, **P<0.01, ***P<0.001, ****P<0.0001.

3.3.9 ROS-mediated telomere attrition in hepatocytes following H_2O_2 exposure

I next thought to establish if modulation of ROS levels accounted for the association of lean MAFLD with shorter telomere lengths. To this end, I treated immortalized human hepatocytes (IHH), a hepatocyte cell line with H2O2 (300 nM) and measured the effect on telomere length. Telomere lengths were significantly decreased in H_2O_2- treated cells (**Fig. 3.7**).

Concurrent treatment with mitochondria targeted antioxidant (Mito-Tempo) (10μM), a ROS inhibitor, abolished H2O2- induced shortening of telomeres (**Fig. 3.7**), confirming the specificity of the effect.

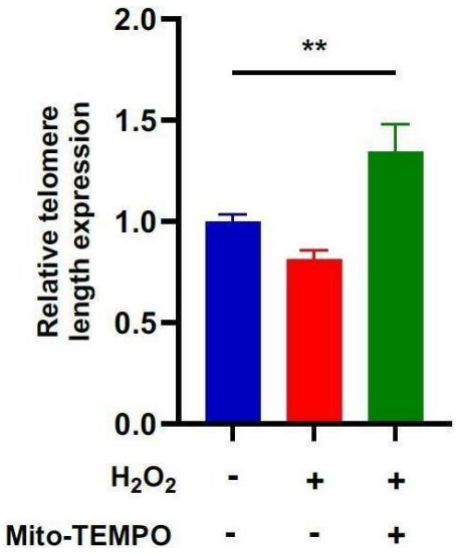

Figure 3.7: Effect of H_2O_2 and Mito-TEMPO on relative telomere length expression. Data are represented by vertical bars and are mean ± SEM. Statistical differences between groups are assessed by one–way ANOVA test. *P<0.05, **P<0.01, ***P<0.001, ****P<0.0001.

3.3.10 Hepatocyte telomerase activity and TERT expression decline following H_2O_2 exposure

In the same line, when treated with H_2O_2, hepatocytes exhibited a significant decrease in telomerase activity compared to mock-treated cells as measured by a telomerase repeat amplification protocol assay (**Fig. 3.8a**) and a reduction of Telomerase reverse transcriptase (TERT) protein expression measured by western blot (**Fig. 3.8b**).

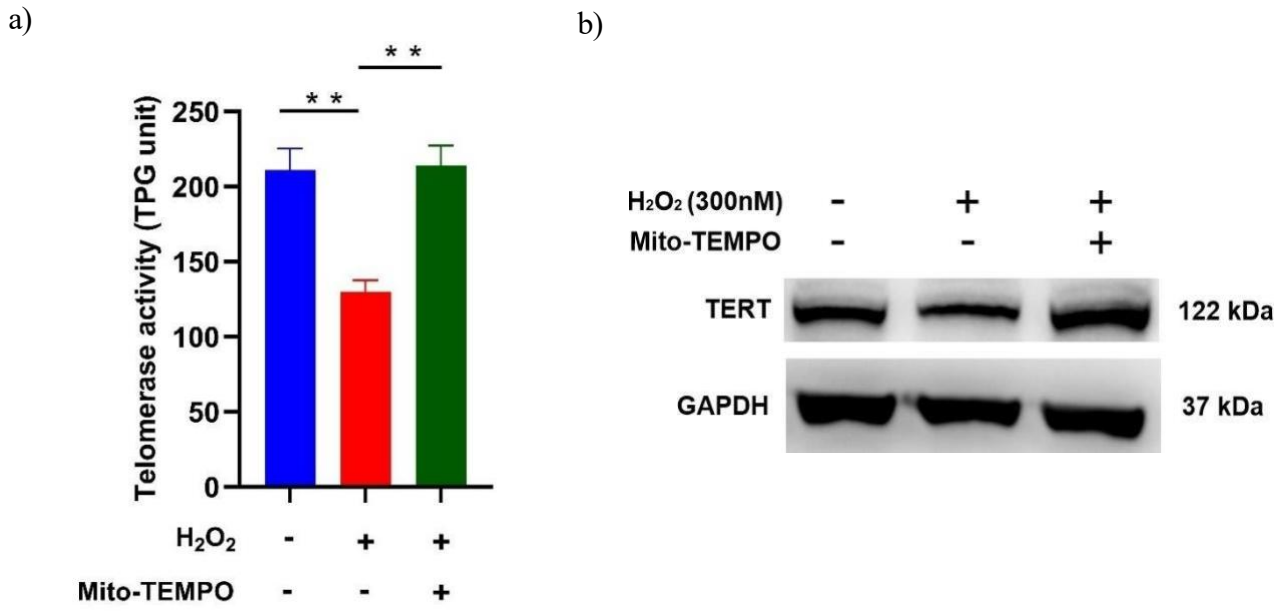

Figure 3.8: Effect of Mito-TEMPO on telomerase activity and TERT expression in H_2O_2-induced oxidative stress. a) Telomerase activity measured by telomerase repeat amplification procedure test (TRAP). **b)** TERT protein expression was evaluated by western blot analysis normalised to GAPDH. Data are represented by vertical bars and are mean ± SEM. Statistical differences between groups are assessed by ordinary one–way ANOVA test. *P<0.05, **P<0.01, ***P<0.001, ****P<0.0001. Abbreviation, TERT: Telomerase reverse transcriptase.

3.3.11 H_2O_2 exposure modulates shelterin complex components

Maintenance of telomere length is affected by telomerase as it recognizes the 3′-OH at the ends of chromosomes and adds telomere repeats de novo using an associated RNA template, Telomerase RNA component (TERC) (223).

In addition, the structure of telomeres is assembled in association with telomere-specific proteins, namely the shelterin complex comprising Protection of telomeres protein 1 (POT1), Telomeric repeat binding factor 1 (TRF1), and Telomeric repeat-binding factor 2 (TRF2). The shelterin complex binds to telomeric repeats and proper function of the complex is necessary to avoid induction of the redox DNA damage response (223).

Therefore, to investigate how H_2O_2 induces telomere shortening, RT-PCR was performed to quantify the mRNA expression levels of POT1, TRF1, TRF2, and TERC. Only the expression levels for POT1 and TRF2 were increased in cells that were treated with H_2O_2, this was reversed with Mito-Tempo, further ascertaining the specificity of this finding (**Fig. 3.9**).

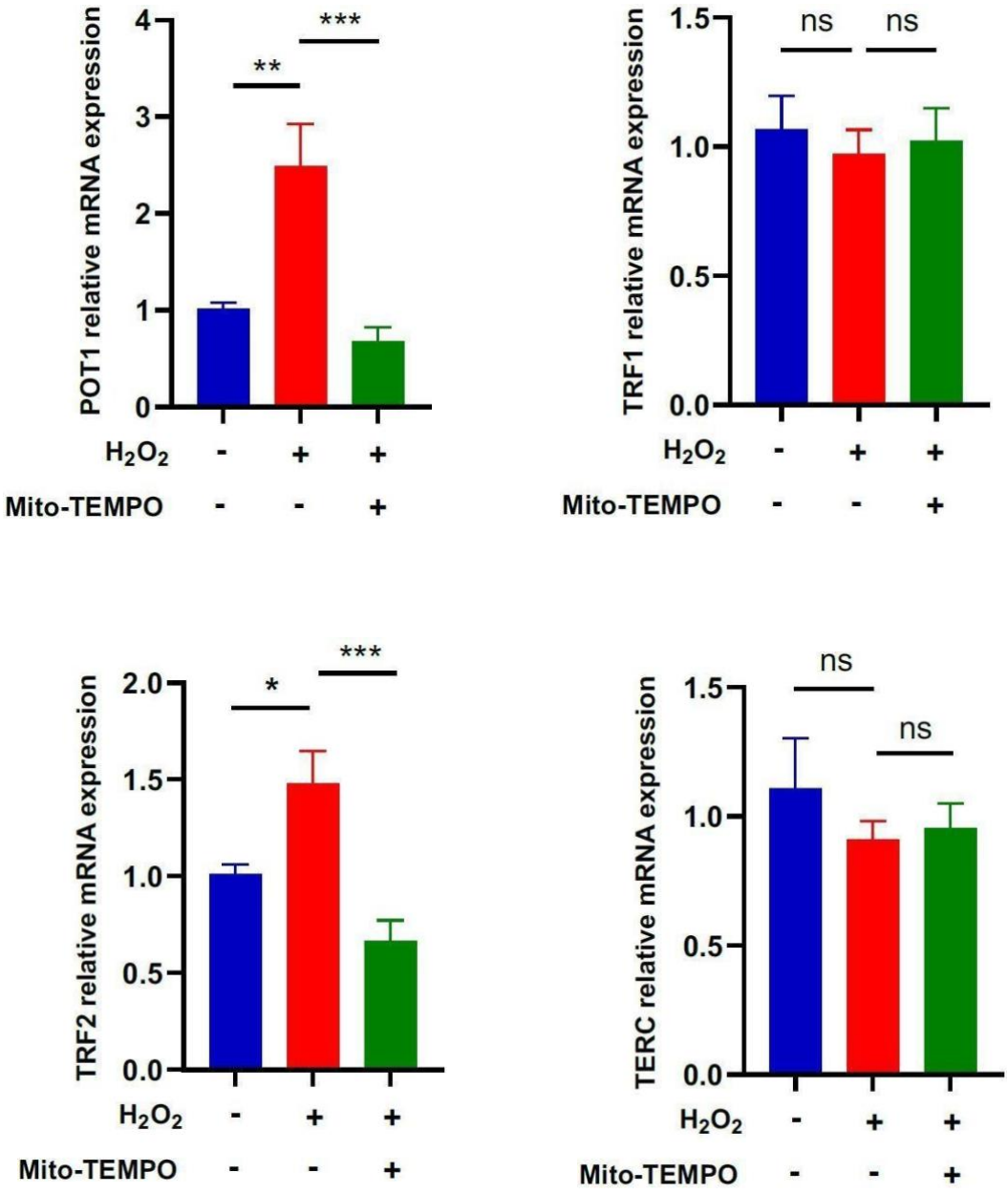

Figure 3.9: Modulation of telomere-specific proteins by H_2O_2. Data are represented by vertical bars and are mean ± SEM. Statistical differences between groups are assessed by ordinary one–way ANOVA test. *P<0.05, **P<0.01, ***P<0.001, ****P<0.0001.

3.3.12 Telomere length and mortality analysis in the NHANES cohort

Various studies and meta-analysis have shown that obese patients with MAFLD have better survival than their lean counterparts (216, 218). Finally, to further substantiate that my observed difference in telomere length could be actually an underlying explanation for this, I used the NHANES cohort the 1999-2002 cycle database with available Telomere length and mortality data (210).

During the specified period, DNA samples were collected from participants (≥20 years age). 7,827 out of the 21,004 participants provided DNA specimens and consented for future research. Of the 7,827 participants with available leucocyte telomere length, participants who were 85 years of age and older were eliminated from the study (n=226) to mitigate survivor bias. Pregnant individuals (n=445), participants who did not have the essential laboratory tests for defining liver disease (n=13), as well as subjects with viral hepatitis (HBV or HCV) (n=176), were excluded from the analysis. Thus, the study cohort comprised 6,967 individuals (**Fig. 3.10**).

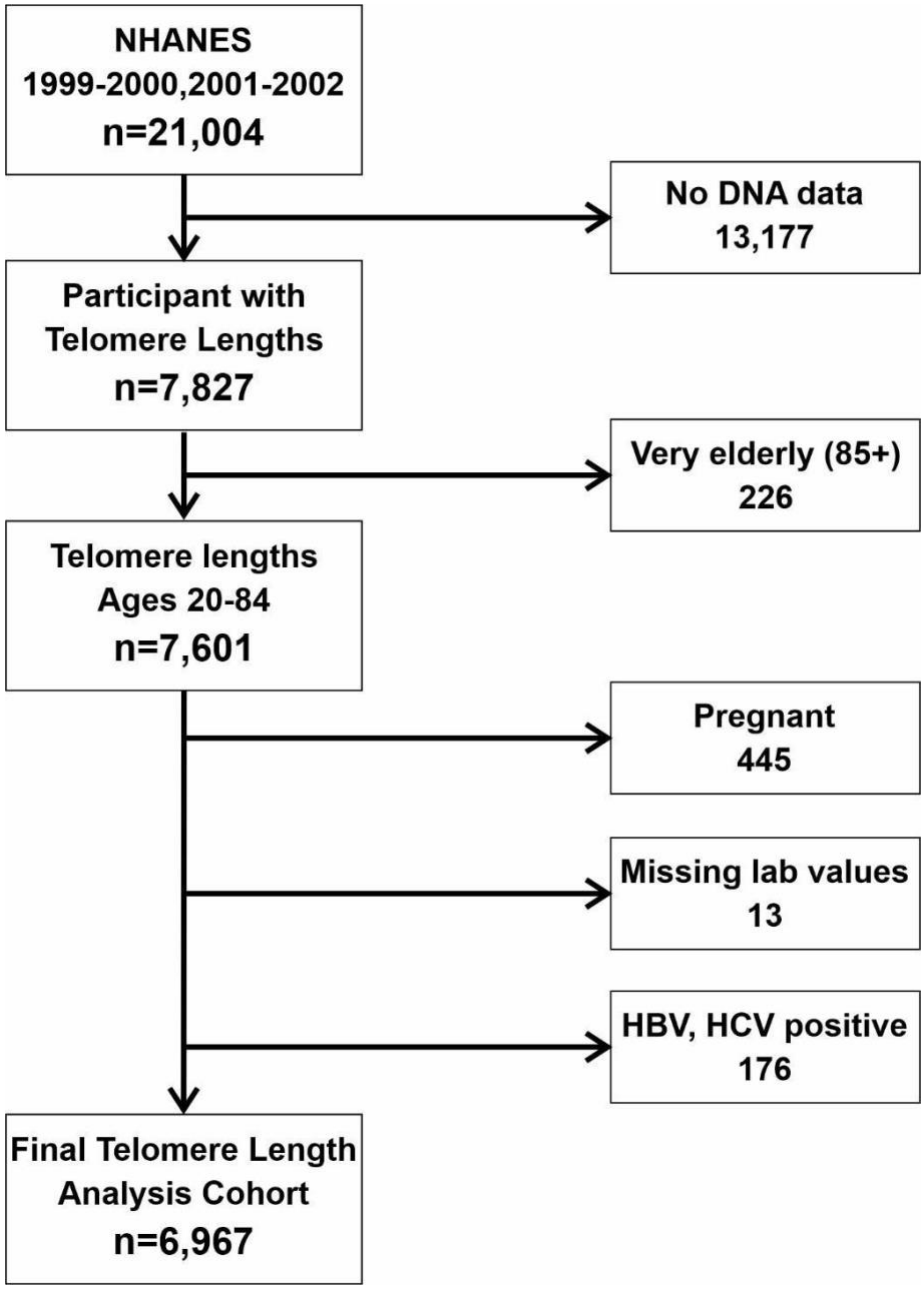

Figure 3.10: Flowchart of cohort selection for analysis from NHANES 1999-2002.

3.3.13 Telomere length and all-cause mortality in lean and non-lean individuals: NHANES 1999–2002

I examined the association between telomere length and survival among lean and non-lean groups in the NHANES cohort. The 6,964 participants from the telomere length analysis cohort with available mortality data had a median follow-up of 218 months (interquartile range, 202–233). During this period, all-cause cumulative mortality was 1,999 deaths (28.7%).

A decrease in telomere length was associated with increased all-cause mortality in the full cohort. The hazard ratio (HR) and 95% confidence intervals (CI) for the shortest quartile of leucocyte telomeres compared with the longest quartile was 1.412 (1.302–1.533; P=<0.001) in the univariate model and 1.374 (1.260–1.500; P=<0.001) in multivariate model after adjusting for age, sex, ethnicity, and fibrosis severity (**Table. 3.6**).

I then examined the relationship between telomere length and all-cause mortality stratified by lean and non-lean status. Univariate Cox regression analysis of lean (HR 1.5; 95% CI, 1.3-1.78; P=<0.001) and non-lean (HR 1.4; 95% CI,1.4-1.5; P=<0.001) and multivariate Cox regression analysis of lean (HR 1.5; 95% CI, 1.3-1.8; P=<0.001) and non-lean (HR 1.3; 95% CI, 1.2-1.5; P=<0.001) showed that the association between telomere shortening and mortality is more pronounced among lean (**Table. 3.6**).

Table 3.6: Univariable and multivariable Cox regression survival models in the NHANES cohort and in lean and non-lean subsets: Effect of telomere length quartiles (compared with longest telomere quartile [Quartile 1]) on all-cause mortality

	Univariable model HR (95% CI)	P value	Multivariable model HR (95% CI)	P value
Total population				
Quartile 1				
Quartile 2	1.298 (1.192-1.413)	<0.001	1.271 (1.165-1.387)	<0.001
Quartile 3	1.352 (1.242-1.472)	<0.001	1.324 (1.213-1.446)	<0.001
Quartile 4	1.412 (1.302-1.533)	<0.001	1.374 (1.260-1.500)	<0.001
Lean				
Quartile 1				
Quartile 2	1.382 (1.172-1.629)	<0.001	1.372 (1.160-1.624)	<0.001
Quartile 3	1.376 (1.168-1.621)	<0.001	1.378 (1.163-1.633)	<0.001
Quartile 4	1.524 (1.306-1.777)	<0.001	1.496 (1.269-1.764)	<0.001
Non-lean				
Quartile 1				
Quartile 2	1.266 (1.145-1.399)	<0.001	1.231 (1.111-1.364)	<0.001
Quartile 3	1.333 (1.206-1.474)	<0.001	1.291 (1.163-1.433)	<0.001
Quartile 4	1.365 (1.237-1.506)	<0.001	1.322 (1.191-1.468)	<0.001

P value was calculated for the test of trend across HR. Abbreviations: HR: hazard ratio; CI: confidence interval. The multivariable model was adjusted for age, sex, ethnicity, and severe fibrosis.

3.3.14 Association between telomere length and mortality in the presumed MAFLD cohort

Next, in another set of models created to confirm the observed relationship between telomere length and mortality is stand also with patient of MAFLD. A decrease in telomere length was associated with increased all-cause mortality in the full cohort of presumed MAFLD. The HR and 95% CI for the shortest quartile of leukocyte telomeres compared with the longest quartile was 1.400 (1.23–1.594; P=<0.001) in the univariate model and 1.393 (1.213–1.599; P=<0.001) in multivariate model after adjusting for age, sex, ethnicity, and fibrosis severity (**Table. 3.7**). I then examined the relationship between telomere length and all-cause mortality stratified by lean and non-lean status. Univariate Cox regression analysis of lean (HR 1.581; 95% CI, 1.162-2.151; P=<0.001) and non-lean (HR 1.363; 95% CI, 1.179-1.575; P=<0.001). The multivariate Cox regression analysis of lean (HR 1.526; 95% CI ,1.093-2.130; P=<0.001) and non-lean (HR 1.354; 95% CI, 1.160-1.580; P=<0.001) showed that the association between telomere shortening and mortality is more pronounced among lean presumed MAFLD (**Table. 3.7**).

Table 3.7: Univariable and multivariable Cox regression survival models in the presumed MAFLD cohort and in lean and non-lean subsets: Effect of telomere length quartiles (compared with longest quartile [Quartile1]) on all-cause mortality

	Univariable model HR (95% CI)	P value	Multivariable model HR (95% CI)	P value
Total population				
Quartile 1				
Quartile 2	**1.377 (1.208-1.571)**	**<0.001**	**1.370 (1.198-1.568)**	**<0.001**
Quartile 3	1.463 (1.282-1.669)	<0.001	1.467 (1.279-1.682)	<0.001
Quartile 4	**1.400 (1.23-1.594)**	**<0.001**	**1.393 (1.213-1.599)**	**<0.001**
Lean				
Quartile 1				
Quartile 2	1.437 (1.050-1.967)	0.02	1.403 (1.013-1.945)	0.04
Quartile 3	**1.558 (1.139-2.129)**	**0.005**	**1.541 (1.107-2.144)**	**0.01**
Quartile 4	1.581 (1.162-2.151)	0.004	1.526 (1.093-2.130)	0.01
Non-lean				
Quartile 1				
Quartile 2	**1.369 (1.183-1.583)**	**<0.001**	**1.365 (1.176-1.584)**	**<0.001**
Quartile 3	1.436 (1.240-1.663)	<0.001	1.434 (1.231-1.670)	<0.001
Quartile 4	**1.363 (1.179-1.575)**	**<0.001**	**1.354 (1.160-1.580)**	**<0.001**

P value was calculated for the test of trend across HR. Abbreviations: HR: hazard ratio; CI: confidence interval. The multivariable model was adjusted for age, sex, ethnicity, and severe fibrosis.

3.3.15 Association between continuous telomere length and mortality in lean and non-lean MAFLD

In addition, when telomere length was represented as a continuous variable, a decrease in telomere length was associated with an increased risk of all-cause mortality of total population in the univariate model (HR 1.508; 95% CI, 1.275–1.782; P=<0.001) and in multivariate model (HR 1.519; 95% CI, 1.265–1.825; P=<0.001) (**Table. 3.8**).

I then stratified the telomere length into lean and non-lean. This again was more profound among lean patients with MAFLD in univariate model (HR 1.728; 95% CI, 1.190–2.511; P=0.004) and in multivariate model (HR 1.712; 95% CI, 1.125–2.606; P=0.01), non-lean univariate model (HR 1.455; 95% CI, 1.204–1.759; P=<0.001) and in multivariate model (HR 1.461; 95% CI, 1.188–1.796; P=<0.001) (**Table. 3.8**).

Table 3.8: Univariable and multivariable Cox regression survival model in the presumed MAFLD cohort and in lean and non-lean subsets: Effect of telomere length (as a continuous variable) on all-cause mortality

	Univariable model HR (95% CI)	P value	Multivariable model HR (95% CI)	P value
Total population				
	1.508 (1.275-1.782)	<0.001	1.519 (1.265-1.825)	<0.001
Lean				
	1.728 (1.190-2.511)	0.004	1.712 (1.125-2.606)	0.01
Non-lean				
	1.455 (1.204-1.759)	<0.001	1.461 (1.188-1.796)	<0.001

P value was calculated for the test of trend across HR. Abbreviations: HR: hazard ratio; CI: confidence interval. The multivariable model was adjusted for age, sex, ethnicity, and severe fibrosis.

3.4 Discussion

Lean individuals represent a significant subgroup of MAFLD patients who experience worse long-term outcomes despite more favorable metabolic and histological features at diagnosis (224). Still, the underlying mechanisms driving disease progression in this population remain poorly understood (225).

In this chapter, I identified an unrecognized mechanism that helps explain the apparent contradiction, demonstrating that lean MAFLD patients have significantly shorter telomeres compared to their non-lean counterparts. This shortening is strongly associated with higher oxidative stress, more fibrosis, and increased all-cause mortality, which at least partially accounts for this clinical paradox.

Previous studies suggest that lean MAFLD exhibits distinct metabolic adaptations, including increased bile acid signaling and upregulation of the Farnesoid X Receptor (FXR) pathway. These changes are thought to contribute to more favorable metabolic and histological features (103). However, the long-term clinical results of lean patients remain challenging to understand (68, 216). The current work presents a novel testable hypothesis that identifies telomere shortening as the reason behind these paradoxical clinical findings. I speculate that due to the energy costly maintenance of telomere, this telomere attrition in lean MAFLD patients represents the unwanted negative consequences of the adaptive metabolic mechanisms among them, in line with the metabolic telomere attrition hypothesis (219).

The fundamental principle of the costly maintenance hypothesis states that telomere maintenance requires energy expenditure for both preventing telomere shortening and extending telomeres (68). The body shortens telomeres as an adaptive response when energy demands become extremely high or metabolic stress occurs to redirect essential resources toward urgent processes(219). The body chooses to support survival functions that require

immediate attention instead of investing energy in sustaining long telomeres (219). The prolonged existence of metabolic stress, as in the case of MAFLD and telomere shortening, could lead to detrimental effects on survival rates.

To further clarify the underlying mechanisms of these changes in telomere among lean MAFLD, I explored if it is mediated by changes in oxidative stress, a known primary factor responsible for telomere shortening (226). Consistently, I confirmed that patients with lean MAFLD have increased circulating and tissue ROS levels, which I confirmed to induce telomere shortening and decrease telomeric activity in hepatocyte cell line. An effect could be reversed using specific ROS inhibitors, further ascertaining the specificity of this pathway.

To further clarify the underlying mechanisms for these effects, my study showed that the mRNA expression level of telomere length regulatory proteins TRF2 and POT1 function, which acts as cis-negative regulators of telomere length (227) increased in hepatocytes when exposed to H_2O_2 under oxidative stress conditions, implying that ROS contributes to telomere shortening in hepatocytes by inducing the expression of both POT1 and TRF2.

Mitochondria represent the main site of ATP synthesis and are considered the powerhouse of the cells, but they also produce most of the endogenous ROS (228). The process of ATP production creates a natural trade-off between energy supply and oxidative stress reduction, as ROS production increases with ATP generation efficiency. The shift in the trade-off between energy production and ROS generation could ultimately contribute to the discerned telomere shortening in lean MAFLD patients.

Recent evidence indicates that telomere attrition is consistently linked to higher mortality across a diverse range of diseases, including cardiovascular, respiratory, hepatic, digestive, and musculoskeletal diseases (217). Notably, my analysis utilizing the NHANES cohort, revealed that the relationship between telomere length and mortality varies between lean and non-lean

patients with liver disease, as it was more pronounced in lean individuals. Supporting this observation, a recent study using the same cohort found an inverse association between leukocyte telomere length and advanced fibrosis exclusively in lean participants, with no significant association observed in non-lean individuals (229).

The strengths of this study include the use of both large-scale population data and well characterized clinical cohorts and supportive functional analysis, aiming to address the long-standing clinically relevant paradox of the natural history of lean MAFLD patients. However, several limitations include, first, that telomere length was assessed in whole blood, rather than liver tissue or specific blood cells. However, previous studies have shown that measurements in peripheral blood strongly correlate with telomere length in liver tissue (230). Second, due to the cross-sectional nature of our study, the telomere length data were obtained from a single time point. However, this analysis was supported by our analysis in the NHANES cohort, with available outcome data.

In summary, my study identifies shorter telomere length as a significant and independent predictor of increased fibrosis and higher all-cause mortality in patients with lean MAFLD, which is mediated by greater oxidative stress compared to their non-lean counterparts. This telomere shortening was closely associated with worse clinical outcomes. These findings suggest that telomere dynamics, driven by oxidative stress, may help explain the poor long-term prognosis in this subgroup. Recognizing telomere shortening as a marker of disease severity offers a potential avenue for improved risk stratification and targeted intervention in lean MAFLD.

Chapter 4: GDF-15 and mortality in Lean MAFLD

4.1 Introduction

While lean individuals with MAFLD often appear metabolically healthier compared to their non-lean counterparts, they paradoxically experience higher mortality (231, 232). In the previous chapter, I identified that lean MAFLD patients had greater oxidative stress and shorter telomeres than non-lean MAFLD patients, suggesting that stress-induced telomere shortening may contributing to poorer outcomes (233, 234). This observation may be driven by impaired increases in ROS production, which can not only damage DNA and accelerate telomere shortening (228), but may also limits the activation of protective stress-response pathways such as GDF-15 (235).

GDF-15 is a key stress-responsive cytokine that has been implicated in various adverse health outcomes and is widely used as a marker of increased mortality risk (236). GDF-15 is induced under physiological stress such as that resulting from an obesogenic diet, and play a role in regulating energy homeostasis (237). Furthermore, it is induced by mitochondrial stress and can reduce oxidative stress and ROS generation (238). Therefore, impaired GDF-15 signaling may hinder mitochondrial stress adaptation, promote oxidative damage, and contribute to telomere attrition in lean MAFLD. One potential mechanism underlying this dysregulation is DNA methylation, which can suppress GDF-15 transcription and lower circulating protein levels (239, 240). In this chapter, I explore the hypothesis that epigenetic suppression of GDF-15 contributes to greater oxidative stress, telomere shortening, and increased mortality risk in lean MAFLD. To test this, I examined differences in circulating GDF-15 andGDF15 between lean and non-lean MAFLD patients, and their correlation with telomere length in a biopsy-proven MAFLD cohort from Westmead Hospital and the National Health and Nutrition Examination Survey (NHANES) dataset, respectively. This was complemented by in vitro hepatocyte experiments to validate the mechanistic effects of GDF-15 on oxidative stress and

telomere regulation.

4.2 Method

Patient cohort

A total of 153 patients with biopsy-proven MAFLD were included from Westmead Hospital, Australia.

Lean MAFLD was defined according to the international consensus guidelines (209). Individuals with dual aetiologies were excluded, including concomitant diagnosis of excess alcohol intake (> 20 g per day for females and > 30 g per day for males), chronic viral hepatitis (hepatitis B and hepatitis C), and drug-induced liver injury.

Ethics approval was obtained from the Human Research Ethics Committees of the Western Sydney Local Health District and the University of Sydney.

The NHANES database from 1999 to 2002 which collected blood samples from adults aged 50 years and above for DNA purification purposes was used (210). Among the 21,004 participants, 2,532 had their DNAm-GDF15 measured. 189 participants were excluded due to incomplete mortality data and therefore the final analysis cohort comprised 2,343 individuals. Mortality data were obtained by linking participant information from NHANES to the NDI. Follow-up time was calculated from the date of the initial survey to the earlier of either the most recent mortality update or the NDI database cut-off date (December 31, 2019). The main outcomes assessed were deaths from all-cause mortality, cardiovascular mortality, cancer mortality and other cause mortality.

Cell culture and molecular assays

IHH were cultured in Williams' E medium supplemented with 10% fetal bovine serum and 1% penicillin/streptomycin. Cells were treated with H2O2 with or without GDF-15. Total RNA

was extracted and converted to cDNA, and gene expression of GDF-15 was assessed using RT-PCR (reverse transcription-polymerase chain reaction). In addition, GDF-15 protein levels were quantified by ELISA.

Telomerase activity assay

Telomerase activity was measured using the TRAPeze telomerase detection kit. Cell lysates were processed with telomerase repeat amplification procedure (TRAP) PCR under standard cycling conditions. Products were separated by agarose gel electrophoresis and visualized with ethidium bromide using a ChemiDoc imaging system.

Statistical analysis

Data analysis was conducted with GraphPad Prism software version 10. Data are presented as the mean ± standard error of the mean (SEM). One-way analysis of variance (ANOVA) was used for multi-group research, whereas the student's t-test was applied for two groups comparisons. IBM SPSS Statistics was used for the analysis of public datasets. P-value <0.05 denote the presence of a statistically significant difference.

4.3 Results

4.3.1 Circulating GDF-15 protein levels are associated with inflammation and fibrosis in MAFLD

GDF-15 is a mitochondrial stress–induced cytokine known to raise in response to inflammation and tissue injury (241, 242). To assess whether GDF-15 reflects disease severity in MAFLD, I measured circulating GDF-15 protein levels in the serum samples in a cohort of 153 MAFLD patients by ELISA. In this analysis, no difference in levels of GDF-15 was observed according to steatosis stage (**Fig. 4.1a**), but this was observed according to inflammation level and fibrosis stage, respectively (**Fig. 4.1b, c**).

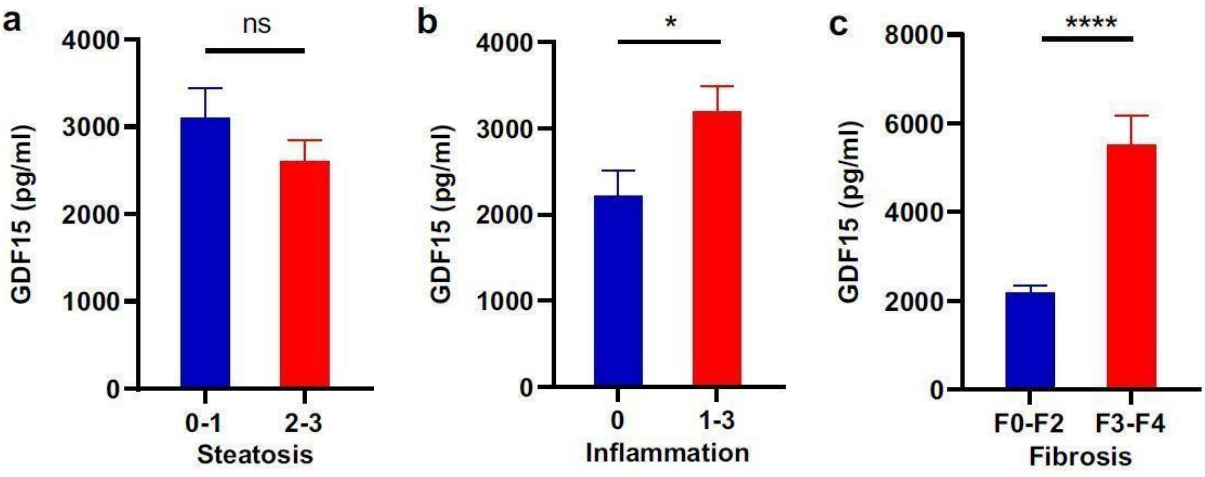

Figure 4.1: Circulating GDF-15 protein levels and histological features in patients with MAFLD: a) steatosis, **b)** inflammation, **c)** fibrosis. Data are represented by vertical bars and are mean ± SEM. Statistical differences between groups are assessed by Mann–Whitney test. *P<0.05, **P<0.01, ***P<0.001, ****P<0.0001.

Next, in a multivariable logistic regression analysis, the association between circulating GDF-15 protein levels and fibrosis remained significant after adjusting for age, BMI, sex, ALT, and platelets (OR=1.001; 95% CI: 1.000–1.001; P=<0.001) (Table. 4.1).

Table 4.1: Multivariable analysis of factors associated with fibrosis stage ≥3

Variable	Odd Ratio	95% CI	P value
GDF-15 (pg/ml)	1.001	1.000-1.001	<0.001
Age (years)	0.98	0.93-1.03	0.4
Male	3.39	1.02-11.27	0.04
AST (IU/mL)	1.009	0.99-1.02	0.1
Platelets (×109/L)	0.99	0.98-0.99	0.01

P value was calculated using multivariable logistic regression analysis. Abbreviations: GDF-15: Growth differentiation factor 15; AST: Aspartate aminotransferase.

4.3.2 Circulating GDF-15 protein levels are lower in lean compared to non-lean MAFLD patients

Given that GDF-15 is a marker of mitochondrial stress and inflammation (243), and lean MAFLD patients were previously found to have elevated oxidative stress and telomere shortening in chapter 3. I then investigated whether GDF-15 protein levels differed by BMI. Patients with lean MAFLD were found to have significantly lower GDF-15 protein levels compared with their non-lean counterparts (P=0.03) (**Fig. 4.2**).

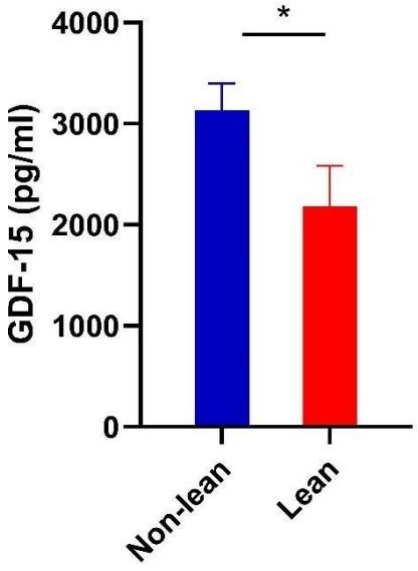

Figure 4.2: Mean concentration of GDF-15 protein levels in patients with lean and non-lean MAFLD. Data are represented by vertical bars and are mean ± SEM (n=153). Statistical differences between groups are assessed by Mann–Whitney test. *p<0.05, **p<0.01, ***p<0.001, ****p<0.0001.

To determine whether circulating GDF-15 protein levels are independently associated with lean MAFLD. I performed multivariable logistic regression. The association between GDF-15 protein levels and lean MAFLD remained significant after adjusting for age, BMI, sex, ALT, and platelets in a multivariable logistic regression analysis (OR=1.000; 95% CI: 1.000–1.001; P=0.03). (**Table. 4.2**).

Table 4.2: Multivariable analysis of factors associated with lean MAFLD

Variable	Odd Ratio	95% CI	P value
GDF-15 (pg/ml)	1.000	1.000-1.001	0.03
Age (years)	0.98	0.94-1.02	0.4
Male	0.85	0.32-2.29	0.7
AST (IU/mL)	0.99	0.98-1.009	0.5
Platelets (×109/L)	0.99	0.99-1.005	0.6

P value was calculated using multivariable logistic regression analysis. Abbreviations: GDF-15: Growth differentiation factor 15; AST: Aspartate aminotransferase.

4.3.3 DNAm-GDF15 levels are elevated in lean MAFLD

As I have identified that circulating GDF-15 protein levels were lower in lean compared to non-lean MAFLD patients. I next considered whether this reduction could be due to epigenetic silencing. Therefore, I next investigated if the DNAm-GDF15 levels differ between those with lean and non-lean MAFLD. This analysis was performed in the NHANES database, where among the 21,004 participants, 2,343 had their DNAm-GDF15 measured. Consistently, DNAm-GDF15 levels were significantly elevated in lean compared to non-lean MAFLD patients (951.6±151.7 vs. 918.9±143.7, P=0.01, respectively) (**Fig. 4.3**).

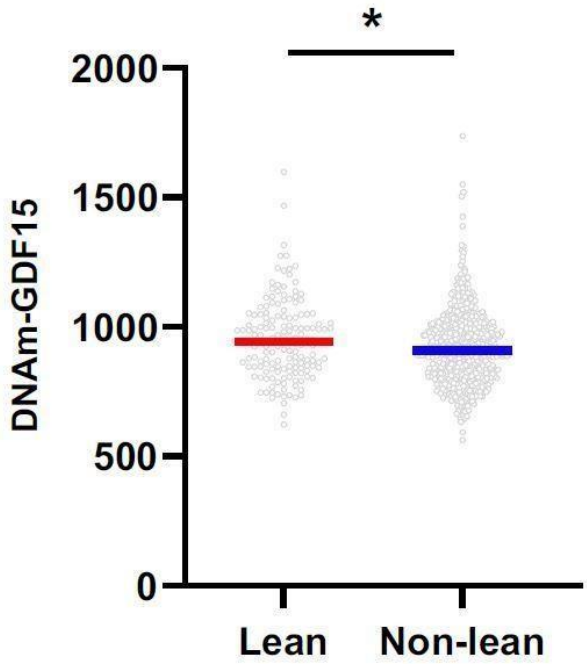

Figure 4.3: DNAm-GDF15 comparison between lean MAFLD and non-lean MAFLD. Data are represented by individual values and are median. Statistical differences between groups are assessed by Mann-Whitney test. *p<0.05, **p<0.01, ***p<0.001, ****p<0.0001.

4.3.4 Higher DNAm-GDF15 predicts increased all-cause mortality

DNA methylation also has the potential to affect gene expression and is being increasingly examined as a predictor of disease risk and mortality (244). Given the elevated DNAm-GDF15 in lean MAFLD patients, I next examined whether higher DNAm-GDF15 predicts mortality in a large population cohort. The study included 2,343 participants from the NHANES database with available DNAm-GDF15 and outcome data who had a median follow-up of 250 months (interquartile range, 123-226). During this period, all-cause cumulative mortality was 1,202 deaths (51.3%).

First, I explored the link between DNA methylation-predicted GDF15 (DNAm-GDF15) levels stratified by quartiles and all-cause mortality in the overall cohort. In this analysis, a stepwise increase in mortality risk with higher DNAm-GDF15 quartiles was observed, with individuals in the highest quartile (Q4) exhibited a (HR: 8.33; 95% CI: 6.84–10.15, P<0.001) for all-cause mortality compared to those in the lowest quartile (Q1) (**Fig. 4.4**).

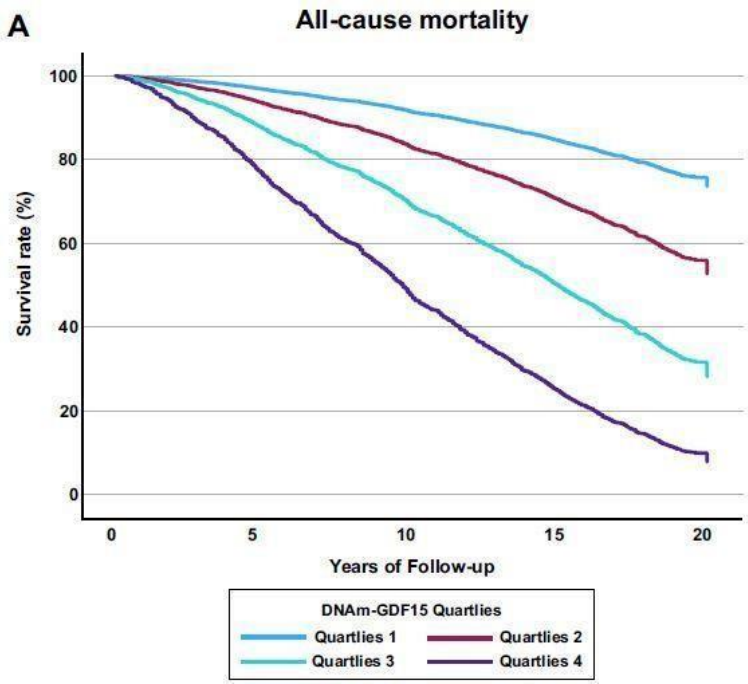

Figure 4.4: Mortality stratified by DNAm-GDF15 quartiles in the all-cause mortality. Data presented by Cox Regression survival curves.

4.3.5 Stepwise increase in cause-specific mortality across DNAm-GDF15 quartiles

After establishing that higher DNAm-GDF15 is associated with increased all-cause mortality. I next examined whether this epigenetic marker is associated with cause-specific mortality. Similarly, individuals in the highest quartile (Q4) exhibited higher cardiovascular disease (CVD)-related mortality (HR: 20.53; 95% CI: 13.22–31.87; P<0.001) **(Fig. 4.5a**), cancer-related mortality (HR: 9.78; 95% CI: 6.65–14.38; P<0.001) (**Fig. 4.5b**), and other causes mortality (HR: 11.91; 95% CI: 9.07–15.65; P<0.001) (**Fig. 4.5c**). compared to those in the lowest quartile (Q1).

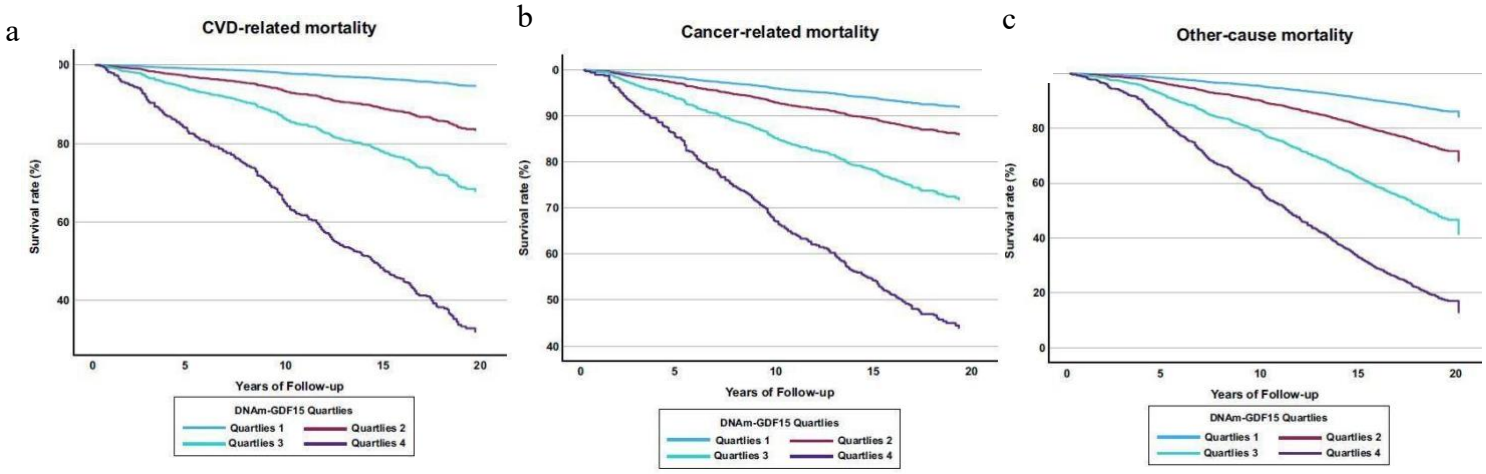

Figure 4.5: Mortality stratified by DNAm-GDF15 quartiles in cause-specific mortality. a) CVD-related mortality. **b)** Cancer-related mortality. **c)** Other causes mortality. Data presented by Cox Regression survival curves.

4.3.6 Independent association of DNAm-GDF15 with all-cause and cause-specific mortality

To confirm that DNAm-GDF15 is independently associated with mortality outcomes, I also performed multivariate Cox regression analysis using quartiles of DNAm-GDF15 after adjusting for age, sex, ethnicity, ALT, AST. The association remained significant with the hazard ratio for the highest quartile of DNAm-GDF15 compared with the lowest quartile was (HR: 2.52; 95% CI: 1.93–3.28; P<0.001) for all-cause mortality, (HR: 3.7; 95% CI: 2.10–6.51; P<0.001) for CVD-related mortality, (HR: 2.66; 95% CI: 1.56–4.53; P<0.001) for cancer-related mortality, and (HR: 2.81; 95% CI: 1.95–4.05; P<0.001) for other causes of death (**Table. 4.4**).

Table 4.4: Multivariate Cox regression analysis of DNAm-predicted GDF-15 and risk of all-cause and cause-specific mortality in overall cohort

	Overall cohort HR (95% CI)	P value
All-cause mortality		
Quartile 1		
Quartile 2	1.35 (1.08-1.68)	0.008
Quartile 3	1.79 (1.41-2.27)	<0.001
Quartile 4	2.52 (1.93-3.28)	<0.001
CVD related mortality		
Quartile 1		
Quartile 2	1.77 (1.08-2.88)	0.02
Quartile 3	2.18 (1.29-3.66)	0.003
Quartile 4	3.7 (2.1-6.51)	<0.001
Cancer related mortality		
Quartile 1		
Quartile 2	1.09 (0.7-1.67)	0.6
Quartile 3	1.57 (0.99-2.51)	0.05
Quartile 4	2.66 (1.56-4.53)	<0.001
Other cause related mortality		
Quartile 1		
Quartile 2	1.32 (0.97-1.81)	0.07
Quartile 3	1.8 (1.29-2.51)	<0.001
Quartile 4	2.81 (1.95-4.05)	<0.001

P value was calculated using the test of trend of HR. The multivariable model was adjusted for age, sex, ethnicity, ALT, AST. Abbreviations: HR: hazard ratio; CI: confidence intervals; CVD: cardiovascular disease.

4.3.7 DNAm-GDF15 as a predictor of increased all-cause mortality in the presumed MAFLD cohort

After I confirmed the association between DNAm-GDF15 and mortality in the overall cohort, then I investigated whether the same relationship exists within the subgroup of individuals with presumed MAFLD. Notably, a similar trend was observed within the subset of 789 patients with presumed MAFLD, 158 (20%) of them were lean. The mortality risk increased with higher DNAm-GDF15 quartiles, with individuals in the highest quartile (Q4) exhibiting a (HR: 8.18; 95% CI: 5.78–11.59; P<0.001) for all-cause mortality compared to those in the lowest quartile (Q1) (**Fig. 4.6**).

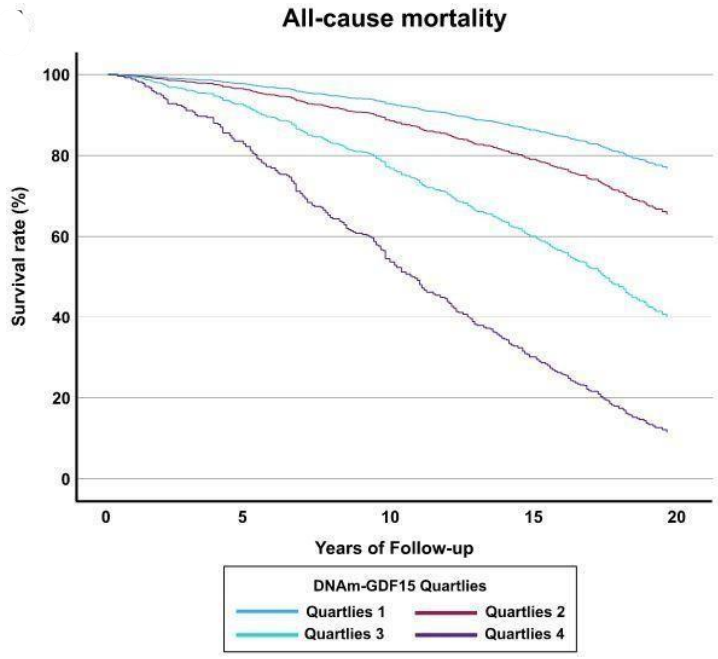

Figure 4.6: Mortality stratified by DNAm-GDF15 quartiles in the all-cause mortality of presumed MAFLD cohort. Data presented by Cox Regression survival curves.

4.3.8 Higher DNAm-GDF15 predicts CVD, cancer, and other causes mortality in the presumed MAFLD cohort

I next examined whether this epigenetic marker is also associated with cause-specific mortality in the presumed MAFLD cohort. A stepwise increase in mortality risk with higher DNAm-GDF15 quartiles was observed. Individuals in the highest quartile (Q4) exhibited for cause-specific mortality compared to those in the lowest quartile (Q1), namely cardiovascular disease (CVD)-related mortality (HR: 19.8; 95% CI: 8.32–47.16; P<0.001) (**Fig. 4.7a**), cancer-related mortality (HR: 10.57; 95% CI: 5.25–21.29; P<0.001) **(Fig. 4.7b**), and other causes mortality (HR: 10.15; 95% CI: 6.45–15.97; P<0.001) (**Fig. 4.7c**).

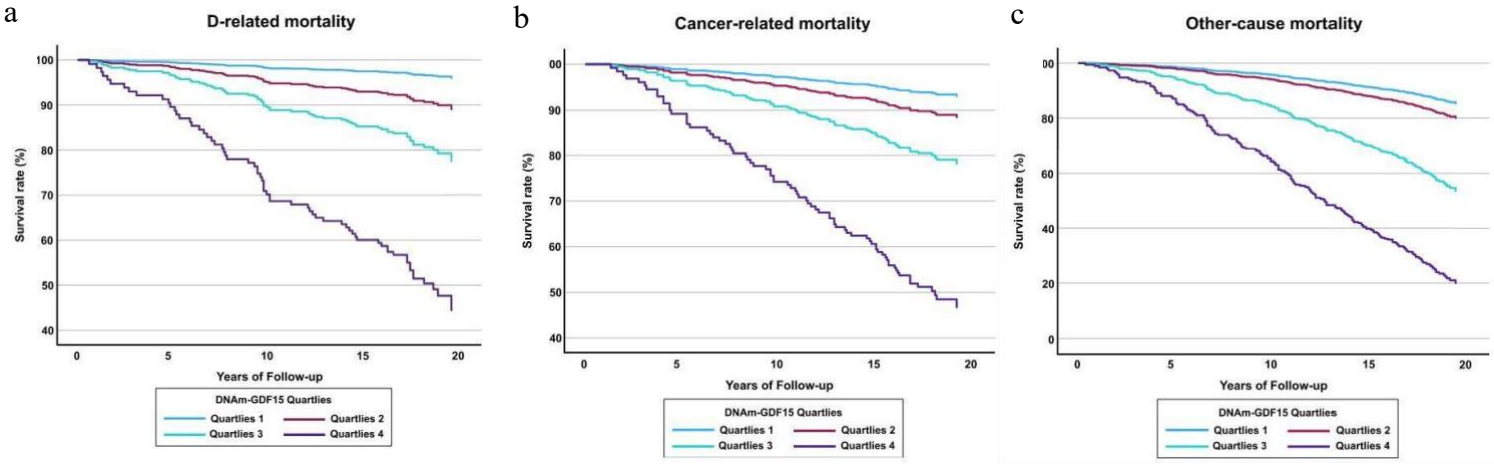

Figure 4.7: Mortality stratified by DNAm-GDF15 quartiles in cause-specific mortality of presumed MAFLD cohort. a) CVD-related mortality**. b)** Cancer-related mortality. **c)** Other causes mortality. Data presented by Cox Regression survival curves.

4.3.9 Mortality risk increases across DNAm-GDF15 quartiles in MAFLD cohort

To confirm that DNAm-GDF15 is independently associated with mortality outcomes, I performed multivariate Cox regression using quartiles of DNAm-GDF15 after adjusting for age, sex, ethnicity, ALT, AST. The association remained significant with the hazard ratio of the highest quartile of DNAm-GDF15 compared with the lowest quartile was (HR: 3.19; 95% CI: 2.00–5.07; P<0.001) for all-cause mortality, (HR: 3.34; 95% CI: 1.06–10.52; P=0.04) for CVD-related mortality, (HR: 7.48; 95% CI: 3.11–17.95; P<0.001) for cancer-related mortality, and (HR: 3.07; 95% CI: 1.62–5.82; P<0.001) for other causes of death (**Table. 4.5**).

Table 4.5: Multivariate Cox regression analysis of DNAm-predicted GDF-15 and risk of all-cause and cause-specific mortality in presumed MAFLD cohort

	Presumed MAFLD HR (95% CI)	P value
All-cause mortality		
Quartile 1		
Quartile 2	1.21 (0.82-1.77)	0.3
Quartile 3	1.86 (1.24-2.79)	0.003
Quartile 4	3.18 (2.-5.07)	<0.001
CVD related mortality		
Quartile 1		
Quartile 2	1.59 (0.63-3.98)	0.3
Quartile 3	1.73 (0.64-4.7)	0.2
Quartile 4	3.34 (1.06-10.51)	0.039
Cancer related mortality		
Quartile 1		
Quartile 2	1.34 (0.65-2.75)	0.425
Quartile 3	2.65 (1.22-5.78)	0.014
Quartile 4	7.47 (3.11-17.95)	<0.001
Other cause related mortality		
Quartile 1		
Quartile 2	1.03 (0.61-1.75)	0.891
Quartile 3	1.81 (1.04-3.13)	0.034
Quartile 4	3.06 (1.61-5.81)	<0.001

P value was calculated using the test of trend of HR. The multivariable model was adjusted for age, sex, ethnicity, ALT, AST. Abbreviations: HR: hazard ratio; CVD: cardiovascular disease.

4.3.10 Negative association between DNAm-GDF15 and telomere length, stronger in lean MAFLD

Telomere length is negatively associated with morality risk (245), and patients with lean MAFLD were found to have shorter telomere length, linked with the observed higher mortality in them compared with their non-lean counterparts in the chapter 3.

Thus, I next sought to determine whether DNAm- GDF15 level correlated with telomere length. Consistently, a significant negative correlation between DNAm-GDF15 and telomere length was discerned (r=–0.19, P<0.0001) (**Fig. 4.8a**). This negative correlation was stronger in lean (r= –0.23, P=0.003) (**Fig. 4.8b**) compared to non-lean MAFLD subjects (r= –0.19, P<0.0001) (**Fig. 4.8c**).

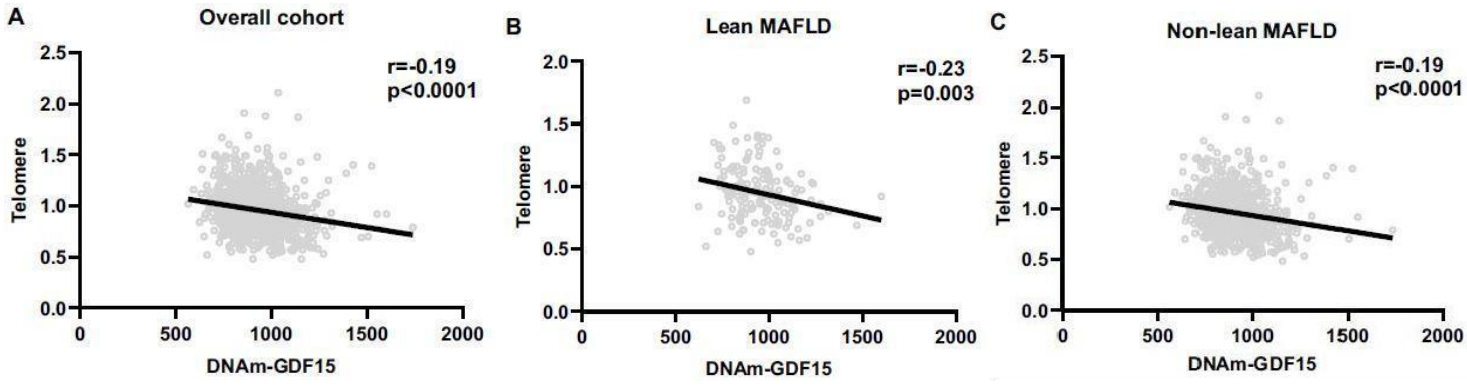

Figure 4.8: Correlation between DNAm-GDF15 and Telomere. a) Overall cohort. **b)** Lean MAFLD cohort. **c)** Non-lean MAFLD cohort. Data were analysed using Spearman's rank correlation. *p<0.05, **p<0.01, ***p<0.001, ****p<0.0001.

4.3.11 DNAm-GDF15 mediates the association between telomere length and mortality

To explore whether DNAm-GDF15 levels mediate the correlation between telomere length and mortality, I conducted a mediation analysis. The analysis revealed that while longer telomere length was associated with a reduced risk of mortality, with a direct effect size of -1.02 (P<0.001), interestingly, the indirect effect mediated by DNAm-GDF15 was more profound, with an effect size of -1.15 (P=0.008) (**Fig. 4.9**).

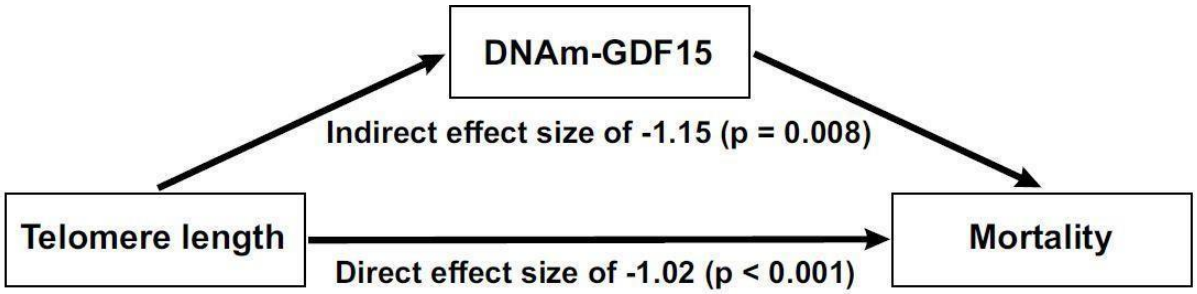

Figure 4.9: Mediation analyses of DNAm-GDF15, telomere effect on mortality.

Data were analysed using mediation analysis. *p<0.05, **p<0.01, ***p<0.001, ****p<0.0001.

4.3.12 GDF-15 prevents oxidative stress-induced telomere attrition in hepatocytes

Finally, to experimentally validate the role of GDF-15 in protecting against telomere damage under oxidative stress, I pretreated IHH cells with GDF-15 before challenging with H_2O_2, a known inducer of ROS and telomere damage (246). GDF-15 led to a marked reverse of the H_2O_2 effect on telomere length (**Fig. 4.10a**) and telomerase activity (**Fig. 4.10b**).

a b

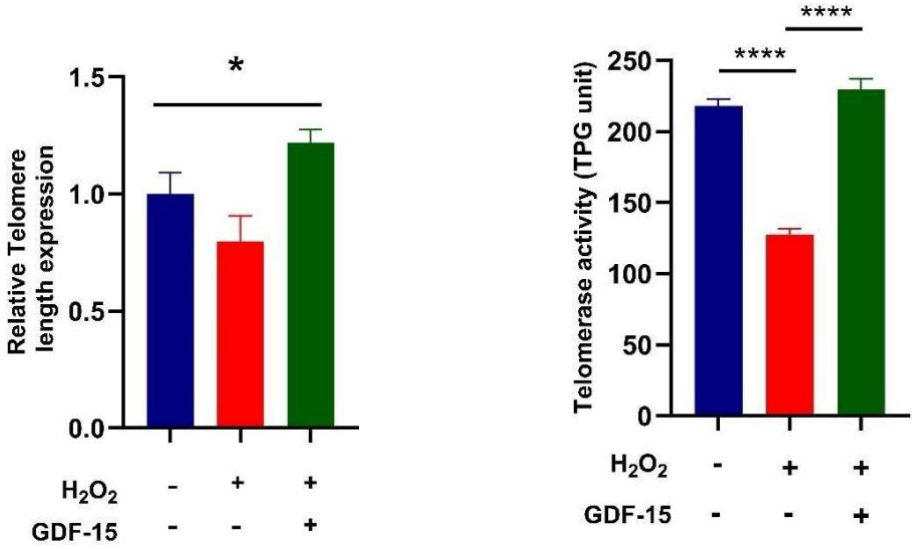

Figure 4.10: Role of the GDF-15 in regulating telomere length: a) Relative telomere length expression. **b)** Telomerase activity in IHH cells challenged with H2O2 (n=3). Data are represented by vertical bars and are mean ± SEM. Statistical differences between groups are assessed by Ordinary one-way ANOVA test. *p<0.05, **p<0.01, ***p<0.001, ****p<0.0001.

4.4 Discussion

In this chapter, I identified a novel additional and possibly hitherto unknown mechanism that provides an integrated explanation of the observed paradox of increased mortality risk among lean MAFLD patients, despite having more favorable metabolic profiles, compared to their non-lean MAFLD counterparts. Collectively, my findings demonstrate that lean MAFLD patients have significantly lower circulating GDF-15 protein compared with their non-lean MAFLD counterparts. Consistently, DNAm-GDF15 was elevated in lean MAFLD patients relative to non-lean patients, and higher DNAm-GDF15 was strongly associated with both all-cause and cause-specific mortality. DNAm-GDF15 also showed a negative correlation with telomere length, which was more pronounced in lean MAFLD. Mediation analysis further revealed that DNAm-GDF15 mediates the association between telomere attrition and mortality. Finally, GDF-15 treatment significantly reversed the effect of H2O2 on telomere length.

To elaborate, the clinical trajectory of lean MAFLD is still not well understood. Recently, it was identified that this entity represents a distinct entity mediated by metabolic adaptations, including enhanced bile acid signaling, which initially contributes to a more favorable histological profile. However, as the disease progresses, these adaptations may become ineffective, potentially due to endotoxemia-driven epigenetic changes that attenuate bile acid signalling (103, 104).

Paradoxically, despite more favorable clinical and metabolic characteristics, epidemiological evidence consistently shows that lean MAFLD patients have higher mortality rates than their obese counterparts (247, 248). My findings across this chapter and previous chapter suggest that telomere attrition, driven by heightened oxidative stress and reduced GDF-15 levels, may explain this paradox.

The increased levels of serum and hepatic lean individuals with MAFLD in the previous chapter may be explained by the current finding of suppressed GDF-15 protein levels. GDF-15 is known to reduce oxidative stress by modulating mitochondrial membrane potential and limiting ROS production. A reduction in GDF-15 may impair this protective mechanism against oxidative stress, leading to elevated ROS levels (249, 250). This finding is consistent with evidence from the general population, where GDF-15 is recognized as a stress-responsive cytokine typically elevated in individuals with obesity compared to healthy lean individuals (251).

Interestingly, previous studies have found no significant difference in fibroblast growth factor 21 (FGF-21) levels between lean and non-lean MAFLD patients (142, 252) FGF-21 is another important hepatic metabolite that responds to mitochondrial dysfunction and plays a role in systemic metabolic adaptation to the mitochondrial integrated stress response (253). The unique suppression of GDF-15 in lean MAFLD patients suggests a specific role for this pathway in this population.

To explain the reduction of GDF-15, my study demonstrates that DNAm-GDF15 levels are significantly elevated in individuals with lean MAFLD compared to non-lean MAFLD, supporting the hypothesis that DNA methylation may epigenetically suppress GDF-15 expression. Given that hypermethylation is known to downregulate gene transcription (254), this mechanism likely contributes to the lower circulating GDF-15 levels observed in these patients. Notably, elevated DNAm-GDF15 levels were strongly associated with increased all-cause and cause-specific mortality, independent of potential confounders, underscoring their prognostic significance.

A negative correlation between DNAm-GDF15 and telomere length was more pronounced in

lean MAFLD, and mediation analysis indicated that DNAm-GDF15 mediates the association between telomere shortening and mortality. Collectively, these findings suggest that DNAm-GDF15 may represent a potential pathway linking telomere attrition, mitochondrial dysfunction, and adverse clinical outcomes in lean MAFLD.

This study has several strengths, including the integration of a large-scale population-based cohort with another well-characterized biopsy-proven cohort. It employs a multipronged analytical approach, incorporating cause-specific mortality data, mediation analysis, and mechanistic analysis. Together, these methods provide valuable insights into a long-standing clinical paradox of lean MAFLD. However, the study also has multiple noteworthy limitations. The small sample size of lean MAFLD patients and the lack of data on methylation and GDF15 expression within the same cohort restrict the potential for direct causal inferences. Additionally, DNAm-GDF15 was measured in peripheral blood rather than in liver tissue within the NHANES dataset.

In conclusion, my work in this chapter identifies that individuals with lean MAFLD have significantly lower circulating levels of GDF-15 compared to their non-lean MAFLD counterparts. Additionally, they have elevated DNAm-GDF15 levels that were found to inversely correlate with telomere length, while also showing a positive correlation with higher mortality risk. This presents a novel mechanism that explains the increased mortality risk in lean MAFLD patients compared to those who are non-lean.

Chapter 5: Differential mitochondrial profile in lean MAFLD

5.1 Introduction

Lean MAFLD represents a substantial subgroup, accounting for approximately 20% of all patients with MAFLD worldwide (68, 78). Despite this, lean patients remain less investigated than their non-lean counterparts, and the mechanisms that drive disease in this population are poorly defined (255).

Mitochondria are essential hubs of metabolism, energy homeostasis, and redox balance. They generate ATP through oxidative phosphorylation and produce ROS that activate adaptive stress pathways (256, 257). When mitochondrial structure or function is impaired, protective signaling fails, leading to hepatocellular injury, inflammation, and fibrosis (258, 259). While mitochondrial impairment is well recognized in metabolic liver disease (260), it remains unclear whether lean and non-lean MAFLD differ in their mitochondrial profile including structure, function, or adaptive capacity.

Building on my findings from Chapter 4, I demonstrated that lean MAFLD is characterised by suppressed circulating GDF-15 protein levels and elevated DNAm-GDF15, consistent with epigenetic suppression of GDF-15 expression and impaired stress adaptation. Given that GDF-15 is a stress-responsive cytokine induced by mitochondrial dysfunction (261), its suppression in lean MAFLD suggested that mitochondrial features may differ in this subgroup.

This chapter therefore tests the hypothesis that mitochondrial differ between lean and non-lean MAFLD. To address this, I compared mitochondrial morphology, mtDNA content, and respiratory complex expression in lean versus non-lean MAFLD, using both well-established dietary mouse models and human liver tissue. By integrating ultrastructural and molecular data, this chapter characterises the mitochondrial profile of lean MAFLD.

5.2 Methods

Molecular assays

Mitochondrial DNA (mtDNA) was extracted from frozen mouse liver tissue and analysed following the manufacturer's protocols. Total RNA was extracted from mouse models and converted to cDNA, and gene expression of oxidative phosphorylation complexes components was assessed using RT-PCR (reverse transcription-polymerase chain reaction). Protein expression of oxidative phosphorylation complexes was examined by Western blot analysis using liver tissue lysates.

Anial Models

Several dietary models for MAFLD have been developed such as the Methionine-Choline-Deficient (MCD) diet and the High Cholesterol (ChR) diet model, which represent lean MAFLD, as well as the High-Fat Diet (HFD) model for non-lean disease. Animal experimental protocols received approval from the Western Sydney Local Health District animal ethics committee (Ethics protocol: 4249, 4302) and adhered to the guidelines set by the Australian Council on Animal Care.

Transmission electron microscopy (TEM)

Human liver biopsies and mouse frozen liver samples were collected. The samples were embedded and sectioned into ultrathin slices. The prepared tissue sections were examined using transmission electron microscopy.

Statistical analysis

Data analysis was conducted with GraphPad Prism software version 10. Data are presented as the mean ± standard error of the mean (SEM). The Mann-Whitney test was applied for two-group comparisons.

5.3 Results

5.3.1 Lean MAFLD have a larger mitochondrial size in mouse models

Building on my Chapter 4 findings of suppressed GDF-15 protein, and given that GDF-15 is a key mitochondrial regulator (261), I next examined whether mitochondrial morphology differs between lean and non-lean groups. To address this, I used dietary mouse models: mice were fed either a MCD diet for 6 weeks or a HFD for 24 weeks. Mice on the MCD diet remain lean while developing MAFLD, recapitulating features of lean MAFLD, aligning with findings from other studies (262, 263). In contrast, mice on a HFD exhibit weight gain and characteristics of non-lean MAFLD, mirroring aspects of non-lean disease (264). To assess the difference in mitochondrial size between lean MCD and non-lean HFD, I performed transmission electron microscopy (TEM) on liver tissue and found that mitochondria were larger in MCD than in HFD (**Fig. 5.1**).

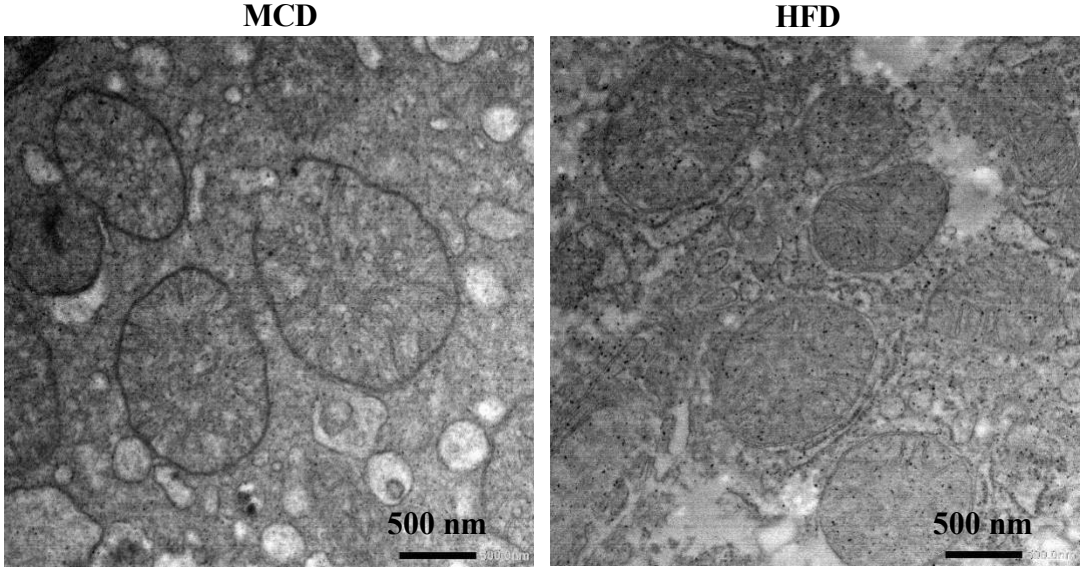

Figure 5.1: Representative TEM images of mouse liver mitochondria (MCD vs HFD). Representative TEM images (n=2 per group) of mouse liver mitochondria. Scale bar, 500 nm.

5.3.2 Quantification of mitochondrial area, perimeter and length in mice liver tissue

To further assess the mitochondrial ultrastructure in liver tissue, I measured the area, perimeter, and length. Mitochondrial area (P=0.01; **Fig. 5.2a**), perimeter (P=0.04; **Fig. 5.2b**) and length (P=0.01; **Fig. 5.2c**) were significantly increased in MCD mice compared to HFD.

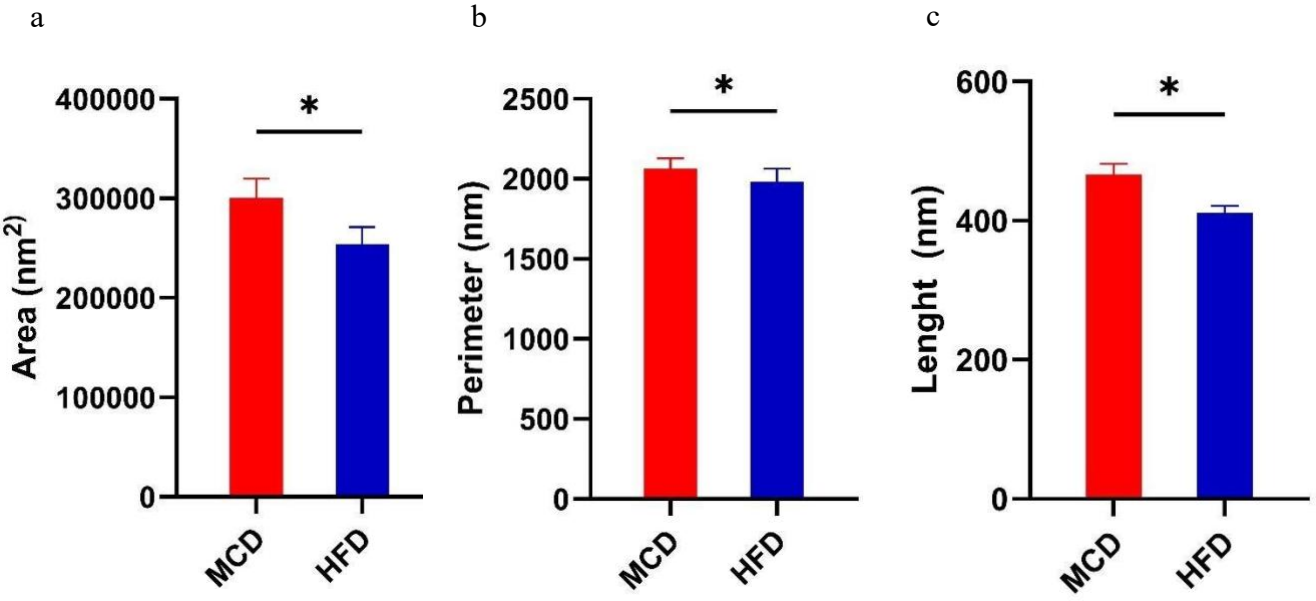

Figure 5.2: Mitochondrial size metrics in mouse liver. a) area. **b)** perimeter. **c)** length. Over 100 mitochondria in each group were quantified for area, perimeter and length. Data are represented by vertical bars and are mean ± SEM. Statistical differences between groups are assessed by Mann-Whitney test. *p<0.05, **p<0.01, ***p<0.001, ****p<0.0001.

5.3.3 Clinical and histopathological characteristics of lean and non-lean MAFLD patients for TEM study

To validate the findings observed in the mouse model, I next examined liver biopsy samples from patients with lean and non-lean MAFLD. The clinical and histopathological characteristics of these patients are summarised in (**Table 5.1**).

Table 5.1: Clinical and histopathological characteristics of lean and non-lean MAFLD patients.

	Lean MAFLD (n = 2)	Non-lean MAFLD (n = 2)
Age (years)	**50.5 ± 6.5**	**62 ± 14**
Male (%) **Female (%)**	 2 (100)	1 (50) 1 (50)
BMI (kg/m2)	**23.2 ± 0.17**	**28.9 ± 3.13**
Homa-IR	20.6 ± 2.1	3.7 ± 5.9
ALT (IU/mL)	**36 ± 15**	**33 ± 17**
AST (IU/mL)	27 ± 8	17 ± 2
GGT (IU/L)	**149.5 ± 123.5**	**32 ± 5**
Platelets (× 109 /L)	204 ± 4	338.5 ± 132.5
Total cholesterol (mmol/L)	**4.4 ± 0.1**	**3.3 ± 0.3**
Triglyceride (mmol/L)	0.9 ± 0.2	2.4 ± 1.3
Fibrosis (F0-F1) (%)	**2 (100)**	**2 (100)**

Abbreviations: BMI: Body Mass Index; Homa-IR: Homeostatic Model Assessment for Insulin Resistance; ALT: Alanine Aminotransferase; AST: aspartate aminotransferase; GGT: gamma-glutamyl transferase

5.3.4 Lean MAFLD patients also show enlarged mitochondria

Consistently, transmission electron microscopy of liver biopsy samples showed larger mitochondrial size in lean than in non-lean MAFLD (**Fig. 5.3**).

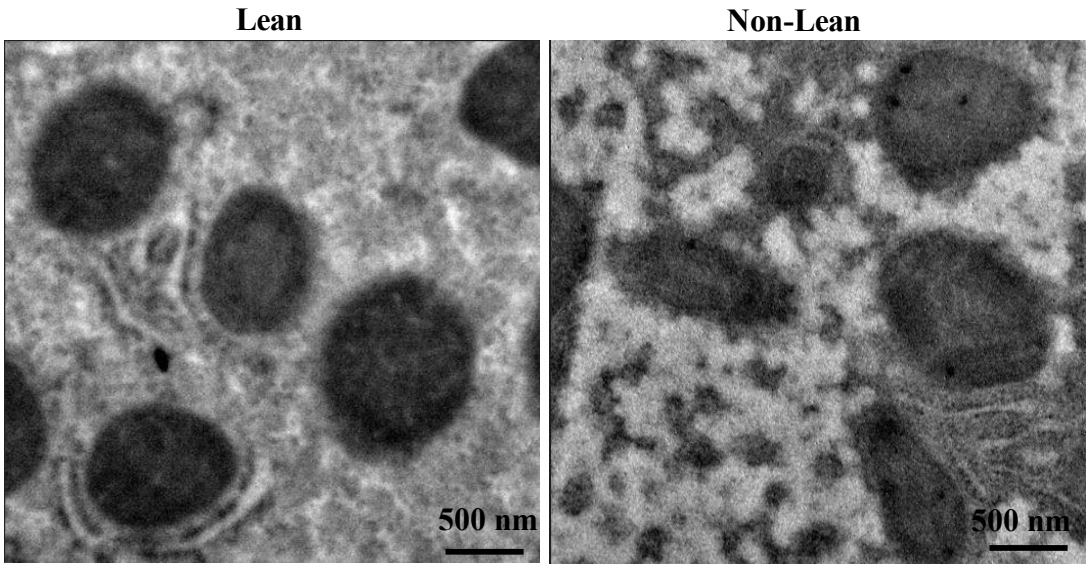

Figure 5.3: Representative TEM images of human liver mitochondria (lean vs non-lean MAFLD). Representative TEM images (n=2 per group) of human liver mitochondria. Scale bar, 500 nm.

5.3.5 Quantification of mitochondrial area, perimeter and length in human liver biopsy

To further assess the mitochondrial ultrastructure in liver biopsy tissue, I measured the area, perimeter and length. Mitochondrial area (P=<0.0001; **Fig. 5.4a**), perimeter (P=<0.0001; **Fig. 5.4b**) and length (P=0.01; **Fig. 5.4c**) were significantly increased in lean liver biopsies compared to non-lean MAFLD.

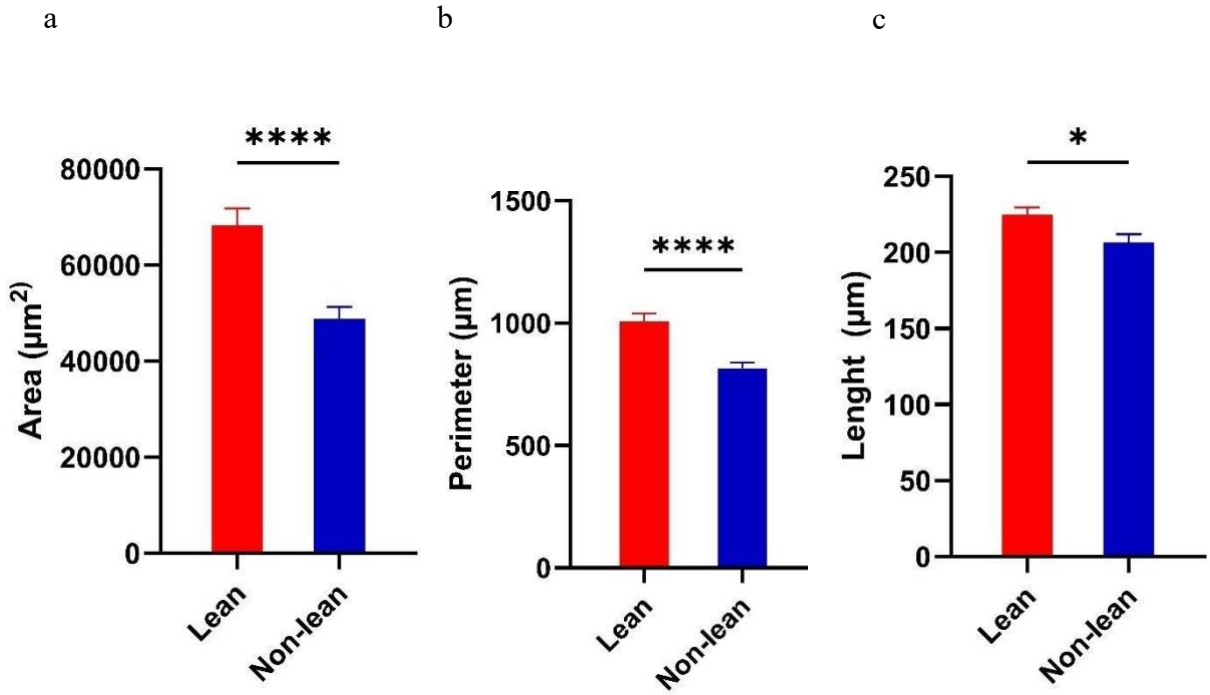

Figure 5.4: Mitochondrial size metrics in human liver biopsies. a) area. **b)** perimeter. **c)** length. Over 100 mitochondria in each group were quantified for area, perimeter and length. Data are represented by vertical bars and are mean ± SEM. Statistical differences between groups are assessed by Mann-Whitney test. *p<0.05, **p<0.01, ***p<0.001, ****p<0.0001.

5.3.6 Reduced mRNA expression of mitochondrial complexes in the lean MAFLD mouse model

To further explore the differential mitochondrial profiles of the lean and obese two subtypes of MAFLD, I examined the hepatic mRNA expression of mitochondrial complexes in the MCD and HDF mouse models. These complexes are crucial components of oxidative phosphorylation and are essential for the production of ATP. A significant reduction in mRNA expression of mitochondrial respiratory complexes was observed for complex I (CI) (P=0.0002) (**Fig. 5.5a**), complex III (CIII) (P=0.002) (**Fig. 5.5c**), and complex IV (CIV) (P=0.0002) **(Fig. 5.5d**) in MCD compared with HFD.

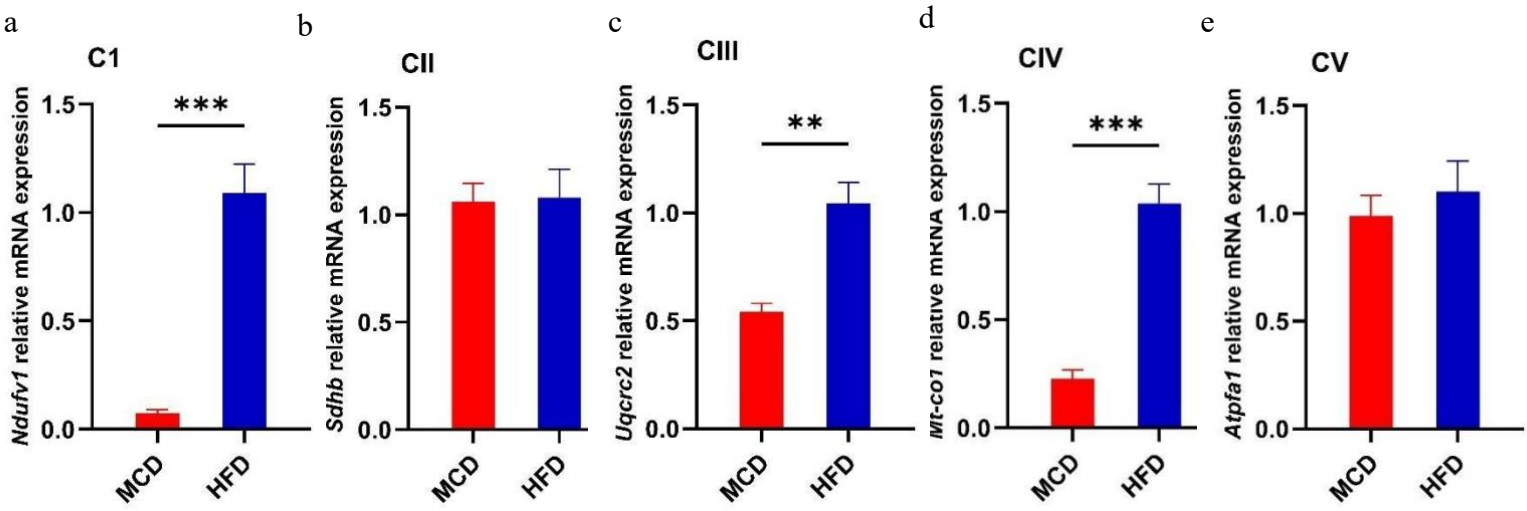

Figure 5.5: Reduced mRNA expression of mitochondrial respiratory complexes in the MCD model. a) CI. **b)** CII. **c)** CIII. **d)** CIV. **e)** CV. Data are represented by vertical bars and are mean ± SEM. Statistical differences between groups are assessed by Mann-Whitney test. *p<0.05, **p<0.01, ***p<0.001, ****p<0.0001.

5.3.7 Decreased mitochondrial complex protein expression in lean MAFLD mouse model

To complement the mRNA expression findings, western blotting was used to assess protein expression of mitochondrial complexes. Consistently, protein expression of complexes I–V was markedly decreased (~70–80%) in MCD compared with HFD (**Fig. 5.6**).

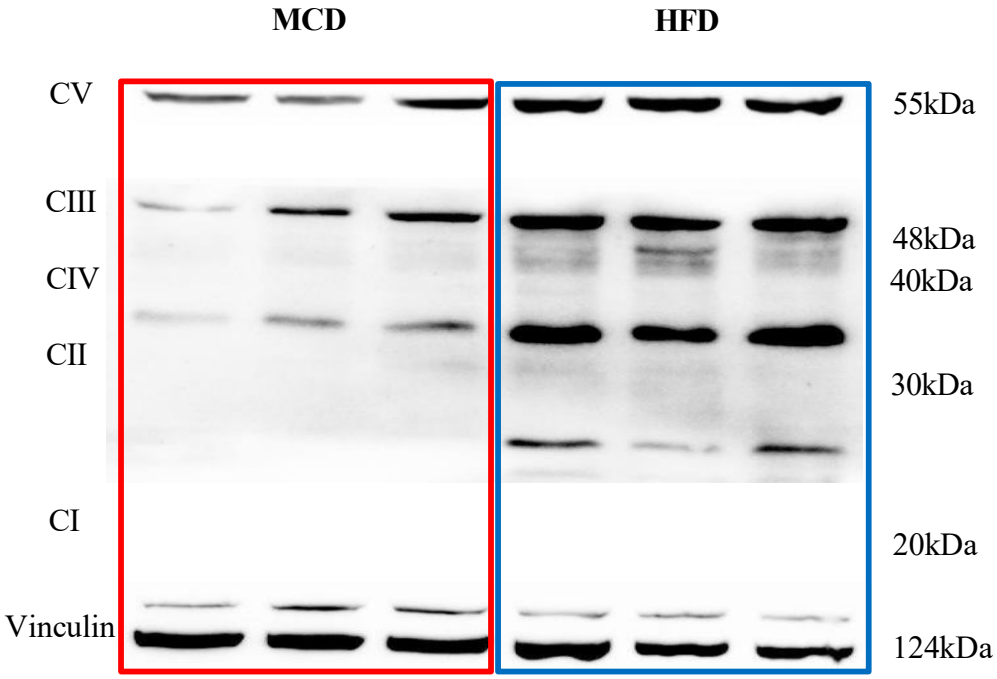

Figure 5.6: Reduced protein expression of mitochondrial respiratory complexes in the MCD model. Mitochondrial complexes (CI-CV) protein expression was evaluated by western blot analysis normalised to vinculin.

5.3.8 Decreased mitochondrial DNA in lean MAFLD mouse model

The mitochondrial DNA (mtDNA) copy number is crucial for encoding numerous critical proteins involved in the assembly and functioning of mitochondrial respiratory complexes (265, 266). As an additional indicator of mitochondrial function, I measured mtDNA copy number, which was notably reduced in MCD compared with HFD model (P=0.0002, **Fig. 5.7**).

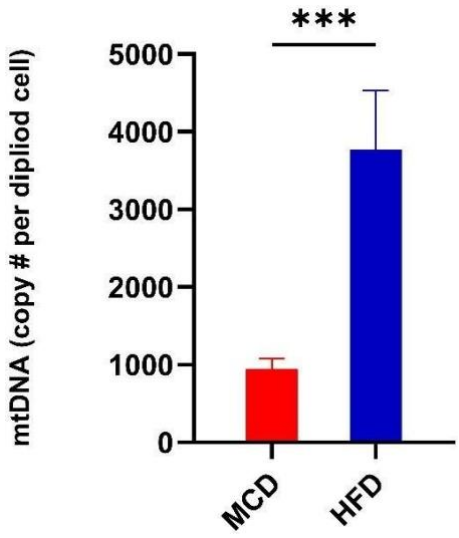

Figure 5.7: Reduced mitochondrial DNA copy number in the MCD model. Data are represented by vertical bars and are mean ± SEM. Statistical differences between groups are assessed by Mann-Whitney test. *p<0.05, **p<0.01, ***p<0.001, ****p<0.0001.

5.3.9 Reduced mRNA expression of mitochondrial complexes in the ChR model

To verify that the observed changes were not model-specific, I also assessed another lean MAFLD model using a high-cholesterol diet (ChR). Mice were fed the ChR diet for eight weeks and remained lean despite developing MAFLD, consistent with previous reports (103). Consistently, a reduction in mRNA expression of mitochondrial respiratory complexes was observed in the ChR model for complex I (CI) (P=0.007; **Fig. 5.8a**), complex II (CII) (P=0.04; **Fig. 5.8b**), complex III (CIII) (P=0.003; **Fig. 5.8c**), and complex IV (CIV) (P=0.02; **Fig. 5.8d**), and complex V (CV) (P=0.007; **Fig. 5.8e**) compared with HFD model.

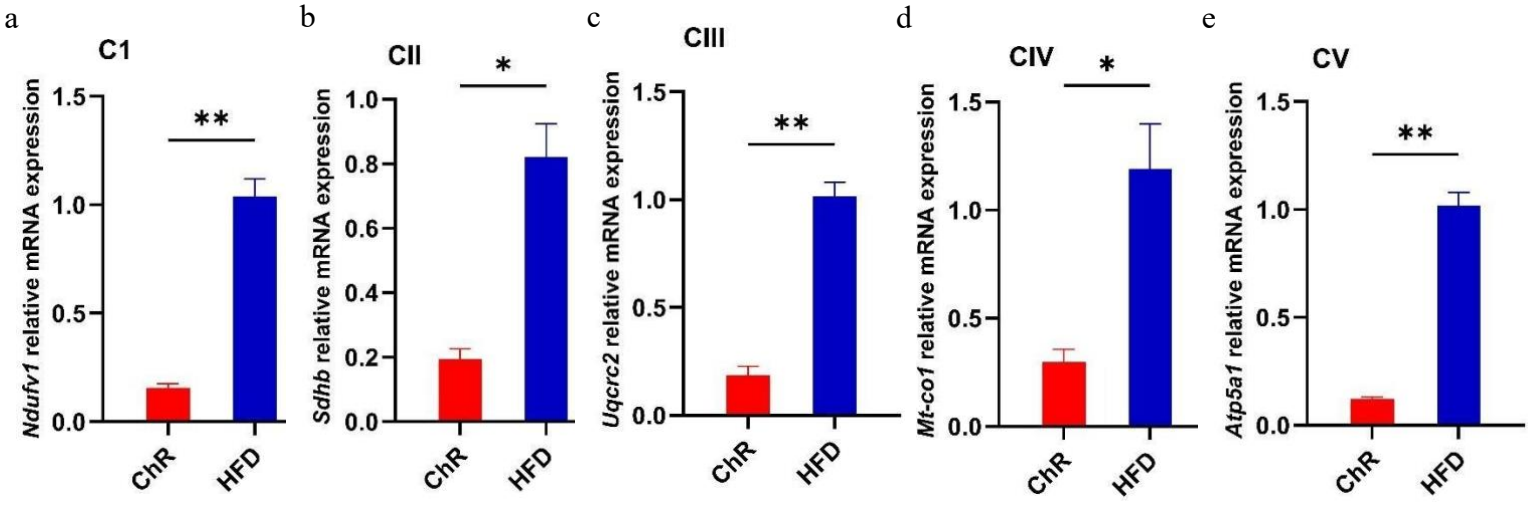

Figure 5.8: Reduced mRNA expression of OXPHOS complexes in the ChR model. a) CI. **b)** CII. **c)** CIII. **d)** CIV. **e)** CV. Data are represented by vertical bars and are mean ± SEM. Statistical differences between groups are assessed by Mann-Whitney test. *p<0.05, **p<0.01, ***p<0.001, ****p<0.0001.

5.3.10 Decreased mitochondrial DNA in ChR model

In order to confirm my finding of lower mtDNA in the MCD model, I measured mtDNA copy number in the ChR model. Similarly, mtDNA copy number was significantly reduced in ChR compared to HFD (P=0.005, **Fig. 5.9**).

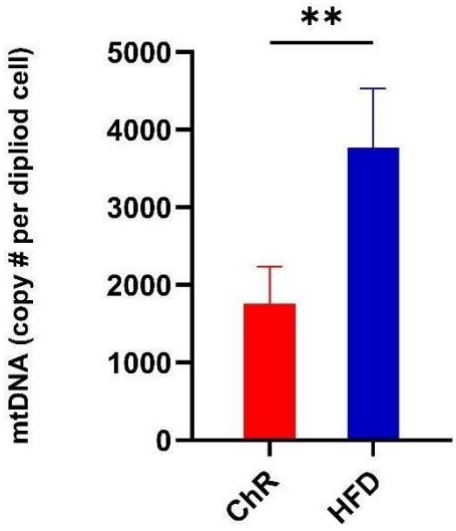

Figure 5.9: Reduced mitochondrial DNA copy number in the ChR model. Data are represented by vertical bars and are mean ± SEM. Statistical differences between groups are assessed by Mann-Whitney test. *p<0.05, **p<0.01, ***p<0.001, ****p<0.0001.

5.4 Discussion

In this chapter, I identified a distinct mitochondrial profile in lean MAFLD, which may provide critical mechanistic clues advance our understanding of the pathogenesis of this subtype of MAFLD patients. Collectively, using two dietary mouse models of lean MAFLD (MCD and ChR diets) and obese MAFLD mouse using HFD, as well as human liver biopsies, I identified a consistent mitochondrial signature that differentiates lean from non-lean disease. Across both animal and human samples, mitochondria in lean MAFLD were significantly enlarged, with increased area, perimeter, and length observed on transmission electron microscopy. Morphological enlargement, however, was accompanied by reduced mRNA and protein expression of oxidative phosphorylation complexes, indicating impaired respiratory capacity. Furthermore, mitochondrial DNA (mtDNA) copy number, an established surrogate for mitochondrial content, was significantly reduced in lean MAFLD. Together, these findings describe a phenotype of structurally enlarged but functionally compromised mitochondria, consistent with maladaptive remodeling.

These findings extend prior work from Chapters 3 and 4, in which I showed that lean MAFLD patients display significant telomere attrition associated with oxidative stress, fibrosis, and mortality and demonstrated suppressed circulating GDF-15 alongside elevated DNAm-GDF15, linking epigenetic dysregulation of this stress-responsive cytokine to telomere shortening and adverse outcomes. Because GDF-15 is a mitochondria-regulated cytokine (251, 267), the mitochondrial dysfunction identified in this chapter is consistent with, and may help contextualize, the increased oxidative stress and telomere attrition previously observed in lean MAFLD, while also providing a basis for the impaired GDF-15 stress-response signaling described in the previous chapter. Collectively, providing the first cohesive and plausible mechanistic explanation for clinically observed higher adverse outcomes in lean MAFLD,

despite their favourable metabolic and histological profile compared to their obese counterparts.

Mitochondrial pathology is increasingly recognized as a hallmark of progressive liver disease (268). Prior studies have reported reduced oxidative phosphorylation activity, and altered cristae architecture in MAFLD (191). However, whether such changes differ between lean and non-lean phenotypes has remained unresolved. The current data suggest that lean MAFLD is characterised by defective mitochondrial plasticity, mitochondria become enlarged, yet exhibit reduced respiratory capacity and diminished genomic content. Such maladaptive remodeling may reflect an attempted compensatory response to metabolic stress, which may increase susceptibility to oxidative stress and hepatocellular injury (269).

The observation of reduced mtDNA is particularly relevant, as mtDNA copy number is a surrogate marker of mitochondrial mass and is required for encoding essential subunits of respiratory complexes I, III, IV, and V (270, 271). Depletion of mtDNA has been linked to adverse outcomes across cardiovascular, oncologic, and hepatic disorders (272). Its reduction in lean MAFLD strengthens the evidence for a fundamental defect in mitochondrial homeostasis in this phenotype.

Strengths of this study include the integration of ultrastructural, transcriptional, and genomic analyses across both experimental murine models and human samples. However, the work has some noteworthy limitations, including the relatively small human sample size and reliance on indirect markers of mitochondrial function rather than direct bioenergetic assays.

In summary, my work identifies that lean MAFLD has a distinct mitochondrial profile characterized by enlarged mitochondria that are, however, functionally compromised. This includes reduced expression of respiratory complexes and depleted mitochondrial DNA (mtDNA), which collectively indicate impaired mitochondrial biogenesis and stress adaptation.

When integrated with prior findings of oxidative stress, telomere attrition, and suppressed GDF-15 signaling, these data highlight mitochondria as central to the pathophysiology of lean MAFLD and a possible focus for future translational studies.

Chapter 6: Differential mitochondrial dynamics in lean MAFLD

6.1 Introduction

Lean MAFLD accounts for a substantial proportion of MAFLD cases and is increasingly recognised as a distinct clinical subtype of the disease that develops hepatic steatosis in the absence of obesity (273), though the mechanisms underlying disease development in this subgroup remain poorly understood (274).

Mitochondria are central to hepatic energy metabolism and stress adaptation (275). Their function is maintained through several coordinated quality-control processes, including mitochondrial biogenesis, fusion and fission dynamics, and the selective removal of damaged organelles through mitophagy (276). These processes sustain mitochondrial renewal and energy balance while limiting the accumulation of dysfunctional organelles and reactive oxygen species (ROS) (277, 278). Disruption of these pathways can lead to mitochondrial injury, oxidative stress, and activation of the ER stress response (279).

In Chapter 5, I demonstrated that lean MAFLD has distinct mitochondrial profile characterised by enlarged but functionally compromised mitochondria with reduced respiratory complex expression and depleted mtDNA content, compared to their obese counterpart. These findings suggest that mitochondrial dysfunction in lean MAFLD might extend beyond structural abnormalities. Building on my earlier findings, the current chapter extends characterization of the differential mitochondrial profile between lean and non-lean MAFLD by examining whether transcriptional regulation of mitochondrial biogenesis, dynamics, and mitophagy varies between these two subtypes. It also investigates whether these alterations are accompanied by activation of ER stress and oxidative stress pathways, which may represent secondary responses to defective mitochondrial maintenance.

To address this, I analysed the expression of genes involved in mitochondrial biogenesis, fusion, fission, and mitophagy, as well as key markers of ER stress and oxidative damage, in

both the methionine–choline-deficient (MCD) and high-cholesterol (ChR) dietary models compared with the high-fat-diet (HFD) model. Thisntegrating molecular and functional data, this chapter characterises the regulatory profile of mitochondrial quality control in lean MAFLD.

6.2 Methods

Animal Models

Several dietary models for MAFLD have been developed such as the Methionine-Choline-Deficient (MCD) diet and the High Cholesterol (ChR) diet model, which represent lean MAFLD, as well as the High-Fat Diet (HFD) model for non-lean disease (280, 281). Animal experimental protocols received approval from the Western Sydney Local Health District animal ethics committee (Ethics protocol: 4249, 4302) and adhered to the guidelines set by the Australian Council on Animal Care.

Molecular assays

Total RNA was extracted from mouse models and converted to cDNA, and gene expression of biogenesis, fusion, fission, mitophagy and ER Stress were assessed using RT-PCR (reverse transcription-polymerase chain reaction).

Protein expression of ER Stress marker (Ire1) was examined by Western blot analysis using liver tissue lysates. Oxidative DNA damage assessment, IHC was performed on liver tissue sections using antibodies against 4-HNE. ROS, liver homogenates were incubated with DCFH-DA (10 μM) for 30 min at 37 °C, and fluorescence was measured at 482/528 nm. Values were normalized to protein content.

Immunofluorescence (IF)

Frozen sections were rinsed twice with PBS, permeabilized in 0.3% Triton X-100, incubated

overnight at 4 °C with the primary antibody, and then for 1 h at room temperature with a FITC-conjugated secondary antibody. Images were captured using a Leica confocal microscope.

Statistical analysis

Data analysis was conducted with GraphPad Prism software version 10. Data are presented as the mean ± standard error of the mean (SEM). The t-test was applied for two-group comparisons.

6.3 Results

6.3.1 Suppression of mitochondrial biogenesis, fusion and fission in MCD model

In Chapter 5, I identified a distinct mitochondrial phenotype in lean MAFLD, characterised by structurally enlarged but functionally compromised organelles, reduced respiratory complex expression, and depleted mtDNA content. These findings suggested a defect in mitochondrial homeostasis that extends beyond morphology. Because mitochondrial quality is maintained not only by biogenesis but also by the continuous processes of fusion and fission (282, 283), I next examined whether mitochondrial biogenesis, fusion and fission are differentially regulated in the lean MAFLD. Together, these pathways coordinate mitochondrial renewal, structural remodeling, and distribution, and their impairment has been associated with metabolic liver disease (283). Consistently, the mRNA expression levels of biogenesis (Sirt1, Tfam), fusion (Mfn1, Mfn2), and fission (Stat2, Mief1, Drp1; P<0.01, for all) in MCD model were significantly lower than HFD model (**Fig. 6.1**).

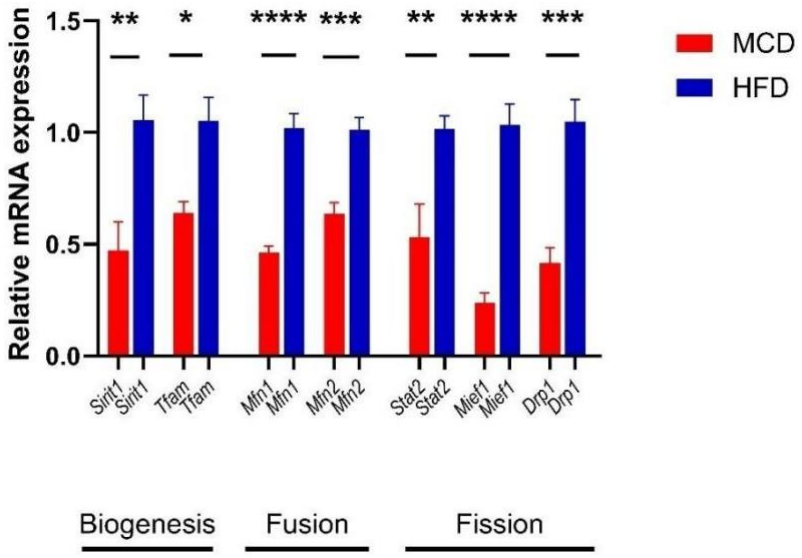

Figure 6.1: Reduced miochondrial biogenesis, fusion, and fission in MCD model. Data are represented by vertical bars and are mean ± SEM. Statistical differences between groups are assessed by t test. *p<0.05, **p<0.01, ***p<0.001, ****p<0.0001.

6.3.2 Suppression of mitochondrial mitophagy in MCD model

Mitochondrial homeostasis relies not only on biogenesis and dynamics but also on the selective removal of damaged organelles through mitophagy (284). This process is critical for preserving a functional mitochondrial pool and preventing the accumulation of dysfunctional mitochondria that exacerbate oxidative stress (285). Since biogenesis, fusion, and fission were suppressed in the MCD model, I next investigated whether mitophagy pathways were also altered. Consistently, the mRNA expression levels of mitophagy (Bnip3, Fundc1, and Pink1; P<0.01, for all) were significantly lower in the MCD model compared with HFD (**Fig. 6.2**).

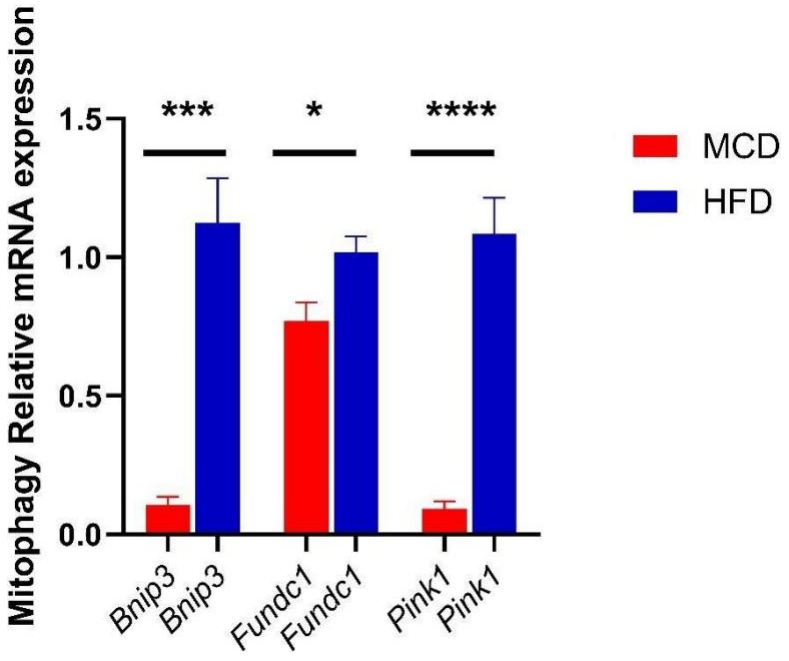

Figure 6.2: Reduced miochondrial mitophagy in MCD model. Data are represented by vertical bars and are mean ± SEM. Statistical differences between groups are assessed by t test. *p<0.05, **p<0.01, ***p<0.001, ****p<0.0001.

6.3.3 Upregulation of ER Stress related UPR Genes in MCD model

Mitochondria and the ER are closely linked functionally, and impaired mitochondrial activity or the buildup of damaged mitochondria can trigger ER stress responses, contributing to metabolic imbalance (286). Therefore, I assessed key markers of the UPR between the lean and non-lean mouse models. The mRNA expression levels of Ire1, Perk and Atf6 in MCD model were significantly higher than HFD model (P<0.01, for all) (**Fig. 6.3a**). To complement these transcriptional data, protein expression of UPR components was evaluated by Western blotting. Consistently, protein expression of Ire1 was markedly increased in MCD compared with HFD (**Fig. 6.3b**).

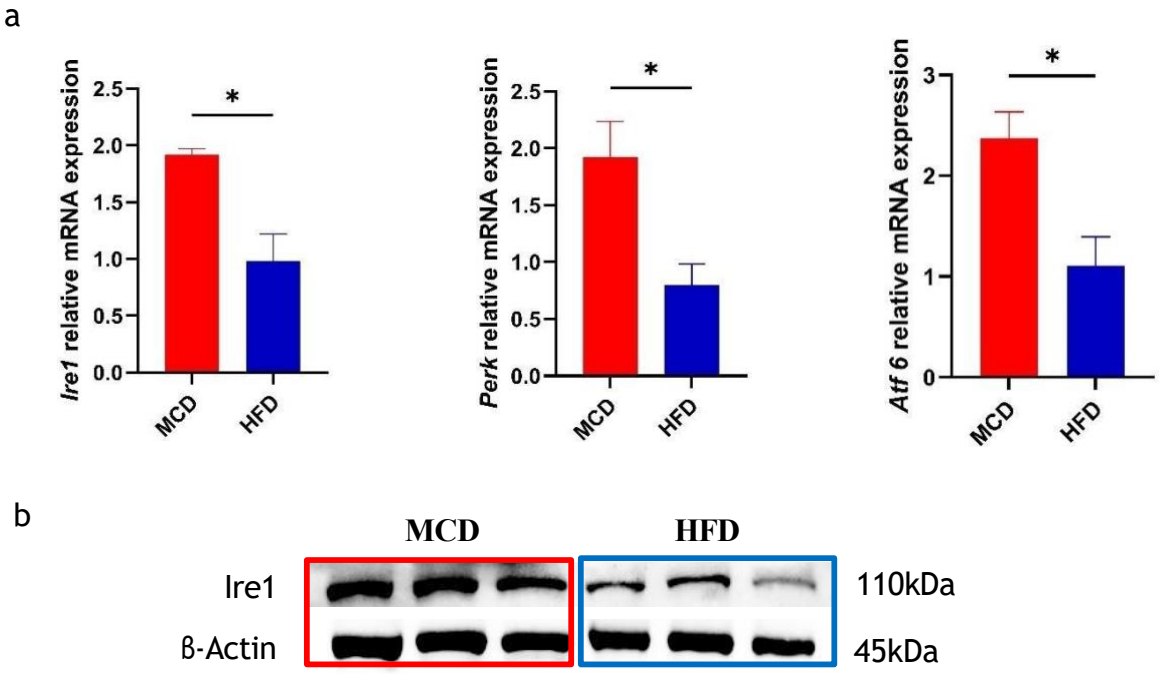

Figure 6.3: Elevated expression of unfolded protein response (UPR) markers. a) Elevated mRNA expression of Ire1, Perk and Atf6 by PCR. **b)** Elevated protein expression of Ire1 by WB. Data are represented by vertical bars and are mean ± SEM. Statistical differences between groups are assessed by t test. *p<0.05, **p<0.01, ***p<0.001, ****p<0.0001. Protein

expression was evaluated by western blot analysis normalised to β-Actin.

6.3.4 Increased hepatic Ire1 expression in the MCD model

To confirm the activation of ER stress observed at the transcriptional and protein levels, I next examined the hepatic localization and expression of Ire1 using immunofluorescence staining. Consistent with the mRNA and Western blot results, Ire1 staining intensity was markedly higher in the MCD model compared with the HFD model (**Fig. 6.4a**). Quantitative analysis confirmed that Ire1 expression was siginfcantly higher in MCD compared with the HDF model (P=0.008; **Fig. 6.4b**).

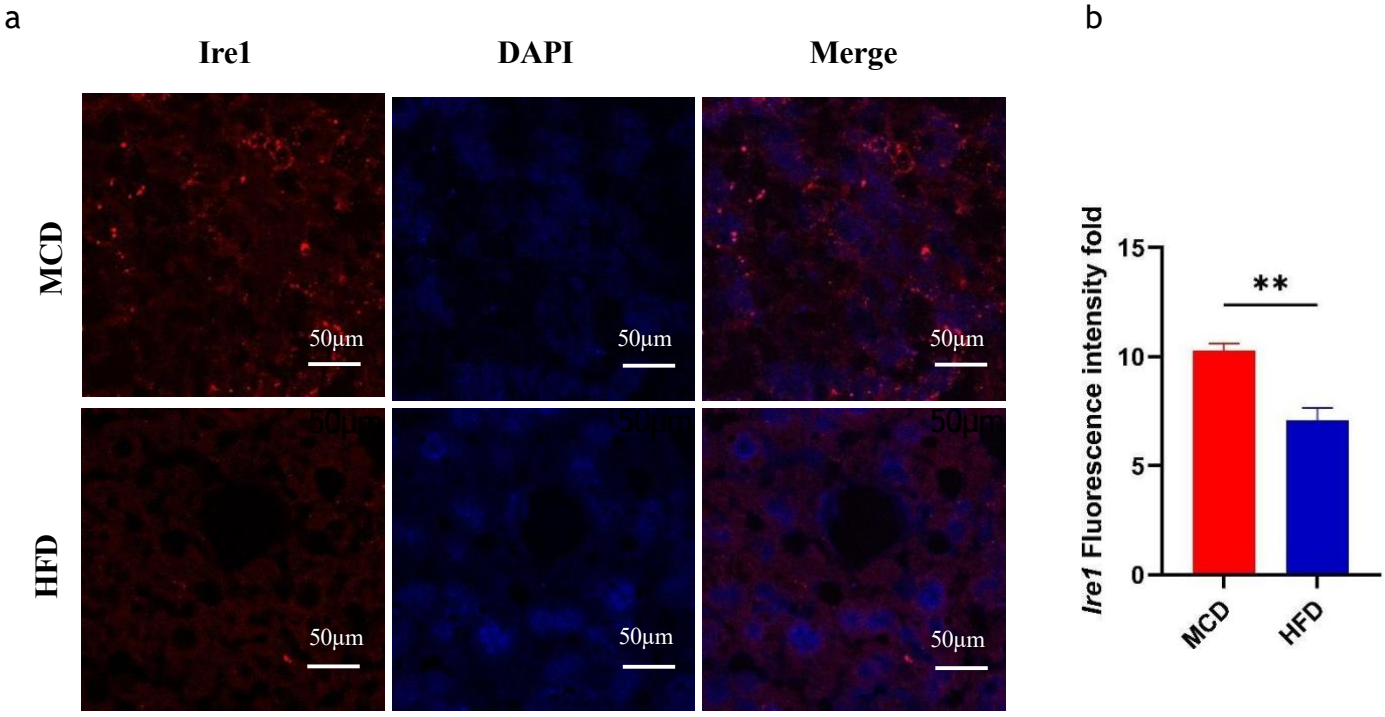

Figure 6.4: Increased hepatic Ire1 expression in the MCD model. a) Immunofluorescence shows ER stress marker Ire1 in two different models, MCD and HFD. **b)** Quantitative analysis of Ire1 immunofluorescence expression. Imaging was undertaken using Leica confocal microscope and analysed using image J. Data are represented by vertical bars and are mean ± SEM. Statistical differences between groups are assessed by t test. *p<0.05, **p<0.01, ***p<0.001, ****p<0.0001.

6.3.5 Elevated hepatic ROS Levels in the MCD model

Given that mitochondrial dysfunction and ER stress are major sources of oxidative stress (287), I next measured hepatic ROS levels to assess oxidative burden in the two dietary models. Consistantly, ROS levels were significantly increased in the MCD model compared with the HFD model (P=0.0002; **Fig. 6.5**).

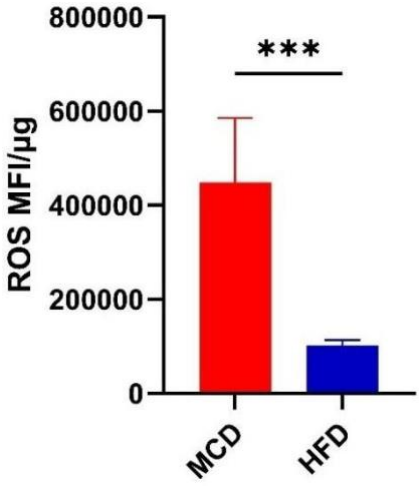

Figure 6.5: Increased ROS production in the MCD model. ROS level was measured by ELISA between MCD and HFD. Data are represented by vertical bars and are mean ± SEM. Statistical differences between groups are assessed by t test. *p<0.05, **p<0.01, ***p<0.001, ****p<0.0001.

6.3.6 Increased hepatic lipid peroxidationin the MCD model

ROS overproduction can lead to lipid peroxidation (288). To assess oxidative damage, hepatic 4-HNE expression was examined by immunohistochemistry. As shown in (**Fig. 6.6a**) the MCD model exhibited a markedly higher level of 4-HNE positive area compared with the HFD model. Quantitative analysis confirmed a of 4-HNE shows significant increase in MCD model compared with HFD (P=<0.0001; **Fig. 6.6b**).

a b

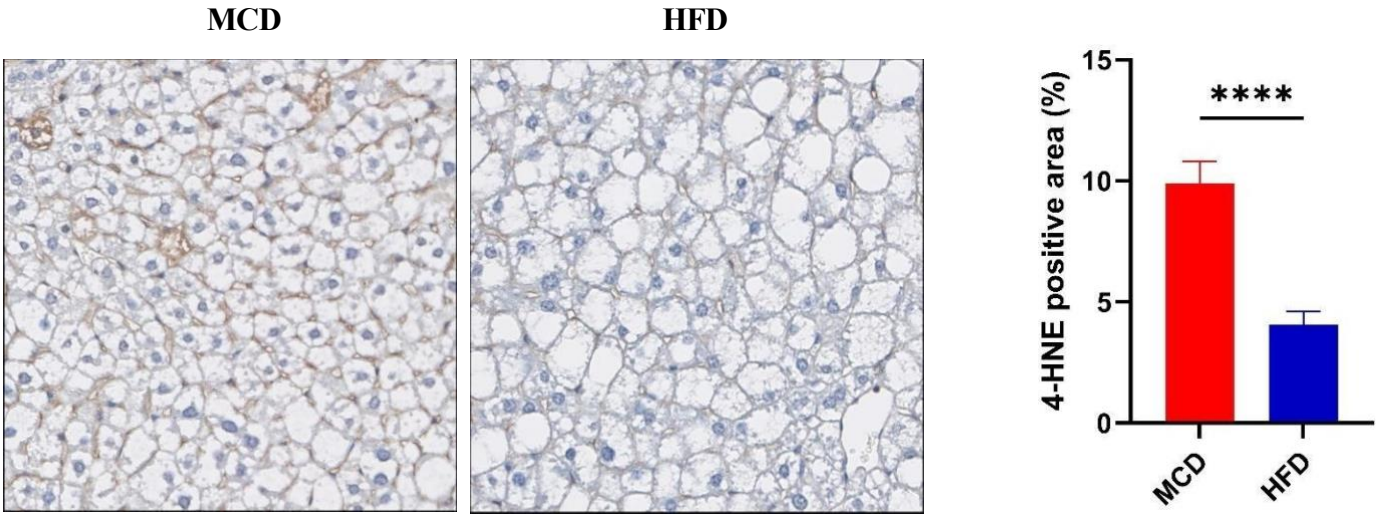

Figure 6.6: Increased hepatic 4-HNE expression in the MCD model. a) Immunohistochemistry shows oxidative marker 4-HNE in two different models, MCD and HFD. **b)** Quantification of 4-HNE by ImageJ. Data are represented by vertical bars and are mean ± SEM. Statistical differences between groups are assessed by t test. *p<0.05, **p<0.01, ***p<0.001, ****p<0.0001.

6.3.7 Suppression of mitochondrial biogenesis, fusion and fission in ChR model

To confirm that the suppression of mitochondrial regulatory pathways was not model specific. I next examined the expression of genes involved in mitochondrial biogenesis, fusion, and fission in the ChR model. Consistently, the ChR model exhibited a significant reduction in the mRNA expression of biogenesis related genes (Sirt1, Tfam), fusion (Mfn1, Mfn2), and fission (Stat2, Mief1, Drp1; P<0.01, for all) compared with the HFD model (**Fig. 6.7**).

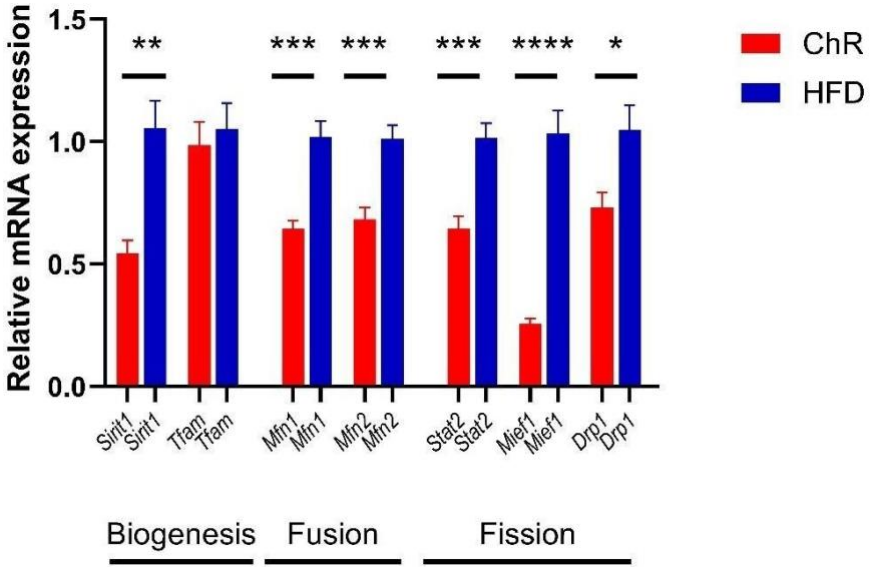

Figure 6.7: Reduced mitochondrial biogenesis, fusion, and fission in ChR model. Data are represented by vertical bars and are mean ± SEM. Statistical differences between groups are assessed by t test. *p<0.05, **p<0.01, ***p<0.001, ****p<0.0001.

6.3.8 Suppression of mitochondrial mitophagy in ChR model

To further determine whether impaired mitochondrial quality control observed in the MCD model also occurs in the ChR model. I assessed the expression of key mitophagy related genes. Consistently, the ChR model showed that mRNA expression levels of mitophagy (Bnip3, Fundc1, and Pink1; P<0.01, for all) were significantly lower in the ChR model compared with HFD (**Fig. 6.8**).

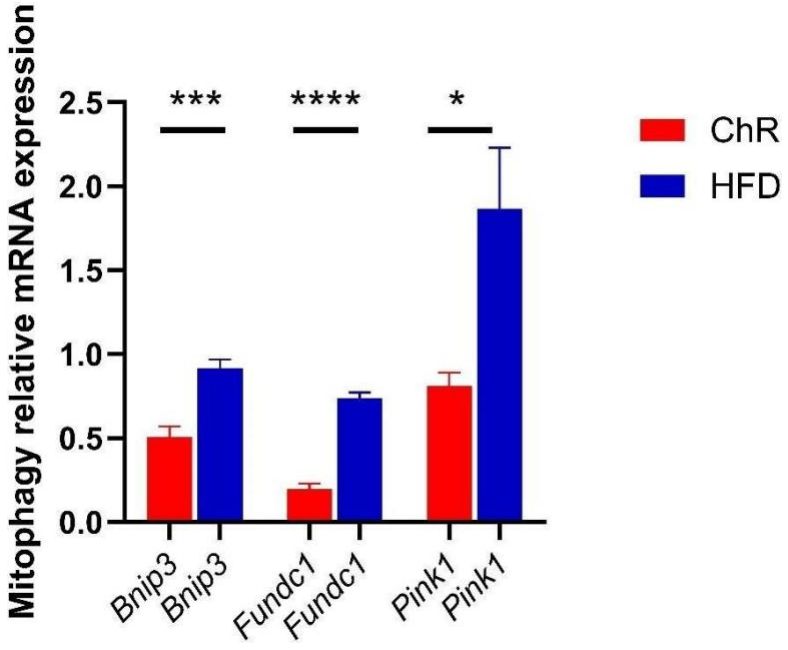

Figure 6.8: Reduced miochondrial mitophagy in ChR model. Data are represented by vertical bars and are mean ± SEM. Statistical differences between groups are assessed by t test. *p<0.05, **p<0.01, ***p<0.001, ****p<0.0001.

6.3.9 Upregulation of ER Stress related UPR Genes in ChR model

To determine whether activation of ER stress observed in the MCD model also occurs in the ChR model. I examined the expression of UPR genes. Consistently, the ChR model showed significantly higher mRNA expression of Ire1, Perk, and Atf6 compared with the HFD model (P=0.0008, P=0.002 and P=0.01, respectively) (**Fig. 6.9**).

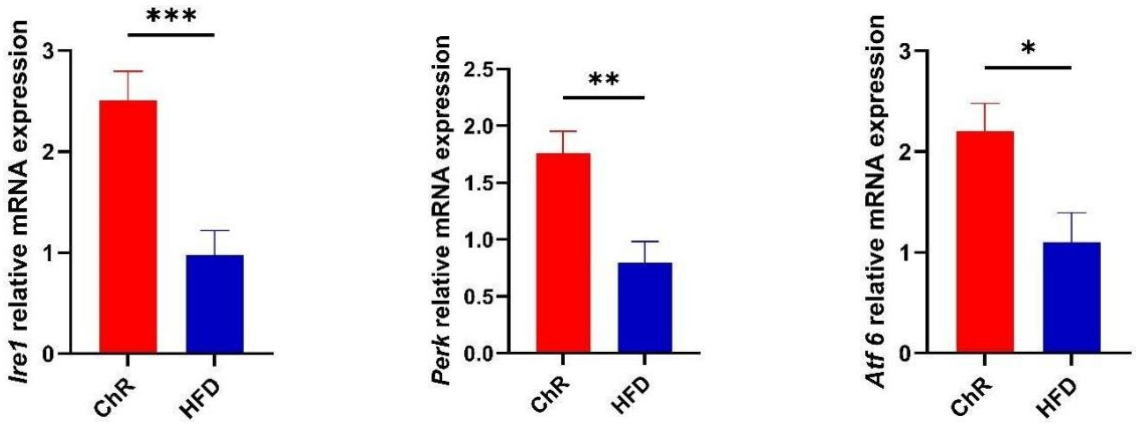

Figure 6.9: Elevated expression of UPR markers. Data are represented by vertical bars and are mean ± SEM. Statistical differences between groups are assessed by t test. *p<0.05, **p<0.01, ***p<0.001, ****p<0.0001.

6.3.10 Increased hepatic Ire1 expression in the ChR model

To confirm the activation of ER stress observed at MCD model. I next examined the hepatic localization and expression of Ire1 using immunofluorescence staining. Consistentaly, Ire1 staining intensity was markedly higher in the ChR model compared with the HFD model (**Fig. 6.10a**). Quantitative analysis confirmed that Ire1 expression was siginfcantly higher in ChR compared with the HDF model (P=0.01; **Fig. 6.10b**).

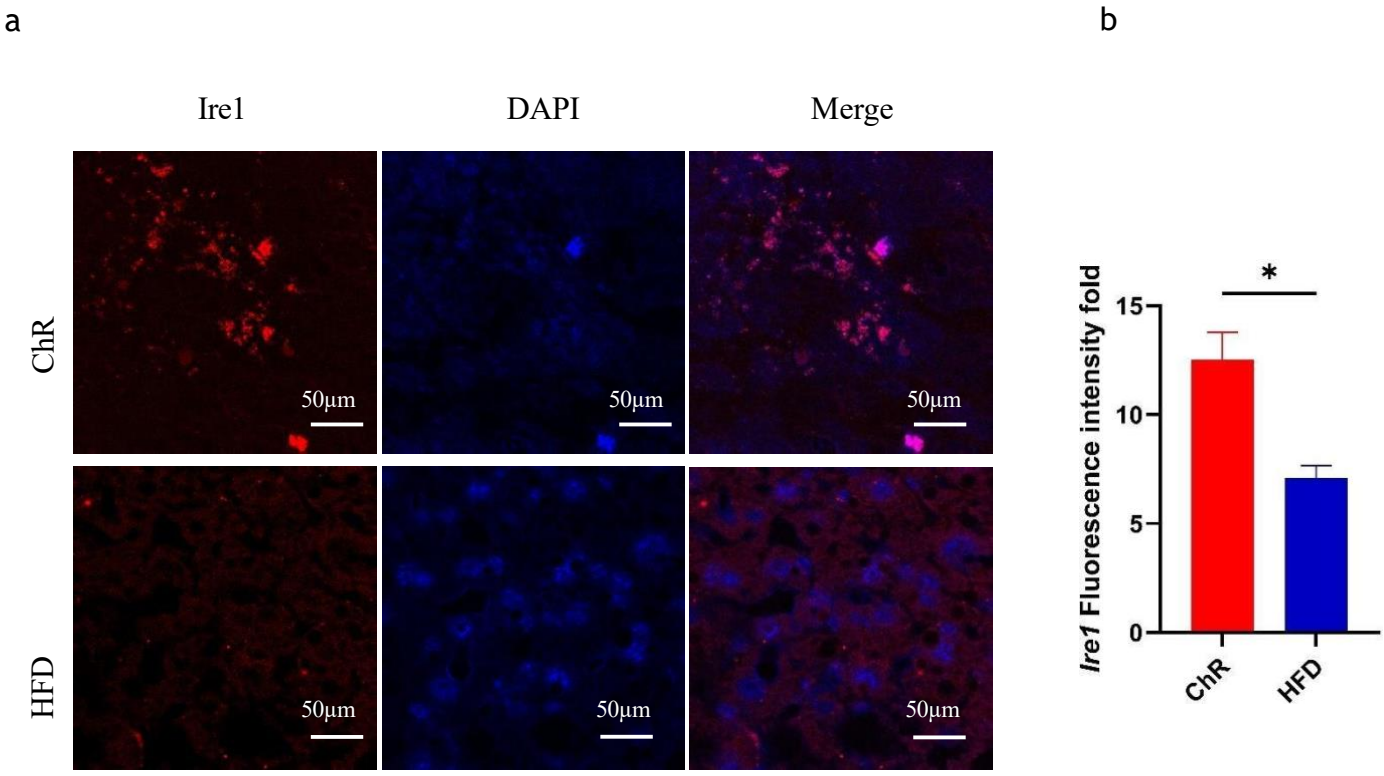

Figure 6.10: Increased hepatic Ire1 expression in the ChR model. a) Immunofluorescence shows ER stress marker Ire1 in two different models, ChR and HFD. **b)** Quantitative analysis of Ire1 immunofluorescence expression. Imaging was undertaken using Leica confocal microscope and analysed using image J. Data are represented by vertical bars and are mean ± SEM. Statistical differences between groups are assessed by t test. *p<0.05, **p<0.01, ***p<0.001, ****p<0.0001.

6.3.11 Elevated hepatic ROS levels in the ChR model

To determine whether oxidative stress is also increased in the ChR model, I quantified hepatic ROS levels. Similar to the findings in the MCD model, ROS levels were significantly higher in the ChR model compared with the HFD model (P=0.02; **Fig. 6.11**).

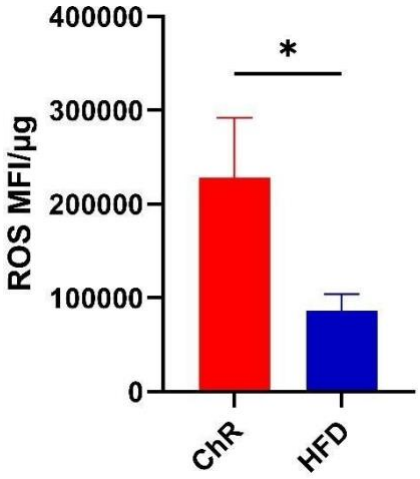

Figure 6.11: Increased ROS production in the ChR model. ROS level was measured by ELISA between MCD and HFD. Data are represented by vertical bars and are mean ± SEM. Statistical differences between groups are assessed by t test. *p<0.05, **p<0.01, ***p<0.001, ****p<0.0001.

6.4 Discussion

In this chapter, I identified that lean MAFLD is associated with reduced expression of mitochondrial biogenesis, fusion, fission, and mitophagy pathways using two mouse models. I also observed an activation of the UPR, evidenced by an increase in ER stress markers at both transcript and protein levels. Immunofluorescence confirmed the elevated levels of ER stress. Additionally, oxidative stress significantly increased in lean MAFLD, with higher levels of reactive oxygen species and lipid peroxidation.

These findings, along with those previously discussed in Chapter 5, provide a comprehensive characterization of the mitochondrial profile in lean MAFLD. The observed reduction in mitochondrial biogenesis, fusion, fission, and mitophagy is consistent with earlier reports describing suppressed mitochondrial renewal and altered dynamics in lean MAFLD (289, 290). Disruption of these regulatory pathways compromises mitochondrial quality control, leading to the accumulation of damaged and dysfunctional organelles. This buildup of defective mitochondria contributes to ongoing cellular stress and disturbed energy metabolism, which may increase the risk of adverse outcomes in individuals with lean MAFLD compared to those wit non-lean MAFLD (291).

The observed activation of ER stress pathways supports this, with increased expression of Ire1, Perk, and Atf6 at both transcript and protein levels. Immunofluorescence analysis further confirmed higher hepatic expression of Ire1. These changes indicate sustained activation of the UPR, likely triggered by the buildup of damaged mitochondria.

Increased oxidative stress in lean MAFLD was marked by elevated ROS levels and lipid peroxidation. ROS are known to promote hepatocellular injury, damage mitochondrial DNA, and trigger pro-inflammatory signaling, which together accelerate disease progression (292). Oxidative stress further disrupts redox homeostasis, impairs mitochondrial function, and

activates fibrogenic pathways that contribute to liver damage (293).

A key strength of this chapter is the use of two independent dietary models of lean MAFLD, both of which consistently demonstrated impairments in mitochondrial regulation and increased cellular stress. The integration of transcript-level data, protein expression, and tissue level imaging provides a robust and multi-layered assessment of organelle dysfunction. However, there are some limitations. Direct measurements of mitochondrial respiration were not performed, so functional impairment was inferred from transcriptional and molecular markers rather than dynamic assays. Lack of human validation limits the direct translational relevance of these findings. Future studies should incorporate functional assays and human cohorts to confirm and extend these observations.

In conclusion, this chapter demonstrates that lean MAFLD has disntic mitochondrial profile characterized by impaired mitochondrial quality control, sustained ER stress, and increased oxidative damage. These abnormalities were consistent across two independent dietary models and involved multiple levels of regulation, from gene expression to protein localization. The combined disruption of mitochondrial dynamics, stress adaptation, and redox balance defines a distinct pathophysiological profile in lean MAFLD, which may contribute to disease progression and adverse clinical outcomes.

Chapter 7: Comprehensive Discussion

7.1 Discussion

Lean MAFLD represents a significant subset of patients diagnosed with MAFLD, yet the clinical characteristics, natural history, and underlying pathogenic mechanisms of this condition remain poorly understood. This has led some experts to debate whether lean MAFLD is a distinct entity or simply a variation within the spectrum of non-obese MAFLD (294, 295). Such uncertainty has resulted in its underrepresentation in both clinical trials and mechanistic studies. However, emerging evidence suggests that lean MAFLD possesses a unique clinical and metabolic profile, likely driven by specific pathogenic pathways that are yet to be fully characterized.

In my work, I identified an unanticipated mechanism that helps to reconcile the apparently contradictory reports regarding a better histological profile in cross-sectional studies on the one hand and a worse survival on the other hand of lean patients with MAFLD, compared with their non-lean counterparts. I show that greater ROS generation in lean MAFLD is associated with accelerated telomere attrition compared to those with non-lean MAFLD, and at least partially explains the clinical paradox.

Mechanistically, at the subcellular level, I identified that lean MAFLD patients demonstrated a distinct mitochondrial profile characterized by larger mitochondrial size but impaired respiratory function, reduced mtDNA content, disrupted mitochondrial dynamics, and elevated oxidative and ER stress.

Additionally, I discerned that circulating GDF15 levels, a key mitochondrial regulator, were significantly lower in patients with lean MAFLD compared to their obese counterparts. This effect is likely mediated by their higher DNAm-GDF15 levels. Ultimately, elevated DNAm-GDF15 was also identified as a robust indicator of mortality in the general population and MAFLD patients, with a stronger negative correlation in lean MAFLD subjects with shorter

telomere length. Collectively, these findings represent a significant step towards enhancing our understanding of the pathogenesis of MAFLD, particularly among non-obese subjects and reconciling many of the frequently reported and apparently paradoxical findings about this subgroup of patients.

In previous studies, our team identified that patients with lean MAFLD have better metabolic adaptation that is mediated by increased bile acids signaling and FXR activity. This likely explains the favorable metabolic and histological profile of lean patients with MAFLD compared to their non-lean counterparts in cross-sectional studies but become less effective as the disease progresses (103). This decline was identified by us in a subsequent study to be mediated by endotoxemia-induced epigenetic modifications that attenuate bile acid signaling (103, 296). Paradoxically, despite these favorable features, epidemiological data consistently show higher mortality among lean MAFLD patients compared with their obese counterparts (247, 248). It remains difficult to reconcile why these patients tend to have worse long-term clinical outcomes (216, 297).

My current work presents a novel testable hypothesis that identifies telomere shortening as a potential explanation for the paradoxical clinical findings in lean MAFLD. The findings from this work suggest that telomere attrition, driven by increased oxidative stress and reduced GDF-15 levels, may underlie this paradoxical outcome (**Fig. 7.1**).

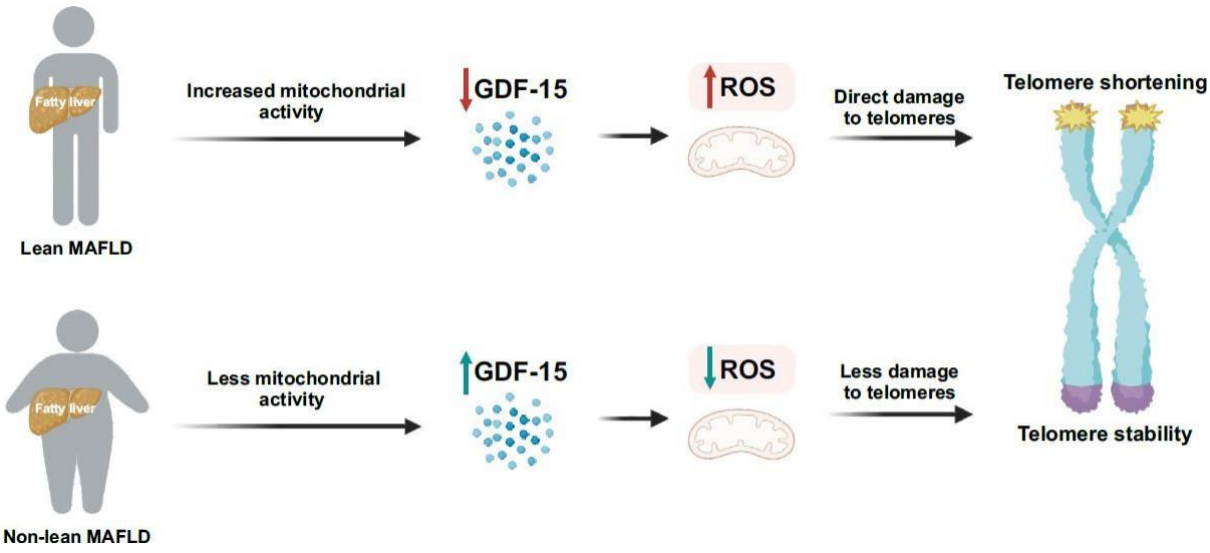

Figure 7.1: Proposed model for the differential mortality outcomes between lean and non-lean MAFLD.

I propose that because telomere maintenance is energetically costly, telomere attrition in lean MAFLD patients represents a maladaptive outcome of their otherwise beneficial metabolic adaptation, in line with the metabolic telomere attrition hypothesis (219). The fundamental premise of the costly maintenance hypothesis is that sustaining telomere length requires continuous energy expenditure for both preventing attrition and promoting elongation (297). When energy demands become excessive or metabolic stress persists, telomeres shorten as resources are redirected from long-term maintenance toward immediate survival needs (219). While this trade-off may temporarily support metabolic stability, persistent telomere attrition under chronic metabolic stress, as seen in MAFLD, may lead to cumulative cellular damage and contribute to poorer long-term survival.

It is suggested that oxidative stress is the main cause of telomere attrition (298), as my data confirm. Mitochondria as the cellular powerhouse generate the majority of adenosine

triphosphate (ATP) and most endogenous ROS is generated in mitochondria (299). The efficiency of ATP production is positively correlated with the rate of ROS production, leading to a physiological trade-off between the body's energy requirements and its need to prevent oxidative stress (300). This trade-off is known to influence telomere attrition through ROS-mediated oxidative damage, and my findings demonstrate that this mechanism is particularly evident in patients with lean MAFLD. Patients with lean MAFLD exhibited higher serum and hepatic ROS levels compared with their non-lean counterparts. Furthermore, my in vitro experiments confirmed that ROS directly attenuates telomere length and telomerase activity in hepatocytes.

In the context of oxidative stress, my work revealed upregulation of the expression of key negative regulators of telomere length in hepatocytes treated upon induction of ROS (301). One of these regulators protection of telomeres 1 (POT1) inhibits the translocation of telomerase to the telomere and suppresses its interaction with it, thereby preventing telomere elongation (302). Furthermore, its promoter contains a binding site for NF-κB (302), suggesting that inflammation and ROS generation can influence its activity. Thus, my data suggest that oxidative stress may inhibit telomere elongation by inducing the expression of negative regulators, linking inflammation and ROS generation to telomere shortening (302).

Telomere attrition is consistently linked to increased morbidity and mortality across multiple diseases (217). A recent study demonstrated that shorter leukocyte telomere length correlates with higher cardiovascular, respiratory, hepatic, digestive, and musculoskeletal mortality, though not with cancer-related deaths (229). Experimental models further implicate telomere dysfunction in aging-related conditions such as liver cirrhosis, while in hepatocarcinogenesis, telomere shortening may act as a tumor-initiating event, as shortened telomeres are more frequent in hepatocellular carcinoma cells than in adjacent noncancerous tissue (303).

Of particular interest, I found that the association between telomere length and mortality differs between lean and non-lean patients with liver disease. This relationship was stronger among lean individuals in the NHANES cohort. Consistently, another analysis using the same dataset reported that leukocyte telomere length was inversely associated with advanced fibrosis only among lean participants, but not among the non-lean (304).

Building on these observations, my further analyses explored the role of GDF-15 and its epigenetic regulation in lean MAFLD. The higher serum and hepatic ROS observed in lean patients may be partly explained by impaired activation of stress-responsive pathways involving GDF-15 and FGF21, two key hepatic metabokines that mediate systemic adaptation to mitochondrial stress (305, 306).

I demonstrated that lean MAFLD patients have significantly lower serum GDF-15 levels even after adjusting for age and sex. This aligns with reports in the general population showing that GDF-15, typically elevated in obesity, acts as a stress-induced cytokine regulating energy balance and suppressing oxidative stress (307). Under mitochondrial stress, increased GDF-15 secretion normally limits energy intake and reduces intracellular ROS by modulating mitochondrial membrane potential (308).

In contrast, circulating FGF21, which rises during mild mitochondrial dysfunction under obesogenic conditions, did not differ between lean and non-lean MAFLD in a previous report (309). Together, these findings indicate distinct regulatory roles for these metabokines: GDF-15 primarily modulates energy intake and protects against hepatic steatosis, whereas FGF21 enhances glucose clearance and energy expenditure (310).

Subsequent findings revealed that DNAm-GDF15 levels are markedly higher in individuals with lean MAFLD, consistent with the epigenetic suppression of GDF-15 expression through DNA methylation. Because hypermethylation typically reduces gene transcription, this likely

explains the lower circulating GDF-15 observed in these patients.

Higher DNAm-GDF15 levels was identidfed to be strongly associated with increased all-cause and cause-specific mortality, even after adjustment for confounders, underscoring their prognostic significance. A negative correlation between DNAm-GDF15 and telomere length was also observed, and being more pronounced in lean MAFLD. Mediation analysis further indicated that DNAm-GDF15 mediates the link between telomere attrition and mortality, identifying a potential pathway connecting telomere dysfunction, mitochondrial impairment, and adverse clinical outcomes in lean MAFLD.

Collectivtely, these findngs provked a further question whether there is a differntail mitochondrial profile between lean and non-lean MAFLD. In this work, I identifed that lean MAFLD exhibited a distinct mitochondrial phenotype characterized by enlarged mitochondria with reduced respiratory capacity and increased ROS production. Consistent with mitochondrial dysfunction, I also observed lower mitochondrial DNA content, which is associated with impaired biogenesis and reduced oxidative phosphorylation capacity (311).

To further explore these mechanisms, mitochondrial quality control and cellular stress pathways were examined in experimental models of lean MAFLD. The observed downregulation of genes involved in mitochondrial fusion, fission, and mitophagy indicates impaired organelle turnover, contributing to metabolic stress, oxidative damage, and ER stress key hallmarks of lean MAFLD physiology (**Fig. 7.2**).

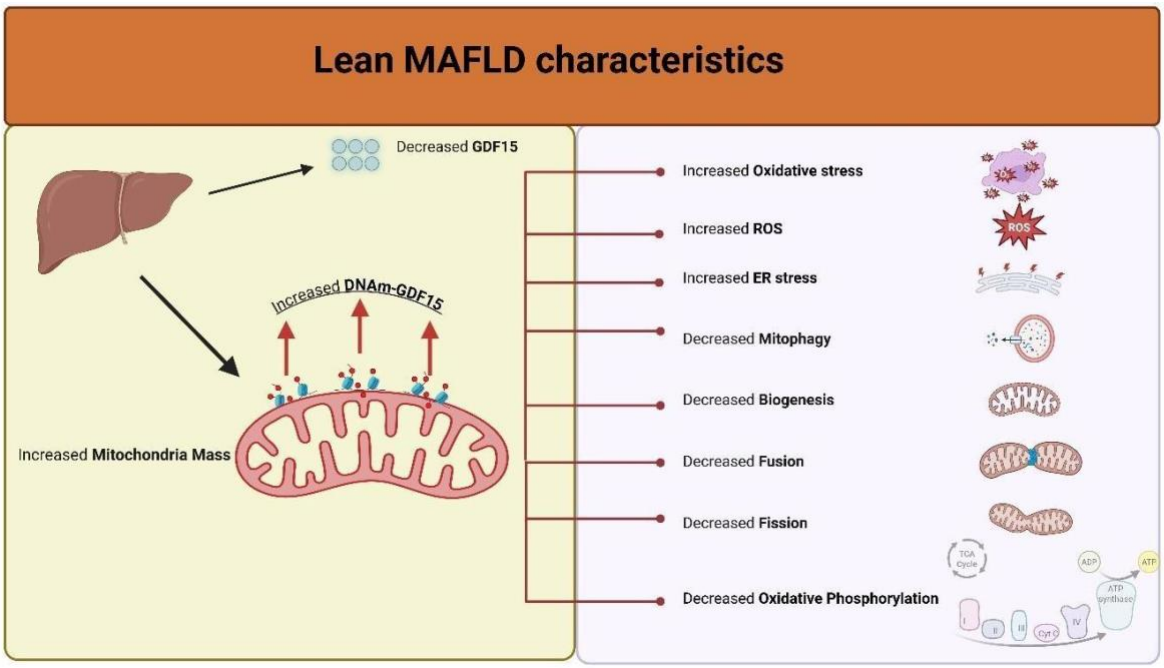

Figure 7.2: Characteristic features of lean MAFLD compared to non-lean MAFLD.

The strengths of this study include incorporating a multi-pronged approach integrating human cross-sectional and observational data with mechanistic insights from murine models, accompanied by a wide array of functional studies and analysis, providing a novel and coherent model of work that advances our understanding of the pathogenesis of lean MAFLD and heterogeneity within MAFLD phenotypes.

Nevertheless, several limitations should also be acknowledged. Telomere length was measured only in whole blood; although previous studies show strong correlations between leukocyte and hepatic telomere length, tissue-specific differences may still exist (312). Measurements were also obtained at a single time point, preventing assessment of longitudinal telomere dynamics that could influence mortality risk. Furthermore, leukocytes comprise multiple cell types with variable telomere lengths, which may introduce heterogeneity into the measurements. The study also relied in parts on murine models that, while replicating several

features of lean MAFLD, do not fully capture the complexity or long-term progression of human disease. The absence of fresh liver tissue limited direct functional assays of mitochondrial activity, and detailed evaluation of mitochondrial function in human lean and non-lean MAFLD was not undertaken. Lastly, due to sample size constraints, it was not possible to confirm MAFLD diagnosis within the NHANES cohort. Despite these limitations, the findings provide important mechanistic insight and serve as a proof of concept supporting the proposed framework.

In conclusion, I demonstrate that lean MAFLD is characterized by shorter telomeres, greater oxidative stress, and a distinct mitochondrial profile compared with non-lean disease, with GDF15 emerging as a key regulator mediating the link between these changes and adverse outcomes, making it a potential prognostic and therapeutic target. These findings provide a mechanistic framework for understanding disease progression in lean MAFLD and highlight the need for studies clarifying the interplay between energy balance, metabolic regulators, and telomere maintenance in MAFLD.

7.2 Future directions

7.2.1 Validation in larger human cohorts

Future work should aim to validate these findings in independent, larger, and well-characterized human cohorts from diverse ethnicities and geographic backgrounds. By incorporating both clinical and molecular data, the associations between telomere attrition, DNAm-GDF15, and mitochondrial alterations in lean MAFLD can cbe confirmed, thereby ensuring the generalizability of our findings.

7.2.2 Longitudinal assessment of telomere dynamics

Longitudinal studies are required to determine whether temporal changes in telomere length

and GDF-15 methylation predict disease progression and mortality. Repeated measurements will allow a better understanding of dynamic cellular ageing in MAFLD.

7.2.3 Functional evaluation of mitochondrial activity

Further work should investigate mitochondrial respiration, biogenesis, and turnover using patient-derived hepatocytes and high-resolution functional assays to verify the molecular alterations identified in this thesis.

7.2.4 Integrating epigenetic and mitochondrial pathways

Future studies integrating epigenetic, metabolic, and mitochondrial datasets within the same cohort will enhance causal interpretation and reveal mechanistic interactions between oxidative stress, DNA methylation, and organelle dysfunction.

7.2.5 Development of biomarkers and therapeutic Targets

Translating these findings into clinical practice will involve evaluating telomere length, DNAm-GDF15, and mitochondrial parameters as potential biomarkers for disease stratification and as targets for therapeutic intervention in lean MAFLD.

Chapter 8: References

1. Devarbhavi H, Asrani SK, Arab JP, Nartey YA, Pose E, Kamath PS. Global burden of liver disease: 2023 update. Journal of hepatology. 2023;79(2):516-37.

2. Lou T-W, Yang R-X, Fan J-G. The global burden of fatty liver disease: the major impact of China. Hepatobiliary surgery and nutrition. 2024;13(1):119.

3. Asrani SK, Devarbhavi H, Eaton J, Kamath PS. Burden of liver diseases in the world. J Hepatol. 2019;70(1):151-71.

4. Wu X-N, Xue F, Zhang N, Zhang W, Hou J-J, Lv Y, et al. Global burden of liver cirrhosis and other chronic liver diseases caused by specific etiologies from 1990 to 2019. BMC Public Health. 2024;24(1):363.

5. Younossi ZM, Koenig AB, Abdelatif D, Fazel Y, Henry L, Wymer M. Global epidemiology of nonalcoholic fatty liver disease-Meta-analytic assessment of prevalence, incidence, and outcomes. Hepatology. 2016;64(1):73-84.

6. Sepanlou SG, Safiri S, Bisignano C, Ikuta KS, Merat S, Saberifiroozi M, et al. The global, regional, and national burden of cirrhosis by cause in 195 countries and territories, 1990–2017: a systematic analysis for the Global Burden of Disease Study 2017. The Lancet gastroenterology & hepatology. 2020;5(3):245-66.

7. Hassan-Kadle MA, Osman MS, Ogurtsov PP. Epidemiology of viral hepatitis in Somalia: systematic review and meta-analysis study. World Journal of Gastroenterology. 2018;24(34):3927.

8. Said ZNA, El-Sayed MH. Challenge of managing hepatitis B virus and hepatitis C virus infections in resource-limited settings. World J Hepatol. 2022;14(7):1333-43.

9. Stanaway JD, Flaxman AD, Naghavi M, Fitzmaurice C, Vos T, Abubakar I, et al. The global burden of viral hepatitis from 1990 to 2013: findings from the Global Burden of Disease Study 2013. The Lancet. 2016;388(10049):1081-8.

10. Eslam M, Sanyal AJ, George J, Sanyal A, Neuschwander-Tetri B, Tiribelli C, et al. MAFLD: a consensus-driven proposed nomenclature for metabolic associated fatty liver disease. Gastroenterology. 2020;158(7):1999-2014. e1.

11. Chalasani N, Younossi Z, Lavine JE, Charlton M, Cusi K, Rinella M, et al. The diagnosis and management of nonalcoholic fatty liver disease: practice guidance from the American Association for the Study of Liver Diseases. Hepatology. 2018;67(1):328-57.

12. Ciardullo S, Perseghin G. From NAFLD to MAFLD and MASLD: a tale of alcohol, stigma and metabolic dysfunction. Metab Target Organ D. 2024;4(4).

13. Eslam M, Newsome PN, Sarin SK, Anstee QM, Targher G, Romero-Gomez M, et al. A new definition for metabolic dysfunction-associated fatty liver disease: An international expert consensus statement. Journal of hepatology. 2020;73(1):202-9.

14. Tsutsumi T, Eslam M, Kawaguchi T, Yamamura S, Kawaguchi A, Nakano D, et al. MAFLD better predicts the progression of atherosclerotic cardiovascular risk than NAFLD: generalized estimating equation approach. Hepatol Res. 2021;51(11):1115-28.

15. Grabherr F, Grander C, Effenberger M, Schwärzler J, Tilg H. MAFLD: what 2 years of the redefinition of fatty liver disease has taught us. Ther Adv Endocrinol Metab. 2022;13:20420188221139101.

16. Wong VW-S, Ekstedt M, Wong GL-H, Hagstrom H. Changing epidemiology, global trends and implications for outcomes of NAFLD. Journal of hepatology. 2023;79(3):842-52.

17. Younossi Z, Anstee QM, Marietti M, Hardy T, Henry L, Eslam M, et al. Global burden of NAFLD and NASH: trends, predictions, risk factors and prevention. Nature reviews Gastroenterology & hepatology. 2018;15(1):11-20.

18. Zelber-Sagi S, Carrieri P, Pericas JM, Ivancovsky-Wajcman D, Younossi ZM, Lazarus JV. Food inequity and insecurity and MASLD: burden, challenges, and interventions. Nature reviews Gastroenterology & hepatology. 2024;21(10):668-86.

19. Mak L-Y, Liu K, Chirapongsathorn S, Yew KC, Tamaki N, Rajaram RB, et al. Liver diseases and hepatocellular carcinoma in the Asia-Pacific region: burden, trends, challenges and future directions. Nature reviews Gastroenterology & hepatology. 2024;21(12):834-51.

20. Pennisi G, Infantino G, Celsa C, Di Maria G, Enea M, Vaccaro M, et al. Clinical outcomes of MAFLD versus NAFLD: A meta-analysis of observational studies. Liver Int. 2024;44(11):2939-49.

21. Farahat TM, Ungan M, Vilaseca J, Ponzo J, Gupta PP, Schreiner AD, et al. The paradigm shift from NAFLD to MAFLD: A global primary care viewpoint. Liver international : official journal of the International Association for the Study of the Liver. 2022;42(6):1259-67.

22. Liang J, Kim N, Yang JD. Hepatocellular carcinoma risk prediction and early detection in patients with metabolic dysfunction associated steatotic liver disease. Transl Gastroent Hep. 2024;9.

23. Teng ML, Ng CH, Huang DQ, Chan KE, Tan DJ, Lim WH, et al. Global incidence and prevalence of nonalcoholic fatty liver disease. Clinical and Molecular Hepatology. 2023;29(Suppl):S32.

24. Tilg H, Petta S, Stefan N, Targher G. Metabolic Dysfunction–Associated Steatotic Liver Disease in Adults: A Review. JAMA. 2025.

25. Gines P, Castera L, Lammert F, Graupera I, Serra-Burriel M, Allen AM, et al. Population screening for liver fibrosis: Toward early diagnosis and intervention for chronic liver diseases. Hepatology (Baltimore, Md). 2022;75(1):219-28.

26. Stefan N, Yki-Jarvinen H, Neuschwander-Tetri BA. Metabolic dysfunction-associated steatotic liver disease: heterogeneous pathomechanisms and effectiveness of metabolism-based treatment. The lancet Diabetes & endocrinology. 2025;13(2):134-48.

27. Kraus N, Uschner FE, Moeslein M, Schierwagen R, Gu W, Brol MJ, et al. Decompensated MASH-Cirrhosis Model by Acute and Toxic Effects of Phenobarbital. Cells. 2024;13(20).

28. Gancheva S, Roden M, Castera L. Diabetes as a risk factor for MASH progression. Diabetes Res Clin Pract. 2024;217:111846.

29. Ezhilarasan D. Hepatic stellate cells in the injured liver: Perspectives beyond hepatic fibrosis. J Cell Physiol. 2022;237(1):436-49.

30. Motta BM, Masarone M, Torre P, Persico M. From Non-Alcoholic Steatohepatitis (NASH) to Hepatocellular Carcinoma (HCC): Epidemiology, Incidence, Predictions, Risk Factors, and Prevention. Cancers (Basel). 2023;15(22).

31. Chen J, Su Y, Su X, Luo F. Remnant cholesterol has a non-linear association with non-alcoholic fatty liver disease. Diabetes Res Clin Pract. 2023;201:110733.

32. Riazi K, Swain MG, Congly SE, Kaplan GG, Shaheen A-A. Race and Ethnicity in Non-Alcoholic Fatty Liver Disease (NAFLD): A Narrative Review. Nutrients. 2022;14(21).

33. Ciardullo S, Vergani M, Perseghin G. Nonalcoholic Fatty Liver Disease in Patients with Type 2 Diabetes: Screening, Diagnosis, and Treatment. J Clin Med. 2023;12(17).

34. Seval GC, Kabacam G, Yakut M, Seven G, Savas B, Elhan A, et al., editors. The natural course of non-alcoholic fatty liver disease. Hepatology Forum; 2020.

35. Wang W, Xu AL, Li ZC, Li Y, Xu SF, Sang HC, et al. Combination of Probiotics and Salvia miltiorrhiza Polysaccharide Alleviates Hepatic Steatosis via Gut Microbiota Modulation and Insulin Resistance Improvement in High Fat-Induced NAFLD Mice. Diabetes Metab J. 2020;44(2):336-48.

36. Ren LP, Chan SMH, Zeng XY, Laybutt DR, Iseli TJ, Sun RQ, et al. Differing Endoplasmic Reticulum Stress Response to Excess Lipogenesis versus Lipid Oversupply in Relation to Hepatic Steatosis and Insulin Resistance. Plos One. 2012;7(2).

37. Zhao Y, Zhou Y, Wang D, Huang Z, Xiao X, Zheng Q, et al. Mitochondrial Dysfunction in Metabolic Dysfunction Fatty Liver Disease (MAFLD). Int J Mol Sci. 2023;24(24).

38. Petrescu M, Vlaicu SI, Ciumarnean L, Milaciu MV, Marginean C, Florea M, et al. Chronic Inflammation-A Link between Nonalcoholic Fatty Liver Disease (NAFLD) and Dysfunctional Adipose Tissue. Medicina (Kaunas). 2022;58(5).

39. Daniele G, Guardado Mendoza R, Winnier D, Fiorentino TV, Pengou Z, Cornell J, et al. The inflammatory status score including IL-6, TNF-alpha, osteopontin, fractalkine, MCP-1 and adiponectin underlies whole-body insulin resistance and hyperglycemia in type 2 diabetes mellitus. Acta Diabetol. 2014;51(1):123-31.

40. Kessoku T, Kobayashi T, Tanaka K, Yamamoto A, Takahashi K, Iwaki M, et al. The Role of Leaky Gut in Nonalcoholic Fatty Liver Disease: A Novel Therapeutic Target. International journal of molecular sciences. 2021;22(15).

41. Kountouras J, Kazakos E, Kyrailidi F, Polyzos SA, Zavos C, Arapoglou S, et al. Innate immunity and nonalcoholic fatty liver disease. Ann Gastroenterol. 2023;36(3):244-56.

42. Bellanti F, Lo Buglio A, Vendemiale G. Hepatic Mitochondria-Gut Microbiota Interactions in Metabolism-Associated Fatty Liver Disease. Metabolites. 2023;13(3).

43. Le Garf S, Negre V, Anty R, Gual P. Metabolic Fatty Liver Disease in Children: A Growing Public Health Problem. Biomedicines. 2021;9(12).

44. Eslam M, George J. Genetic contributions to NAFLD: leveraging shared genetics to uncover systems biology. Nature reviews Gastroenterology & hepatology. 2020;17(1):40-52.

45. Moretti V, Romeo S, Valenti L. The contribution of genetics and epigenetics to MAFLD susceptibility. Hepatology International. 2024;18(Suppl 2):848-60.

46. Li R, Su K, Wu T, Xu L, Song W, Sun D, et al. Genome-wide enhancer-gene regulatory maps of liver reveal novel regulatory mechanisms underlying NAFLD pathogenesis. BMC genomics. 2025;26(1):493.

47. Grimaudo S, Pipitone RM, Pennisi G, Celsa C, Camma C, Di Marco V, et al. Association Between PNPLA3 rs738409 C>G Variant and Liver-Related Outcomes in Patients With Nonalcoholic Fatty Liver Disease. Clinical gastroenterology and hepatology : the official clinical practice journal of the American Gastroenterological Association. 2020;18(4):935-44.e3.

48. Gensluckner S, Schnefeld HL, Embacher J, Hansen CD, Balcar L, Bech KT, et al. PNPLA3 and TM6SF2 exacerbate the impact of alcohol and metabolic dysfunction on liver fibrosis☆. JHEP Reports. 2025:101649.

49. Chen VL, Brady GF. Recent advances in MASLD genetics: Insights into disease mechanisms and the next frontiers in clinical application. Hepatol Commun. 2025;9(1).

50. Li TH, Huang YS, Ma CC, Tsai SY, Tsai HC, Yeh HY, et al. GCKR Polymorphisms Increase the Risks of Low Bone Mineral Density in Young and Non-Obese Patients With MASLD and Hyperuricemia. The Kaohsiung Journal of Medical Sciences. 2025:e70017.

51. Zhu X, Xia M, Gao X. Update on genetics and epigenetics in metabolic associated fatty liver disease. Ther Adv Endocrinol Metab. 2022;13:20420188221132138.

52. Wei S, Guan G, Luan X, Yu C, Miao L, Yuan X, et al. NLRP3 inflammasome constrains liver regeneration through impairing MerTK-mediated macrophage efferocytosis. Science Advances. 2025;11(1):eadq5786.

53. Wang P, Song D, Han J, Zhang J, Chen H, Gao R, et al. Comparing Three Ultrasound-Based Techniques for Diagnosing and Grading Hepatic Steatosis in Metabolic Dysfunction-Associated Steatotic Liver Disease. Acad Radiol. 2025;32(4):1949-57.

54. Malandris K, Katsoula A, Liakos A, Bekiari E, Karagiannis T, Theocharidou E, et al. Accuracy of controlled attenuation parameter for liver steatosis in patients at risk for metabolic dysfunction-associated steatotic liver disease using magnetic resonance imaging: a systematic review and meta-analysis. Ann Gastroenterol. 2024;37(5).

55. Papagianni M, Sofogianni A, Tziomalos K. Non-invasive methods for the diagnosis of nonalcoholic fatty liver disease. World J Hepatol. 2015;7(4):638-48.

56. Boursier J, Hagstrom H, Ekstedt M, Moreau C, Bonacci M, Cure S, et al. Non-invasive tests accurately stratify patients with NAFLD based on their risk of liver-related events. Journal of hepatology. 2022;76(5):1013-20.

57. Kang YW, Baek YH, Moon SY. Sequential Diagnostic Approach Using FIB-4 and ELF for Predicting Advanced Fibrosis in Metabolic Dysfunction-Associated Steatotic Liver Disease. Diagnostics. 2024;14(22).

58. Kim J, Ito T, Arai T, Atsukawa M, Kawanaka M, Toyoda H, et al. Modified FIB-4 Index in Type 2 Diabetes Mellitus with Steatosis: A Non-Linear Predictive Model for Advanced Hepatic Fibrosis. Diagnostics (Basel). 2024;14(22).

59. Viganò M, Pugliese N, Cerini F, Turati F, Cimino V, Ridolfo S, et al. Accuracy of FIB-4 to Detect Elevated Liver Stiffness Measurements in Patients with Non-Alcoholic Fatty Liver Disease: A Cross-Sectional Study in Referral Centers. International Journal of Molecular Sciences. 2022;23(20).

60. Wu YL, Kumar R, Wang MF, Singh M, Huang JF, Zhu YY, et al. Validation of conventional non-invasive fibrosis scoring systems in patients with metabolic associated fatty liver disease. World Journal of Gastroenterology. 2021;27(34).

61. Sung S, Al-Karaghouli M, Tam M, Wong YJ, Jayakumar S, Davyduke T, et al. Age-dependent differences in FIB-4 predictions of fibrosis in patients with MASLD referred from primary care. Hepatol Commun. 2025;9(1).

62. Jang SY, Yoon KT, Cho YY, Jo HG, Baek YH, Moon SY, et al. Aspartate aminotransferase-to-platelet ratio index outperforms Fibrosis-4 in 2843 Korean patients with metabolic dysfunction-associated steatotic liver disease. Hepatol Res. 2025;55(4):479-91.

63. Armstrong S, Rajiah K, Courtenay A, Ali N, Abuelhana A. Evaluating the Diagnostic Potential of the FIB-4 Index for Cystic Fibrosis-Associated Liver Disease in Adults: A Comparison with Transient Elastography. J Clin Med. 2025;14(15):5404.

64. Balestra E, Traunero A, Barbi E. Investigating the role of Vitamin D in NAFLD: is liver biopsy justifiable in children? Eur J Pediatr. 2022;181(11):3985.

65. Singla T, Muneshwar KN, Pathade AG, Yelne S. Hepatocytic Ballooning in Non-alcoholic Steatohepatitis: Bridging the Knowledge Gap and Charting Future Avenues. Cureus. 2023;15(9):e45884.

66. Sumida Y, Nakajima A, Itoh Y. Limitations of liver biopsy and non-invasive diagnostic tests for the diagnosis of nonalcoholic fatty liver disease/nonalcoholic steatohepatitis. World J Gastroenterol. 2014;20(2):475-85.

67. Fraczek J, Sowa A, Agopsowicz P, Migacz M, Dylinska-Kala K, Holecki M. Non-Invasive Tests as a Replacement for Liver Biopsy in the Assessment of MASLD. Medicina (Kaunas). 2025;61(4).

68. Eslam M, El-Serag HB, Francque S, Sarin SK, Wei L, Bugianesi E, et al. Metabolic (dysfunction)-associated fatty liver disease in individuals of normal weight. Nat Rev Gastroenterol Hepatol. 2022;19(10):638-51.

69. Méndez-Sánchez N, Díaz-Orozco LE. International consensus recommendations to replace the terminology of non-alcoholic fatty liver disease (NAFLD) with metabolic-associated fatty liver disease (MAFLD). Medical Science Monitor: International Medical Journal of Experimental and Clinical Research. 2021;27:e933860-1.

70. Ilagan-Ying YC, Banini BA, Do A, Lam R, Lim JK. Screening, diagnosis, and staging of non-alcoholic fatty liver disease (NAFLD): application of society guidelines to clinical practice. Current gastroenterology reports. 2023;25(10):213-24.

71. Njei B, Ameyaw P, Al-Ajlouni Y, Njei L-P, Boateng S. Diagnosis and Management of Lean Metabolic Dysfunction-Associated Steatotic Liver Disease (MASLD): A Systematic Review. Cureus. 2024;16(10):e71451.

72. Rotaru A, Stratina E, Huiban L, Girleanu I, Minea H, Sfarti C, et al. Beyond BMI: revealing metabolic risk in lean MASLD. Archive of Clinical Cases. 2025;12(3):110.

73. Méndez-Sánchez N, Brouwer WP, Lammert F, Yilmaz Y. Metabolic dysfunction associated fatty liver disease in healthy weight individuals. Hepatology international. 2024;18(Suppl 2):884-96.

74. Younossi ZM, Kalligeros M, Henry L. Epidemiology of metabolic dysfunction-associated steatotic liver disease. Clin Mol Hepatol. 2025;31(Suppl):S32-s50.

75. Ye Q, Zou B, Yeo YH, Li J, Huang DQ, Wu Y, et al. Global prevalence, incidence, and outcomes of non-obese or lean non-alcoholic fatty liver disease: a systematic review and meta-analysis. Lancet Gastroenterol Hepatol. 2020;5(8):739-52.

76. Young S, Tariq R, Provenza J, Satapathy SK, Faisal K, Choudhry A, et al. Prevalence and Profile of Nonalcoholic Fatty Liver Disease in Lean Adults: Systematic Review and Meta-Analysis. Hepatol Commun. 2020;4(7):953-72.

77. Pei Y, Goh GB-B. Genetic Risk Factors for Metabolic Dysfunction-Associated Steatotic Liver Disease. Gut Liver. 2025;19(1):8-18.

78. Lu F-B, Zheng KI, Rios RS, Targher G, Byrne CD, Zheng M-H. Global epidemiology of lean non-alcoholic fatty liver disease: A systematic review and meta-analysis. Journal of gastroenterology and hepatology. 2020;35(12):2041-50.

79. Tang A, Ng CH, Phang PH, Chan KE, Chin YH, Fu CE, et al. Comparative Burden of Metabolic Dysfunction in Lean NAFLD vs Non-lean NAFLD - A Systematic Review and Meta-analysis. Clinical gastroenterology and hepatology : the official clinical practice journal of the American Gastroenterological Association. 2023;21(7):1750-60.e12.

80. Spalding KL, Bernard S, Näslund E, Salehpour M, Possnert G, Appelsved L, et al. Impact of fat mass and distribution on lipid turnover in human adipose tissue. Nature communications. 2017;8(1):15253.

81. Njei B, Mezzacappa C, John BV, Serper M, Kaplan DE, Taddei TH, et al. Mortality, Hepatic Decompensation, and Cardiovascular Outcomes in Lean vs. Non-lean MASLD Cirrhosis: A Veterans Affairs Cohort Study. Digestive Diseases and Sciences. 2025;70(2):802-13.

82. Younes R, Govaere O, Petta S, Miele L, Tiniakos D, Burt A, et al. Caucasian lean subjects with non-alcoholic fatty liver disease share long-term prognosis of non-lean: time for reappraisal of BMI-driven approach? Gut. 2022;71(2):382-90.

83. Lebovics N, Heering G, Frishman WH, Lebovics E. Lean MASLD and Cardiovascular Disease: A Review. Cardiology in Review.10.1097.

84. Marjot T, Armstrong MJ, Stine JG. Skeletal muscle and MASLD: Mechanistic and clinical insights. Hepatol Commun. 2025;9(6):e0711.

85. Baffy G, Portincasa P. Gut microbiota and sinusoidal vasoregulation in MASLD: a portal perspective. Metabolites. 2024;14(6):324.

86. Machado MV. Nonalcoholic fatty liver disease in lean subjects: is it all metabolic-associated fatty liver disease? Hepatoma Research. 2020;6(0):84.

87. Hong S-h, Choi KM. Sarcopenic obesity, insulin resistance, and their implications in cardiovascular and metabolic consequences. International journal of molecular sciences. 2020;21(2):494.

88. Orfanidou M, Polyzos SA. Retinopathy in metabolic dysfunction-associated Steatotic liver disease. Medicina. 2024;61(1):38.

89. Wong VW-S. Complex Interaction Between Visceral Adiposity and Metabolic Dysfunction-Associated Steatotic Liver Disease. J Clin Exp Hepatol. 2025;15(1).

90. Orlando FA, Mainous III AG. Inflammation and chronic disease. Frontiers Media SA; 2024. p. 1434533.

91. Chen VL, Du X, Oliveri A, Chen Y, Kuppa A, Halligan BD, et al. Genetic risk accentuates dietary effects on hepatic steatosis, inflammation and fibrosis in a population-based cohort. Journal of Hepatology. 2024;81(3):379-88.

92. Li X, Chen W, Jia Z, Xiao Y, Shi A, Ma X. Mitochondrial Dysfunction as a Pathogenesis and Therapeutic Strategy for Metabolic-Dysfunction-Associated Steatotic Liver Disease. International Journal of Molecular Sciences. 2025;26(9):4256.

93. Jang WB, Rethineswaran VK, Kwon S-M. Targeting Mitochondrial Dysfunction to Prevent Endothelial Dysfunction and Atherosclerosis in Diabetes: Focus on the Novel Uncoupler BAM15. International Journal of Molecular Sciences. 2025;26(10):4603.

94. Ren G, Bai C, Yi S, Cong Q, Zhu Y. Mechanisms and Therapeutic Strategies for MAFLD Targeting TLR4 Signaling Pathways. J Innate Immun. 2024;16(1):45-55.

95. Anirvan P, Khan ZH, Bhuyan P, Dixit S, Dash R, Mishra P, et al. Gut Microbiota and Genetic Polymorphisms Appear to Drive Disease Expression of Nonalcoholic Fatty Liver Disease in Lean Individuals. J Clin Exp Hepatol. 2025;15(3):102503.

96. Patel AH, Peddu D, Amin S, Elsaid MI, Minacapelli CD, Chandler T-M, et al. Nonalcoholic fatty liver disease in lean/nonobese and obese individuals: a comprehensive review on prevalence, pathogenesis, clinical outcomes, and treatment. J Clin Transl Hepato. 2022;11(2):502.

97. Feng Z, Zhao F, Wang Z, Tang X, Xie Y, Qiu L. The relationship between sarcopenia and metabolic dysfunction-associated fatty liver disease among the young and middle-aged populations. BMC Gastroenterol. 2024;24(1):111.

98. Meroni M, Longo M, Tria G, Dongiovanni P. Genetics is of the essence to face NAFLD. Biomedicines. 2021;9(10):1359.

99. Chouchani ET, Kajimura S. Metabolic adaptation and maladaptation in adipose tissue. Nature metabolism. 2019;1(2):189-200.

100. Cheah MC, Crane H, George J. Global prevalence, metabolic characteristics, and outcomes of lean-MAFLD: a systematic review and meta-analysis. Hepatology International. 2025:1-12.

101. Smith RL, Soeters MR, Wüst RC, Houtkooper RH. Metabolic flexibility as an adaptation to energy resources and requirements in health and disease. Endocrine reviews. 2018;39(4):489-517.

102. Heitel P, Faudone G, Helmstädter M, Schmidt J, Kaiser A, Tjaden A, et al. A triple farnesoid X receptor and peroxisome proliferator-activated receptor α/δ activator reverses hepatic fibrosis in diet-induced NASH in mice. Communications chemistry. 2020;3(1):174.

103. Chen F, Esmaili S, Rogers GB, Bugianesi E, Petta S, Marchesini G, et al. Lean NAFLD: a distinct entity shaped by differential metabolic adaptation. Hepatology. 2020;71(4):1213-27.

104. Alharthi J, Pan Z, Gloss BS, McLeod D, Weltman M, George J, et al. Loss of metabolic adaptation in lean MAFLD is driven by endotoxemia leading to epigenetic reprogramming. Metabolism. 2023;144:155583.

105. Duan L, Chang Y, Dai J, Lu H, Zhao W, Shen Y, et al. Lipid metabolism orchestrates liver regeneration: an integrated metabolic network. Journal of Translational Medicine. 2025;23(1):1-20.

106. Boccardi V, Marano L. The telomere connection between aging and cancer: The burden of replication stress and dysfunction. Mechanisms of Ageing and Development. 2025;223:112026.

107. Assalve G, Lunetti P, Rocca MS, Cosci I, Di Nisio A, Ferlin A, et al. Exploring the Link Between Telomeres and Mitochondria: Mechanisms and Implications in Different Cell Types. International Journal of Molecular Sciences. 2025;26(3):993.

108. Prasanna M, Varadan K, Babu A, Arumugaperumal A. A Comprehensive Review on the Telomeric Repeat Sequence in Different Organisms. Medinformatics. 2025;2(4):256-67.

109. Palm W, de Lange T. How shelterin protects mammalian telomeres. Annu Rev Genet. 2008;42:301-34.

110. Ghilain C, Gilson E, Giraud-Panis M-J. Multifunctionality of the Telomere-Capping Shelterin Complex Explained by Variations in Its Protein Composition. Cells. 2021;10(7).

111. de Lange T. Shelterin-Mediated Telomere Protection. Annu Rev Genet. 2018;52:223-47.

112. Maestroni L, Matmati S, Coulon S. Solving the Telomere Replication Problem. Genes (Basel). 2017;8(2).

113. Trybek T, Kowalik A, Gozdz S, Kowalska A. Telomeres and telomerase in oncogenesis. Oncol Lett. 2020;20(2):1015-27.

114. Liu J, Wang L, Wang Z, Liu J-P. Roles of Telomere Biology in Cell Senescence, Replicative and Chronological Ageing. Cells. 2019;8(1).

115. dreamstime. telomerase molecule. dreamstime. 2025.

116. Munroe M, Niero EL, Fok WC, Vessoni AT, Jeong H-C, Brenner KA, et al. Telomere Dysfunction Activates p53 and Represses HNF4alpha Expression Leading to Impaired Human Hepatocyte Development and Function. Hepatology (Baltimore, Md). 2020;72(4):1412-29.

117. Michalopoulos GK, Bhushan B. Liver regeneration: biological and pathological mechanisms and implications. Nature reviews Gastroenterology & hepatology. 2021;18(1):40-55.

118. Han F, Riaz F, Pu J, Gao R, Yang L, Wang Y, et al. Connecting the Dots: Telomere Shortening and Rheumatic Diseases. Biomolecules. 2024;14(10).

119. Kong CM, Lee XW, Wang X. Telomere shortening in human diseases. Febs J. 2013;280(14):3180-93.

120. Shin HK, Park JH, Yu JH, Jin Y-J, Suh YJ, Lee J-W, et al. Association between telomere length and hepatic fibrosis in non-alcoholic fatty liver disease. Scientific Reports. 2021;11(1):18004.

121. Gavia-Garcia G, Rosado-Perez J, Arista-Ugalde TL, Aguiniga-Sanchez I, Santiago-Osorio E, Mendoza-Nunez VM. Telomere Length and Oxidative Stress and Its Relation with Metabolic Syndrome Components in the Aging. Biology. 2021;10(4).

122. Papatheodoridi A-M, Chrysavgis L, Koutsilieris M, Chatzigeorgiou A. The Role of Senescence in the Development of Nonalcoholic Fatty Liver Disease and Progression to Nonalcoholic Steatohepatitis. Hepatology (Baltimore, Md). 2020;71(1):363-74.

123. Alarabi M, Pan Z, Romero-Gomez M, George J, Eslam M. Telomere length and mortality in lean MAFLD: the other face of metabolic adaptation. Hepatol Int. 2024;18(5):1448-58.

124. Wu D, van de Graaf SFJ. Maladaptive regeneration and metabolic dysfunction associated steatotic liver disease: Common mechanisms and potential therapeutic targets. Biochem Pharmacol. 2024;227:116437.

125. Horn P, Tacke F. Metabolic reprogramming in liver fibrosis. Cell Metab. 2024;36(7):1439-55.

126. Rossiello F, Herbig U, Longhese MP, Fumagalli M, d'Adda di Fagagna F. Irreparable telomeric DNA damage and persistent DDR signalling as a shared causative mechanism of cellular senescence and ageing. Curr Opin Genet Dev. 2014;26:89-95.

127. Meijnikman AS, Herrema H, Scheithauer TPM, Kroon J, Nieuwdorp M, Groen AK. Evaluating causality of cellular senescence in non-alcoholic fatty liver disease. JHEP Rep. 2021;3(4):100301.

128. Wijayasiri P, Astbury S, Kaye P, Oakley F, Alexander GJ, Kendall TJ, et al. Role of Hepatocyte Senescence in the Activation of Hepatic Stellate Cells and Liver Fibrosis Progression. Cells. 2022;11(14).

129. Zhou Y, Zhang L, Ma Y, Xie L, Yang Y-Y, Jin C, et al. Secretome of senescent hepatic stellate cells favors malignant transformation from nonalcoholic steatohepatitis-fibrotic progression to hepatocellular carcinoma. Theranostics. 2023;13(13):4430-48.

130. Engelmann C, Tacke F. The potential role of cellular senescence in non-alcoholic fatty liver disease. International journal of molecular sciences. 2022;23(2):652.

131. Plentz RR, Caselitz M, Bleck JS, Gebel M, Flemming P, Kubicka S, et al. Hepatocellular telomere shortening correlates with chromosomal instability and the development of human hepatoma. Hepatology (Baltimore, Md). 2004;40(1):80-6.

132. Martinez P, Blasco MA. Telomere-driven diseases and telomere-targeting therapies. J Cell Biol. 2017;216(4):875-87.

133. Cleal K, Baird DM. Catastrophic endgames: emerging mechanisms of telomere-driven genomic instability. Trends in Genetics. 2020;36(5):347-59.

134. In der Stroth L, Tharehalli U, Gunes C, Lechel A. Telomeres and Telomerase in the Development of Liver Cancer. Cancers (Basel). 2020;12(8).

135. Nault J-C, Ningarhari M, Rebouissou S, Zucman-Rossi J. The role of telomeres and telomerase in cirrhosis and liver cancer. Nature reviews Gastroenterology & hepatology. 2019;16(9):544-58.

136. Tsai VW, Husaini Y, Sainsbury A, Brown DA, Breit SN. The MIC-1/GDF15-GFRAL pathway in energy homeostasis: implications for obesity, cachexia, and other associated diseases. Cell metabolism. 2018;28(3):353-68.

137. Wischhusen J, Melero I, Fridman WH. Growth/differentiation factor-15 (GDF-15): from biomarker to novel targetable immune checkpoint. Frontiers in immunology. 2020;11:951.

138. Girona J, Guardiola M, Barroso E, García-Altares M, Ibarretxe D, Plana N, et al. GDF15 Circulating Levels Are Associated with Metabolic-Associated Liver Injury and Atherosclerotic Cardiovascular Disease. International Journal of Molecular Sciences. 2025;26(5):2039.

139. Schwarz A, Kinscherf R, Bonaterra GA. Role of the stress-and inflammation-induced cytokine GDF-15 in cardiovascular diseases: from basic research to clinical relevance. Reviews in Cardiovascular Medicine. 2023;24(3):81.

140. Boutari C, Stefanakis K, Simati S, Guatibonza-García V, Valenzuela-Vallejo L, Anastasiou IA, et al. Circulating total and H-specific GDF15 levels are elevated in subjects with MASLD but not in hyperlipidemic but otherwise metabolically healthy subjects with obesity. Cardiovasc Diabetol. 2024;23(1):174.

141. Iglesias P, Silvestre RA, Díez JJ. Growth differentiation factor 15 (GDF-15) in endocrinology. Endocrine. 2023;81(3):419-31.

142. Kim KH, Lee M-S. GDF15 as a central mediator for integrated stress response and a promising therapeutic molecule for metabolic disorders and NASH. Biochim Biophys Acta Gen Subj. 2021;1865(3):129834.

143. Johann K, Kleinert M, Klaus S. The role of GDF15 as a myomitokine. Cells. 2021;10(11):2990.

144. Fujita Y, Taniguchi Y, Shinkai S, Tanaka M, Ito M. Secreted growth differentiation factor 15 as a potential biomarker for mitochondrial dysfunctions in aging and age-related disorders. Geriatrics & gerontology international. 2016;16:17-29.

145. Du Y-N, Zhao J-W. GDF15: Immunomodulatory role in hepatocellular carcinoma pathogenesis and therapeutic implications. J Hepatocell Carcinoma. 2024:1171-83.

146. Liu Y, Yong C, Yang M, Qi H, Zheng S, Wang M, et al. The upregulation of GDF15 is controlled epigenetically by oncogenic TCF19 signaling in human hepatocellular carcinoma. iScience. 2025;28(10).

147. Rao S, Chiu T-P, Kribelbauer JF, Mann RS, Bussemaker HJ, Rohs R. Systematic prediction of DNA shape changes due to CpG methylation explains epigenetic effects on protein–DNA binding. Epigenetics & chromatin. 2018;11(1):6.

148. Lu X, He X, Su J, Wang J, Liu X, Xu K, et al. EZH2-mediated epigenetic suppression of GDF15 predicts a poor prognosis and regulates cell proliferation in non-small-cell lung cancer. Molecular Therapy Nucleic Acids. 2018;12:309-18.

149. Winter L-M, Reinhardt D, Schatter A, Tissen V, Wiora H, Gerlach D, et al. Molecular basis of GDF15 induction and suppression by drugs in cardiomyocytes and cancer cells toward precision medicine. Scientific Reports. 2023;13(1):12061.

150. Gadd DA, Smith HM, Mullin D, Chybowska O, Hillary RF, Kimenai DM, et al. DNAm scores for serum GDF15 and NT-proBNP levels associate with a range of traits affecting the body and brain. Clinical Epigenetics. 2024;16(1):124.

151. Luo H, Shen Y. Association between DNA methylation predicted growth differentiation factor 15 and mortality: results from NHANES 1999–2002. Aging Clin Exp Res. 2024;36(1):234.

152. Jiang W-W, Zhang Z-Z, He P-P, Jiang L-P, Chen J-Z, Zhang X-T, et al. Emerging roles of growth differentiation factor-15 in brain disorders. Experimental and Therapeutic Medicine. 2021;22(5):1270.

153. Tsui K-H, Hsu S-Y, Chung L-C, Lin Y-H, Feng T-H, Lee T-Y, et al. Growth differentiation factor-15: a p53-and demethylation-upregulating gene represses cell proliferation, invasion and tumorigenesis in bladder carcinoma cells. Scientific reports. 2015;5(1):12870.

154. Jones PA, Baylin SB. The fundamental role of epigenetic events in cancer. Nature reviews genetics. 2002;3(6):415-28.

155. Drouin SM, Kuo PL, Moore Z, Davatzikos C, Resnick SM, Walker KA. CRP and GDF15 DNA methylation signatures differentially predict brain volume loss. Alzheimer's & Dementia. 2024;20:e095367.

156. Wollweber F, von der Malsburg K, van der Laan M. Mitochondrial contact site and cristae organizing system: A central player in membrane shaping and crosstalk. Biochim Biophys Acta Mol Cell Res. 2017;1864(9):1481-9.

157. Zerbes RM, Bohnert M, Stroud DA, von der Malsburg K, Kram A, Oeljeklaus S, et al. Role of MINOS in mitochondrial membrane architecture: cristae morphology and outer membrane interactions differentially depend on mitofilin domains. J Mol Biol. 2012;422(2):183-91.

158. Colombini M. Mitochondrial outer membrane channels. Chem Rev. 2012;112(12):6373-87.

159. Martinez-Reyes I, Chandel NS. Mitochondrial TCA cycle metabolites control physiology and disease. Nature communications. 2020;11(1):102.

160. Najt CP, Adhikari S, Heden TD, Cui W, Gansemer ER, Rauckhorst AJ, et al. Organelle interactions compartmentalize hepatic fatty acid trafficking and metabolism. Cell Rep. 2023;42(5):112435.

161. Twig G, Hyde B, Shirihai OS. Mitochondrial fusion, fission and autophagy as a quality control axis: the bioenergetic view. Biochimica et biophysica acta. 2008;1777(9):1092-7.

162. Chen H, Chan DC. Mitochondrial dynamics--fusion, fission, movement, and mitophagy--in neurodegenerative diseases. Hum Mol Genet. 2009;18(R2):R169-76.

163. Ma X, McKeen T, Zhang J, Ding W-X. Role and Mechanisms of Mitophagy in Liver Diseases. Cells. 2020;9(4).

164. Archer SL. Mitochondrial dynamics--mitochondrial fission and fusion in human diseases. N Engl J Med. 2013;369(23):2236-51.

165. Eyenga P, Rey B, Eyenga L, Sheu S-S. Regulation of Oxidative Phosphorylation of Liver Mitochondria in Sepsis. Cells. 2022;11(10).

166. Arnold PK, Finley LWS. Regulation and function of the mammalian tricarboxylic acid cycle. J Biol Chem. 2023;299(2).

167. Lee RKY, Ng BYN, Chen DMH. Blended learning in biochemistry: The development of pre-class and post-class learning aids for electron transport chain and oxidative phosphorylation. Biochem Mol Biol Educ. 2024;52(2):220-7.

168. Nolfi-Donegan D, Braganza A, Shiva S. Mitochondrial electron transport chain: Oxidative phosphorylation, oxidant production, and methods of measurement. Redox Biol. 2020;37:101674.

169. Begriche K, Massart J, Robin M-A, Bonnet F, Fromenty B. Mitochondrial adaptations and dysfunctions in nonalcoholic fatty liver disease. Hepatology (Baltimore, Md). 2013;58(4):1497-507.

170. Guerra IMS, Ferreira HB, Melo T, Rocha H, Moreira S, Diogo L, et al. Mitochondrial Fatty Acid beta-Oxidation Disorders: From Disease to Lipidomic Studies-A Critical Review. International journal of molecular sciences. 2022;23(22).

171. Tonazzi A, Giangregorio N, Console L, Palmieri F, Indiveri C. The Mitochondrial Carnitine Acyl-carnitine Carrier (SLC25A20): Molecular Mechanisms of Transport, Role in Redox Sensing and Interaction with Drugs. Biomolecules. 2021;11(4).

172. Savic D, Hodson L, Neubauer S, Pavlides M. The Importance of the Fatty Acid Transporter L-Carnitine in Non-Alcoholic Fatty Liver Disease (NAFLD). Nutrients. 2020;12(8).

173. Adeva-Andany MM, Carneiro-Freire N, Seco-Filgueira M, Fernandez-Fernandez C, Mourino-Bayolo D. Mitochondrial beta-oxidation of saturated fatty acids in humans. Mitochondrion. 2019;46:73-90.

174. Tahri-Joutey M, Andreoletti P, Surapureddi S, Nasser B, Cherkaoui-Malki M, Latruffe N. Mechanisms Mediating the Regulation of Peroxisomal Fatty Acid Beta-Oxidation by PPARalpha. International journal of molecular sciences. 2021;22(16).

175. Zorov DB, Juhaszova M, Sollott SJ. Mitochondrial reactive oxygen species (ROS) and ROS-induced ROS release. Physiol Rev. 2014;94(3):909-50.

176. Onukwufor JO, Berry BJ, Wojtovich AP. Physiologic Implications of Reactive Oxygen Species Production by Mitochondrial Complex I Reverse Electron Transport. Antioxidants (Basel). 2019;8(8).

177. Gusti AMT, Qusti SY, Alshammari EM, Toraih EA, Fawzy MS. Antioxidants-Related Superoxide Dismutase (SOD), Catalase (CAT), Glutathione Peroxidase (GPX), Glutathione Transferase (GST), and Nitric Oxide Synthase (NOS) Gene Variants Analysis in an Obese Population: A Preliminary Case-Control Study. Antioxidants (Basel). 2021;10(4).

178. Lee H-C, Wei Y-H. Oxidative stress, mitochondrial DNA mutation, and apoptosis in aging. Exp Biol Med (Maywood). 2007;232(5):592-606.

179. Seki E, Schwabe RF. Hepatic inflammation and fibrosis: functional links and key pathways. Hepatology (Baltimore, Md). 2015;61(3):1066-79.

180. Thomsen KL, Eriksen PL, Kerbert AJ, De Chiara F, Jalan R, Vilstrup H. Role of ammonia in NAFLD: An unusual suspect. JHEP Rep. 2023;5(7):100780.

181. Kosenko E, Tikhonova L, Alilova G, Montoliu C. A Look into Liver Mitochondrial Dysfunction as a Hallmark in Progression of Brain Energy Crisis and Development of Neurologic Symptoms in Hepatic Encephalopathy. J Clin Med. 2020;9(7).

182. Dadsena S, Zollo C, Garcia-Saez AJ. Mechanisms of mitochondrial cell death. Biochem Soc Trans. 2021;49(2):663-74.

183. Bock FJ, Tait SWG. Mitochondria as multifaceted regulators of cell death. Nat Rev Mol Cell Biol. 2020;21(2):85-100.

184. LeFort KR, Rungratanawanich W, Song B-J. Contributing roles of mitochondrial dysfunction and hepatocyte apoptosis in liver diseases through oxidative stress, post-translational modifications, inflammation, and intestinal barrier dysfunction. Cell Mol Life Sci. 2024;81(1):34.

185. Zhu J-Y, Chen M, Mu W-J, Luo H-Y, Guo L. The functional role of Higd1a in mitochondrial homeostasis and in multiple disease processes. Genes Dis. 2023;10(5):1833-45.

186. Mu C, Wang S, Wang Z, Tan J, Yin H, Wang Y, et al. Mechanisms and therapeutic targets of mitochondria in the progression of metabolic dysfunction-associated steatotic liver disease. Ann Hepatol. 2024;30(1):101774.

187. Lu X, Xuan W, Li J, Yao H, Huang C, Li J. AMPK protects against alcohol-induced liver injury through UQCRC2 to up-regulate mitophagy. Autophagy. 2021;17(11):3622-43.

188. Begriche K, Igoudjil A, Pessayre D, Fromenty B. Mitochondrial dysfunction in NASH: Causes, consequences and possible means to prevent it. Mitochondrion. 2006;6(1):1-28.

189. Mello T, Zanieri F, Ceni E, Galli A. Oxidative Stress in the Healthy and Wounded Hepatocyte: A Cellular Organelles Perspective. Oxidative medicine and cellular longevity. 2016;2016:8327410.

190. Schirrmacher V. Mitochondria at Work: New Insights into Regulation and Dysregulation of Cellular Energy Supply and Metabolism. Biomedicines. 2020;8(11).

191. Koliaki C, Szendroedi J, Kaul K, Jelenik T, Nowotny P, Jankowiak F, et al. Adaptation of hepatic mitochondrial function in humans with non-alcoholic fatty liver is lost in steatohepatitis. Cell metabolism. 2015;21(5):739-46.

192. Amorim R, Magalhaes CC, Borges F, Oliveira PJ, Teixeira J. From Non-Alcoholic Fatty Liver to Hepatocellular Carcinoma: A Story of (Mal)Adapted Mitochondria. Biology. 2023;12(4).

193. Silva AC, Almeida S, Laco M, Duarte AI, Domingues J, Oliveira CR, et al. Mitochondrial respiratory chain complex activity and bioenergetic alterations in human

platelets derived from pre-symptomatic and symptomatic Huntington's disease carriers. Mitochondrion. 2013;13(6):801-9.

194. Tang C, Tao J, Sun J, Lv F, Lu Z, Lu Y. Regulatory mechanisms of energy metabolism and inflammation in oleic acid-treated HepG2 cells from Lactobacillus acidophilus NX2-6 extract. J Food Biochem. 2021;45(10):e13925.

195. Reale M, Pesce M, Priyadarshini M, Kamal MA, Patruno A. Mitochondria as an easy target to oxidative stress events in Parkinson's disease. CNS Neurol Disord Drug Targets. 2012;11(4):430-8.

196. Deng Y, Dong Y, Zhang S, Feng Y. Targeting mitochondrial homeostasis in the treatment of non-alcoholic fatty liver disease: a review. Front Pharmacol. 2024;15:1463187.

197. Li R-L, Wang L-Y, Duan H-X, Zhang Q, Guo X, Wu C, et al. Regulation of mitochondrial dysfunction induced cell apoptosis is a potential therapeutic strategy for herbal medicine to treat neurodegenerative diseases. Front Pharmacol. 2022;13:937289.

198. Seki S, Kitada T, Yamada T, Sakaguchi H, Nakatani K, Wakasa K. In situ detection of lipid peroxidation and oxidative DNA damage in non-alcoholic fatty liver diseases. Journal of hepatology. 2002;37(1):56-62.

199. Rolo AP, Teodoro JS, Palmeira CM. Role of oxidative stress in the pathogenesis of nonalcoholic steatohepatitis. Free Radic Biol Med. 2012;52(1):59-69.

200. Chen Y-R, Zweier JL. Cardiac mitochondria and reactive oxygen species generation. Circ Res. 2014;114(3):524-37.

201. Sharma S, Le Guillou D, Chen JY. Cellular stress in the pathogenesis of nonalcoholic steatohepatitis and liver fibrosis. Nature Reviews Gastroenterology & Hepatology. 2023;20(10):662-78.

202. Pradas I, Huynh K, Cabre R, Ayala V, Meikle PJ, Jove M, et al. Lipidomics Reveals a Tissue-Specific Fingerprint. Front Physiol. 2018;9:1165.

203. Decker ST, Funai K. Mitochondrial membrane lipids in the regulation of bioenergetic flux. Cell metabolism. 2024;36(9):1963-78.

204. Ren LA, Cui HY, Wang Y, Ju F, Cai YJ, Gang XK, et al. The role of lipotoxicity in kidney disease: From molecular mechanisms to therapeutic prospects. Biomedicine & Pharmacotherapy. 2023;161.

205. Caldwell S, Ikura Y, Dias D, Isomoto K, Yabu A, Moskaluk C, et al. Hepatocellular ballooning in NASH. Journal of hepatology. 2010;53(4):719-23.

206. Chen J, Jian L, Guo Y, Tang C, Huang Z, Gao J. Liver Cell Mitophagy in Metabolic Dysfunction-Associated Steatotic Liver Disease and Liver Fibrosis. Antioxidants (Basel). 2024;13(6).

207. Prasun P, Ginevic I, Oishi K. Mitochondrial dysfunction in nonalcoholic fatty liver disease and alcohol related liver disease. Transl Gastroent Hep. 2021;6:4.

208. Trifunovic A, Wredenberg A, Falkenberg M, Spelbrink JN, Rovio AT, Bruder CE, et al. Premature ageing in mice expressing defective mitochondrial DNA polymerase. Nature. 2004;429(6990):417-23.

209. Eslam M, Fan J-G, Yu M-L, Wong VW-S, Cua IH, Liu C-J, et al. The Asian Pacific association for the study of the liver clinical practice guidelines for the diagnosis and

management of metabolic dysfunction-associated fatty liver disease. Hepatology international. 2025;19(2):261-301.

210. Zipf G, Chiappa M, Porter K, Ostchega Y, Lewis B, Dostal J. National Health and Nutrition Examination Survey: Plan and operations, 1999–2010. Vital Health Statistics Series 1, Number 56. National Center for Health Statistics Retrieved from www cdc gov/nchs/data/series/sr_01/sr01_056 pdf. 2013.

211. EL Sharkawy R. MERTK receptor tyrosine kinase: A novel therapeutic target for liver fibrosis: University of Sydney; 2020.

212. Bayoumi A. Mistranslation drives alterations in protein levels and the effects of a synonymous variant at the FGF21 locus 2020.

213. Eslam M, Fan J-G, Mendez-Sanchez N. Non-alcoholic fatty liver disease in non-obese individuals: the impact of metabolic health. The lancet Gastroenterology & hepatology. 2020;5(8):713-5.

214. Elsabaawy M, Naguib M, Abuamer A, Shaban A. Comparative application of MAFLD and MASLD diagnostic criteria on NAFLD patients: insights from a single-center cohort. Clin Exp Med. 2025;25(1):36.

215. Gaspar RC, Macedo APA, Nakandakari SCBR, Munoz VR, Abud GF, Vieira RFL, et al. Notch1 Signalling Is Downregulated by Aerobic Exercise, Leading to Improvement of Hepatic Metabolism in Obese Mice. Liver international : official journal of the International Association for the Study of the Liver. 2025;45(4):e70068.

216. Nabi O, Lapidus N, Boursier J, de Ledinghen V, Petit J-M, Kab S, et al. Lean individuals with NAFLD have more severe liver disease and poorer clinical outcomes (NASH-CO Study). Hepatology. 2023;78(1):272-83.

217. Wang Q, Zhan Y, Pedersen NL, Fang F, Hägg S. Telomere length and all-cause mortality: a meta-analysis. Ageing research reviews. 2018;48:11-20.

218. Ha J, Yim SY, Karagozian R. Mortality and liver-related events in lean versus non-lean nonalcoholic fatty liver disease: a systematic review and meta-analysis. Clinical Gastroenterology and Hepatology. 2023;21(10):2496-507. e5.

219. Casagrande S, Hau M. Telomere attrition: metabolic regulation and signalling function? Biology Letters. 2019;15(3):20180885.

220. Ahmed W, Lingner J. Impact of oxidative stress on telomere biology. Differentiation. 2018;99:21-7.

221. Gupta A, Shyoran D, Meena PK. Determination of Liver Cirrhosis by Liver Function Tests, Lipid Peroxidation (MDA) and Antioxidant Enzyme (SOD). International Journal of Pharmacy Research & Technology (IJPRT). 2025;15(1):757-62.

222. Karataş Ö, Akçakavak G, Eren M, Çelik Z, Tural A, Dağar O, et al. Determination of 8-OHdG and 4-HNE Expressions in Sheep with Hepatic Lipidosis by Immunohistochemical Method. Manas Journal of Agriculture Veterinary and Life Sciences. 2025;15(1):9-15.

223. Chan SW, Blackburn EH. New ways not to make ends meet: telomerase, DNA damage proteins and heterochromatin. Oncogene. 2002;21(4):553-63.

224. Eskridge W, Cryer DR, Schattenberg JM, Gastaldelli A, Malhi H, Allen AM, et al. Metabolic Dysfunction-Associated Steatotic Liver Disease and Metabolic Dysfunction-Associated Steatohepatitis: The Patient and Physician Perspective. J Clin Med. 2023;12(19).

225. Lalloyer F, Mogilenko DA, Verrijken A, Haas JT, Lamaziere A, Kouach M, et al. Roux-en-Y gastric bypass induces hepatic transcriptomic signatures and plasma metabolite changes indicative of improved cholesterol homeostasis. Journal of hepatology. 2023;79(4):898-909.

226. Kawanishi S, Oikawa S. Mechanism of telomere shortening by oxidative stress. Ann N Y Acad Sci. 2004;1019:278-84.

227. van Steensel B, de Lange T. Control of telomere length by the human telomeric protein TRF1. Nature. 1997;385(6618):740-3.

228. Murphy MP. How mitochondria produce reactive oxygen species. Biochem J. 2009;417(1):1-13.

229. Schneider CV, Schneider KM, Teumer A, Rudolph KL, Hartmann D, Rader DJ, et al. Association of Telomere Length With Risk of Disease and Mortality. JAMA Intern Med. 2022;182(3):291-300.

230. Dlouha D, Maluskova J, Kralova Lesna I, Lanska V, Hubacek JA. Comparison of the relative telomere length measured in leukocytes and eleven different human tissues. Physiol Res. 2014;63(Suppl 3):S343-50.

231. Zou B, Yeo Y, Nguyen V, Cheung R, Ingelsson E, Nguyen M. Prevalence, characteristics and mortality outcomes of obese, nonobese and lean NAFLD in the United States, 1999–2016. Journal of internal medicine. 2020;288(1):139-51.

232. Wijarnpreecha K, Li F, Lundin SK, Suresh D, Song MW, Tao C, et al. Higher mortality among lean patients with non-alcoholic fatty liver disease despite fewer metabolic comorbidities. Alimentary pharmacology & therapeutics. 2023;57(9):1014-27.

233. Trusina A. Stress induced telomere shortening: longer life with less mutations? BMC systems biology. 2014;8(1):27.

234. Tang L, Li D, Ma Y, Cui F, Wang J, Tian Y. The association between telomere length and non-alcoholic fatty liver disease: a prospective study. BMC medicine. 2023;21(1):427.

235. Wedel S, Martic I, Guerrero Navarro L, Ploner C, Pierer G, Jansen-Dürr P, et al. Depletion of growth differentiation factor 15 (GDF15) leads to mitochondrial dysfunction and premature senescence in human dermal fibroblasts. Aging Cell. 2023;22(1):e13752.

236. Cimino I, Coll AP. The role of GDF15 in food intake and appetitive behaviour. Current Opinion in Endocrine and Metabolic Research. 2022;22:100299.

237. Lu JF, Zhu MQ, Xia B, Zhang NN, Liu XP, Liu H, et al. GDF15 is a major determinant of ketogenic diet-induced weight loss. Cell metabolism. 2023;35(12):2165-82.e7.

238. Wang Y, Chen C, Chen J, Sang T, Peng H, Lin X, et al. Overexpression of NAG-1/GDF15 prevents hepatic steatosis through inhibiting oxidative stress-mediated dsDNA release and AIM2 inflammasome activation. Redox Biol. 2022;52:102322.

239. Costa VL, Henrique R, Danielsen SA, Duarte-Pereira S, Eknaes M, Skotheim RI, et al. Three epigenetic biomarkers, GDF15, TMEFF2, and VIM, accurately predict bladder cancer from DNA-based analyses of urine samples. Clinical Cancer Research. 2010;16(23):5842-51.

240. Kadowaki M, Yoshioka H, Kamitani H, Watanabe T, Wade PA, Eling TE. DNA methylation-mediated silencing of nonsteroidal anti-inflammatory drug-activated gene (NAG-1/GDF15) in glioma cell lines. International journal of cancer. 2012;130(2):267-77.

241. Gil CI, Coull BM, Jonas W, Lippert RN, Klaus S, Ost M. Mitochondrial stress-induced GFRAL signaling controls diurnal food intake and anxiety-like behavior. Life Science Alliance. 2022;5(11).

242. Huang J, Ding X, Dong Y, Zhu H. Growth Differentiation Factor-15 Orchestrates Inflammation-Related Diseases via Macrophage Polarization. Discovery Medicine. 2024;36(181):248-55.

243. Chen J, Kastroll J, Bello FM, Pangburn MM, Murali A, Smith PM, et al. Skeletal muscle mitochondrial dysfunction is associated with increased Gdf15 expression and circulating GDF15 levels in aged mice. Scientific reports. 2025;15(1):8101.

244. Peterson MD, Collins S, Meier HCS, Brahmsteadt A, Faul JD. Grip strength is inversely associated with DNA methylation age acceleration. J Cachexia Sarcopenia Muscle. 2023;14(1):108-15.

245. Yi J, Guo H, Jiang C, Duan J, Xue J, Zhao Y, et al. Leukocyte telomere length decreased the risk of mortality in patients with alcohol-associated liver disease. Frontiers in Endocrinology. 2024;15:1462591.

246. Coluzzi E, Colamartino M, Cozzi R, Leone S, Meneghini C, O'Callaghan N, et al. Oxidative stress induces persistent telomeric DNA damage responsible for nuclear morphology change in mammalian cells. PloS one. 2014;9(10):e110963.

247. Wongtrakul W, Charatcharoenwitthaya N, Charatcharoenwitthaya P. Lean non-alcoholic fatty liver disease and the risk of all-cause mortality: An updated meta-analysis. Ann Hepatol. 2024;29(3):101288.

248. Chung GE, Yu SJ, Yoo J-J, Cho Y, Lee K-n, Shin DW, et al. Lean or diabetic subtypes predict increased all-cause and disease-specific mortality in metabolic-associated fatty liver disease. BMC medicine. 2023;21(1):4.

249. Li X, Sun H, Zhang L, Liang H, Zhang B, Yang J, et al. GDF15 attenuates sepsis-induced myocardial dysfunction by inhibiting cardiomyocytes ferroptosis via the SOCS1/GPX4 signaling pathway. Eur J Pharmacol. 2024;982:176894.

250. Huang J, Pan B, He Z, Liu Y, Wang C, Tong J, et al. GDF15 attenuates myocardial hypoxic injury by inhibiting mitochondrial damage through BNIP3 pathway. Molecular biology reports. 2025;52(1):825.

251. Kempf T, Guba-Quint A, Torgerson J, Magnone MC, Haefliger C, Bobadilla M, et al. Growth differentiation factor 15 predicts future insulin resistance and impaired glucose control in obese nondiabetic individuals: results from the XENDOS trial. Eur J Endocrinol. 2012;167(5):671-8.

252. Townsend LK, Weber AJ, Day EA, Shamshoum H, Shaw SJ, Perry CGR, et al. AMPK mediates energetic stress-induced liver GDF15. Faseb J. 2021;35(1):e21218.

253. Bayoumi A, Elsayed A, Han S, Petta S, Adams LA, Aller R, et al. Mistranslation Drives Alterations in Protein Levels and the Effects of a Synonymous Variant at the Fibroblast Growth Factor 21 Locus. Adv Sci (Weinh). 2021;8(11):2004168.

254. Li J, Liu X, Tran TT, Lee M, Tsai RY. DNA Methylation and Target Gene Expression in Fatty Liver Progression From Simple Steatosis to Advanced Fibrosis. Liver International. 2025;45(3):e70040.

255. Sun Z, Pan X, Tian A, Surakka I, Wang T, Jiao X, et al. Genetic variants in HFE are associated with non-alcoholic fatty liver disease in lean individuals. JHEP Reports. 2023;5(7):100744.

256. Sokolova IM, Sokolov EP, Haider F. Mitochondrial mechanisms underlying tolerance to fluctuating oxygen conditions: lessons from hypoxia-tolerant organisms. Integrative and comparative biology. 2019;59(4):938-52.

257. Lambrecht R, Rudolf F, Ückert A-K, Sladky VC, Phan TS, Jansen J, et al. Non-canonical BIM-regulated energy metabolism determines drug-induced liver necrosis. Cell Death & Differentiation. 2024;31(1):119-31.

258. Sanyal AJ. Past, present and future perspectives in nonalcoholic fatty liver disease. Nature reviews Gastroenterology & hepatology. 2019;16(6):377-86.

259. Fernández-Tussy P, Cardelo MP, Zhang H, Sun J, Price NL, Boutagy NE, et al. miR-33 deletion in hepatocytes attenuates MASLD-MASH-HCC progression. JCI insight. 2024;9(19):e168476.

260. Chuang C-C, Chen Y-H, Chu F-Y, Yang C-P, Ho H-L, Chang F-P, et al. Temporal Effects of Lipid Oversupply on Energy Metabolism and Mitochondrial Homeostasis in Hepatocytes. International Journal of Medical Sciences. 2025;22(14):3664-81.

261. Pereira RO, Keipert S. Editorial: Role of mitochondrial stress response in metabolic health. Frontiers in endocrinology. 2024;15:1504718.

262. Matthews DR, Li H, Zhou J, Li Q, Glaser S, Francis H, et al. Methionine- and Choline-Deficient Diet-Induced Nonalcoholic Steatohepatitis Is Associated with Increased Intestinal Inflammation. The American journal of pathology. 2021;191(10):1743-53.

263. Gautam J, Aggarwal H, Kumari D, Gupta SK, Kumar Y, Dikshit M. A methionine-choline-deficient diet induces nonalcoholic steatohepatitis and alters the lipidome, metabolome, and gut microbiome profile in the C57BL/6J mouse. Biochimica et Biophysica Acta (BBA)-Molecular and Cell Biology of Lipids. 2024;1869(8):159545.

264. Kuchay MS, Martínez-Montoro JI, Choudhary NS, Fernández-García JC, Ramos-Molina B. Non-alcoholic fatty liver disease in lean and non-obese individuals: current and future challenges. Biomedicines. 2021;9(10):1346.

265. Reznik E, Miller ML, Senbabaoglu Y, Riaz N, Sarungbam J, Tickoo SK, et al. Mitochondrial DNA copy number variation across human cancers. Elife. 2016;5.

266. Spinazzola A, Invernizzi F, Carrara F, Lamantea E, Donati A, Dirocco M, et al. Clinical and molecular features of mitochondrial DNA depletion syndromes. Journal of inherited metabolic disease. 2009;32(2):143-58.

267. Huang Q, Shire D, Hollis F, Abuaish S, Picard M, Monk C, et al. Mitochondrial health, prenatal distress, and gestational age: investigation of cf-mtDNA and GDF15 in two pregnancy studies from the USA and Turkey. Mitochondrion. 2025:102057.

268. Singh V, Chattopadhyay P, Fatima F, Singh P, Pandey R, Agrawal A, et al. Generation and characterization of a chronic in vitro model to study the early stage of metabolic dysfunction-associated steatotic liver disease (MASLD). Biochimica et Biophysica Acta (BBA)-Molecular Basis of Disease. 2025;1871(6):167886.

269. Bellanti F, Coda ARD, Trecca MI, Lo Buglio A, Serviddio G, Vendemiale G. Redox imbalance in inflammation: the interplay of oxidative and reductive stress. Antioxidants-Basel. 2025;14(6):656.

270. Gu S, Fu L, Wang J, Sun X, Wang X, Lou J, et al. MtDNA copy number in oral epithelial cells serves as a potential biomarker of mitochondrial damage by neonicotinoid exposure: a cross-sectional study. Environmental Science & Technology. 2023;57(42):15816-24.

271. Filograna R, Mennuni M, Alsina D, Larsson NG. Mitochondrial DNA copy number in human disease: the more the better? FEBS letters. 2021;595(8):976-1002.

272. Tantu MT, Farhana FZ, Haque F, Koo KM, Qiao L, Ross AG, et al. Pathophysiology, noninvasive diagnostics and emerging personalized treatments for metabolic associated liver diseases. npj Gut and Liver. 2025;2(1):18.

273. Gao L, Xiong W, Wang Y, Wang W, Wang X, Zhang H. Heterogeneity of cardiometabolic and hepatic fibrosis risks in nonalcoholic fatty liver disease among lean, overweight, and obese populations: a multicenter cross-sectional study. Eur J Gastroenterol Hepatol. 2025;37(8):975-81.

274. Ross JM, Kim A, Berthod K, Branca RM, Olin M, Pichardo-Casas I, et al. Mitochondrial Dysfunction Induces Hepatic Lipid Accumulation and Inflammatory Responses in mtDNA Mutator Mice. bioRxiv. 2025:2025.04. 25.650453.

275. Cheng Y, Zheng X. Characteristics and Mechanisms of Liver Injury Caused by Emerging Infectious Diseases. Frontiers in Immunology.16:1647517.

276. Xie H, Huang R, Xu K, Yang X, Xu W, Guo X, et al. Mitochondrial homeostasis dysfunctions during the epithelial-mesenchymal transition process in lens epithelial cells. Experimental Eye Research. 2025:110583.

277. Collins TJ, Berridge MJ, Lipp P, Bootman MD. Mitochondria are morphologically and functionally heterogeneous within cells. The EMBO journal. 2002.

278. Palorini R, De Rasmo D, Gaviraghi M, Danna LS, Signorile A, Cirulli C, et al. Oncogenic K-ras expression is associated with derangement of the cAMP/PKA pathway and forskolin-reversible alterations of mitochondrial dynamics and respiration. Oncogene. 2013;32(3):352-62.

279. Zou Y, Zhang S, Yang J, Qin C, Jin B, Liang Z, et al. Protective Effects of Astaxanthin on Ochratoxin A-Induced Liver Injury: Effects of Endoplasmic Reticulum Stress and Mitochondrial Fission–Fusion Balance. Toxins. 2024;16(2):68.

280. Matsumoto M, Hada N, Sakamaki Y, Uno A, Shiga T, Tanaka C, et al. An improved mouse model that rapidly develops fibrosis in non-alcoholic steatohepatitis. International journal of experimental pathology. 2013;94(2):93-103.

281. Portincasa P, Khalil M, Mahdi L, Perniola V, Idone V, Graziani A, et al. Metabolic dysfunction–associated steatotic liver disease: from pathogenesis to current therapeutic options. International journal of molecular sciences. 2024;25(11):5640.

282. Rehman AS, Kumar P, Parvez S. Dopamine-D2-agonist targets mitochondrial dysfunction via diminishing Drp1 mediated fission and normalizing PGC1-α/SIRT3 pathways in a rodent model of Subarachnoid Haemorrhage. Neuroscience. 2025;564:60-78.

283. Ning X, Tang J, Li X, Wang J, Zhai F, Jiang C, et al. Dexmedetomidine ameliorates hepatic ischemia reperfusion injury via modulating SIRT3 mediated mitochondrial quality control. Scientific Reports. 2025;15(1):5630.

284. Ikeda Y, Shirakabe A, Maejima Y, Zhai P, Sciarretta S, Toli J, et al. Endogenous Drp1 mediates mitochondrial autophagy and protects the heart against energy stress. Circ Res. 2015;116(2):264-78.

285. Steffen J, Ngo J, Wang S-P, Williams K, Kramer HF, Ho G, et al. The mitochondrial fission protein Drp1 in liver is required to mitigate NASH and prevents the activation of the mitochondrial ISR. Molecular Metabolism. 2022;64:101566.

286. Zhang Z, Zhang L, Zhou L, Lei Y, Zhang Y, Huang C. Redox signaling and unfolded protein response coordinate cell fate decisions under ER stress. Redox Biol. 2019;25:101047.

287. Zhong Z, Mao X, Zhang J, Bu W, Guan Z, Wang Y, et al. ER-Localized ERO1α and Caspase-3-Mediated Cleavage of Mitochondrial NDUFS1 Drives Trichothecene-Induced ROS Accumulation in Liver. Available at SSRN 5526005.

288. Yan W, Wang J, Su Y, Zhai X, Zhong Y, Tian L, et al. PM2. 5 Induced Iron Accumulation-Associated Hepatocyte Toxicity and Mice Liver Injury via Activation of Ferroptosis and Pyroptosis. Environment & Health. 2025.

289. Radosavljevic T, Brankovic M, Samardzic J, Djuretić J, Vukicevic D, Vucevic D, et al. Altered mitochondrial function in MASLD: key features and promising therapeutic approaches. Antioxidants-Basel. 2024;13(8):906.

290. Clare K, Dillon JF, Brennan PN. Reactive oxygen species and oxidative stress in the pathogenesis of MAFLD. J Clin Transl Hepato. 2022;10(5):939.

291. Radosavljević T. Mitochondrial Dysfunction in MASLD: Unveiling Mechanisms and Optimizing Therapeutic Strategies. Bentham Science Publishers; 2025. p. 3941-4.

292. Ziolkowska S, Binienda A, Jabłkowski M, Szemraj J, Czarny P. The interplay between insulin resistance, inflammation, oxidative stress, base excision repair and metabolic syndrome in nonalcoholic fatty liver disease. International journal of molecular sciences. 2021;22(20):11128.

293. Ramanathan R, Ali AH, Ibdah JA. Mitochondrial dysfunction plays central role in nonalcoholic fatty liver disease. International Journal of Molecular Sciences. 2022;23(13):7280.

294. Feldman A, Wernly B, Strebinger G, Eder SK, Zandanell S, Niederseer D, et al. Liver-related mortality is increased in lean subjects with non-alcoholic fatty liver disease compared to overweight and obese subjects. Journal of Gastrointestinal and Liver Diseases. 2021;30(3):366-73.

295. Ahmed OT, Gidener T, Mara KC, Larson JJ, Therneau TM, Allen AM. Natural history of nonalcoholic fatty liver disease with normal body mass index: a population-based study. Clinical Gastroenterology and Hepatology. 2022;20(6):1374-81. e6.

296. Alharthi J, Pan Z, Gloss BS, McLeod D, Weltman M, George J, et al. Loss of metabolic adaptation in lean MAFLD is driven by endotoxemia leading to epigenetic reprogramming. Metabolism. 2023;144:155583.

297. Eslam M, El-Serag HB, Francque S, Sarin SK, Wei L, Bugianesi E, et al. Metabolic (dysfunction)-associated fatty liver disease in individuals of normal weight. Nature reviews Gastroenterology & hepatology. 2022;19(10):638-51.

298. Kawanishi S, Oikawa S. Mechanism of telomere shortening by oxidative stress. Ann N Y Acad Sci. 2004;1019(1):278-84.

299. Murphy MP. How mitochondria produce reactive oxygen species. Biochemical journal. 2009;417(1):1-13.

300. Metcalfe NB, Olsson M. How telomere dynamics are influenced by the balance between mitochondrial efficiency, reactive oxygen species production and DNA damage. Mol Ecol. 2022;31(23):6040-52.

301. Van Steensel B, De Lange T. Control of telomere length by the human telomeric protein TRF1. Nature. 1997;385(6618):740-3.

302. Kendellen MF, Barrientos KS, Counter CM. POT1 association with TRF2 regulates telomere length. Mol Cell Biol. 2009;29(20):5611-9.

303. Penrice DD, Jalan-Sakrikar N, Jurk D, Passos JF, Simonetto DA. Telomere dysfunction in chronic liver disease: The link from aging. Hepatology. 2024;80(4):951-64.

304. Kim D, Li AA, Ahmed A. Leucocyte telomere shortening is associated with nonalcoholic fatty liver disease-related advanced fibrosis. Liver International. 2018;38(10):1839-48.

305. Townsend LK, Weber AJ, Day EA, Shamshoum H, Shaw SJ, Perry CG, et al. AMPK mediates energetic stress-induced liver GDF15. The FASEB Journal. 2021;35(1):e21218.

306. Kim KH, Lee M-S. GDF15 as a central mediator for integrated stress response and a promising therapeutic molecule for metabolic disorders and NASH. Biochimica et Biophysica Acta (BBA)-General Subjects. 2021;1865(3):129834.

307. Kempf T, Guba-Quint A, Torgerson J, Magnone MC, Haefliger C, Bobadilla M, et al. Growth differentiation factor 15 predicts future insulin resistance and impaired glucose control in obese nondiabetic individuals: results from the XENDOS trial. Eur J Endocrinol. 2012;167(5):671-8.

308. Li Y-L, Chang JT, Lee L-Y, Fan K-H, Lu Y-C, Li Y-C, et al. GDF15 contributes to radioresistance and cancer stemness of head and neck cancer by regulating cellular reactive oxygen species via a SMAD-associated signaling pathway. Oncotarget. 2016;8(1):1508.

309. Bayoumi A, Elsayed A, Han S, Petta S, Adams LA, Aller R, et al. Mistranslation drives alterations in protein levels and the effects of a synonymous variant at the fibroblast growth factor 21 locus. Advanced Science. 2021;8(11):2004168.

310. Kang SG, Choi MJ, Jung S-B, Chung HK, Chang JY, Kim JT, et al. Differential roles of GDF15 and FGF21 in systemic metabolic adaptation to the mitochondrial integrated stress response. IScience. 2021;24(3).

311. Mposhi A, Cortés-Mancera F, Heegsma J, De Meijer VE, Van de Sluis B, Sydor S, et al. Mitochondrial DNA methylation in metabolic associated fatty liver disease. Front Nutr. 2023;10:964337.

312. Daniali L, Benetos A, Susser E, Kark JD, Labat C, Kimura M, et al. Telomeres shorten at equivalent rates in somatic tissues of adults. Nature communications. 2013;4(1):1597.